TABLE OF CONTENTS

LIST OF TABLES

Page

LIST OF FIGURES

Page

LIST OF ABBREVIATIONS AND ACRONYMS

ASTM	American Society for Testing and Materials
ASME	American Society of Mechanical Engineers
EPP	Elastic Perfectly Plastic
FEA	Finite Element Analysis
HEI	Heat Exchanger Institution
IGA	Intergranular Attack
SCC	Stress Corrosion Cracking
TEMA	Tubular Exchanger Manufacturers Association
LBRB	Leak Before Risk of Break

LIST OF SYMBOLS AND UNITS OF MEAUREMENT
(INTERNATIONAL SYSTEM)

β Constant of Elastic Beam Foundation theory

ν_t , ν_s Poisson's ratio of tube and tubesheet

σ_r Radial stress of tube (MPa)

σ_θ Hoop stress of tube (MPa)

σ_x Axial stress of tube (MPa)

σ_e Equivalent stress of tube (MPa)

σ_l Loading stress(MPa)

σ Residual stress(MPa)

σ_u Unloading stress(MPa)

θ Tube rotation

$A_{\beta x}$, $B_{\beta x}$, $C_{\beta x}$, $D_{\beta x}$ Influence functions in elastic beam foundation theory

c Initial clearance (mm)

c_t , c_s Elasto-plastic radius of tube and tubesheet

E_t Tube elastic modulus (GPa)

E_s Tubesheet elastic modulus (GPa)

E_{tt} , E_{st} Tube and tubesheet tangent modulus (GPa)

f Coefficient of friction

l_t Tubelength

l_s Tubesheetlength

LT_v , LT_M , LT_θ, LT_u Load terms or load and deformation equations

n Dimensionless form of circumferential stress

m Dimensionless form of axial moment

M_{el} Bending moment in elastic beam foundation theory

M_x , M_x^u Axial moment along the transition zone during loading and unloading

N_θ Circumferential hoop stress along the transition zone

P Parameter of plastic analysis

P_{at} Collapse pressure of tube (MPa)

P_c , P_{cm} Contact pressure and its maximal value (MPa)

P_e, P_{em} Expansion pressure and its maximal value *(MPa)*

P_{el} Shear force in elastic beam foundation theory for elastic region

P_{yt} , P_{ys} Tube and tubesheet yield pressure (MPa)

P_u Unit pressure (force per unit area)

q Dimensionless form of shear force in plasticity theory

Q Shear force through the transition zone

r_i , r_o , r_m Inner, outer and mid thickness tube radii (mm)

$\mathbf{R}$ Radius of cylinder for plasticity theory (mm)

$\mathbf{R_i}$, $\mathbf{R_o}$ Inner and equivalent outer tubesheet radii (mm)

$\mathbf{S_{yt}}$ Tubeyield stress (MPa)

$\mathbf{S_{ys}}$ Tubesheet yield stress (MPa)

t_t Tube thicknesses (mm)

u Radial displacement of tube during loading(mm)

u_x Radial displacement of tube in elastic region, through the transition zone during loading(mm)

u_x^u Radial displacement of tube, through the transition zone during unloading(mm)

ω Tube radial displacement at mid thickness (mm)

x Dimensionless form of transition zone length

X Length of transition zone (mm)

Y_s Outer to equivalent inner diameter ratio of tubesheet

Y_t Outer to inner diameter ratio of tube

Y_{tc} Outer to elasto-plastic diameter ratio of tube

V_x^u Shear force of tube, through the transition zone during unloading

INTRODUCTION

The reliability of the tube to tubesheet connection is vital in shell and tube heat exchanger performance, because the residual stresses produced by the expansion process can lead to failure and produce major process safety events. The tube expansion process is conducted to avoid the mixture of the fluids of the two circuits, however the process leaves the residual stresses in the joint. The effect of residual stresses in the tube and tubesheet can cause crack propagation in the presence of a corrosive environment. In fact, the superposition of stresses produced during the manufacturing process, and those generated while the equipment is in service, can eventually provoke the risk of equipment degradation. These stresses are directly affected by the expansion pressure, clearance and material strain hardening, but also by the operating pressure and temperature. When leakage failure of certain connections involving lethal or flammable services takes place, the consequence can be very catastrophic to humans, the environment and the economy. Therefore, the accurate determination of theses stresses in the transition zone of expanded tubes seems to be unavoidable, especially in the cases where the operation conditions are severe.

Objective

As mentioned previously, the main purpose of the expansion process is to improve the integrity of the connection by closing the clearance gap and producing the contact pressure at the interface between the tube and tubesheet. This process often generates high tensile residual stresses, which can be considered the most influential weakness of tube expansion.

Since 1976, when the hydraulic expansion was proposed, many researchers, including Krips (1976), have dedicated their time to this subject and, in particular, to the study of the residual stresses generated during the hydraulic expansion of tube to tubesheet joints. The main interest of the majority of these researchers was the expansion zone. Many failure investigations, however, revealed that the transition zone is the most critical location where the residual stresses reach their highest value through the entire connection.

In this work, in order to analyze residual stresses in the transition zone of a tube, an analytical model to predict these stresses will be developed. The analytical model gives a

cheaper and quick assessment of the joint design as compared to a FEM. It also provides an additional comparative tool that supplements FEM. In the best interest of the analysis, the two steps of loading and unloading will be considered separately in order to evaluate the level of stresses at the two most critical phases of the expansion process. The results will be compared to those of finite element modeling in order to validate the analytical model.

Specific objectives

In order to respect the objective of this analysis and meet the milestones, the following steps are taken into account:

1) A detailed review of literature, which includes our comments, and a high sense of criticism to support this planned research work and the investigation is outlined. Also, a particular attention will be paid to the theories and models proposed by other researchers in both expansion and transition zones to evaluate residual stresses produced by the hydraulic expansion process.
2) Elaborate an analytical model which enables the designers and manufacturers of shell and tube heat exchangers to determine the level of residual stresses in the transition zone and, consequently, to optimize the effective life of expanded connections and required maintenance intervals.
3) Development of a finite element model to validate the compiled data from the analytical model. This 3D FE model is likely according to the numerical models proposed in the literature and will be built using ANSYS Workbench 16.2 structural static tools.

Thesis plan

In the current thesis, the first chapter describes the summary of shell and tube heat exchangers with emphasis on tube to tubesheet joints. Also, principles of tube expansion and common expansion processes used by the pressure vessel industry, as well as design parameters, are outlined in this chapter. The last section is dedicated to various failure mechanisms in expanded tubes and recommended treatments in the literature.

In the second chapter, a literature review with particular attention to the work conducted on the transition zone of tubes and the evaluation of the residual stresses at this zone is conducted. The previous research works are separated into three types; Experimental, Analytical and Finite element sections. In the best interest of data compilation and comparison of the results introduced by different researchers, comments are added at the end of each section. This method allows the author to compile results and findings to justify the objective.

Next chapter explains the main contribution of the author on the topic of hydraulically expanded tube-to-tubesheet joints by proposing an analytical model, which enables the evaluation of the residual stresses in the transition zone during both loading and unloading steps. The main focus of the developed model is to optimize the design of tube expansion by lowering the residual stresses as much as possible while maintaining an adequate contact pressure after unloading or the release of the expansion pressure.

In chapter four, the validation of the analytical model is conducted by means of comparison with 3D finite element modeling, which is considered to be the benchmark. The simulation parameters in the software are described and comparisons of axial and hoop and equivalent stresses according to the two approaches are conducted in order to validate the analytical model.

Finally, the last chapter is devoted to results and discussions. The comparison of the two models and their distribution of stresses along the tube is performed in this chapter. In addition, the effect of reverse yielding during unloading in expansion zone for investigated models is highlighted in this chapter. As is well-known, tube radial displacement through the entire process and especially after unloading is intrinsic due the fact that this parameter contributes in integrity of connection by introducing residual contact pressure and sometimes material strain hardening. Therefore, tube radial displacement throughout the process is manifested.

An accurate model which allows determining the residual stresses in every step of the expansion process can be very interesting for designing an optimum connection. In fact, the effect of various parameters involving in joint analysis necessitates proposing an analytical model which takes into account as many parameters as possible in order to reach an optimal

model. Therefore, this work can be named as a point of departure for a comprehensive study of transition zone which requires the highest attention through the entire tube to tubesheet joint and this is why the last section of this thesis is dedicated to the future work that need to be investigated later.

CHAPTER 1

CONNECTION OUTLINE

1.1 Heat exchangers

A heat exchanger is a piece of equipment which allows the heat transfer from one fluid, which can be liquid or gas, to the second fluid. In this process, there is no contact between the two fluids, but only conventional heat transfer streams between the two circuits. This equipment is widely used in oil and gas, nuclear, power and chemical plants.

There are various classifications of exchangers based on the following criteria and according to the requirements of operation:

1) Fluid combination
    a) Gas to gas,
    b) Gas to liquid,
    c) Liquid to liquid and phase change;
2) Heat transfer mechanisms
    a) Single-phase convection on both sides,
    b) Single-phase convection on one side, two phase convection on the other side,
    c) Two-phase convection on both sides,
    d) Combined convection and radiative heat transfer;
3) Process function
    a) Condensers,
    b) Heaters,
    c) Coolers,
    d) Chillers;
4) Construction
    a) Tubular,
    b) Plate-type,
    c) Regenerative,

   d) Adiabatic wheel;
5) Number of pass
   a) Single-pass,
   b) Multi-pass;
6) Number of fluids passing through the heat exchanger
   a) Two fluids,
   b) Three fluids,
   c) More than three fluids.

As can be seen, this equipment fulfills many needs of industrial plants due to its diversity and availability. The diversity of exchangers makes them very applicable in different industries, although their design is complicated due to the distinct construction and required heat transfer.

1.2 Shell and tube heat exchangers

Shell and tube exchangers are the most common type of exchangers in the industry, due to their high performance. The latter is obtained by the shape of the exchanger, which allows a more effective heat transfer between fluids. Therefore, in comparison with other exchangers, shell and tube affords a wide range of options for the designers by means of modifying the parameters mentioned in the previous section.

The application of shell and tube exchangers is typically in high pressure processes where the operating pressure sometimes can reach up to 70 bar. Figure 1.1 demonstrates a schematic of shell and tube exchangers and flow stream in both head and shell sides.

In order to have a higher efficiency, there are several parameters which must be considered in the design of shell and tube exchangers:

1) Tube diameter,
2) Tube length,
3) Tube thickness,
4) Tube layout,
5) Tube pitch,
6) Tube corrugation,

7) Baffle design.

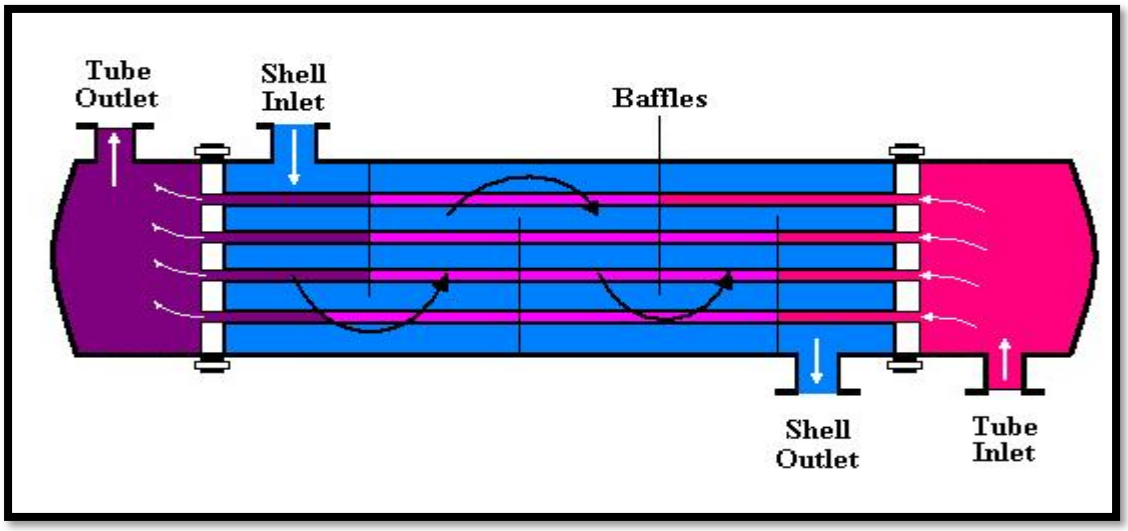

Figure 1.1 Shell and tube heat exchanger
(http://classes.engineering.wustl.edu/)

1.3 Tube to tubesheet joint

The connection of the tube to the tubesheet should be credited as the most critical element of shell and tube exchangers, due to the fact that its rigidity depends upon many parallel tubes. In fact, the high reliability of this joint can ensure a longer life of the exchanger and minimize the risk of exchanger failure. As a solution, expansion of the tube seems to be a useful technique to reduce the possibility of leakage between two circuits. In this process, the tube is expanded to contact the tubesheet bore and close the gap. A weld around the tube is sometimes added to ensure leak-free tightness. By creating this barrier between the tube and tubesheet, the fluid flow in neither direction is allowed.

According to the fundamentals of the expansion process, there are three main affected zones in the tube, as shown in Figure 1.2:

1) Expansion zone,
2) Transition zone,
3) Unexpanded zone.

However, the expansion process enhances the integrity of the tube-to-tubesheet joint. This process can initiate failure of the tube and tubesheet, which sometimes leads to a complete

degradation of the heat exchangers. The presence of high residual stresses developed during expansion can reach critical values when coupled with the stresses created during the operation, which threatens the strength of the connection with the initiation of crack propagation under a corrosive environment. Hence, the latter necessitates an analysis of the fundamentals to clarify the cause of failure.

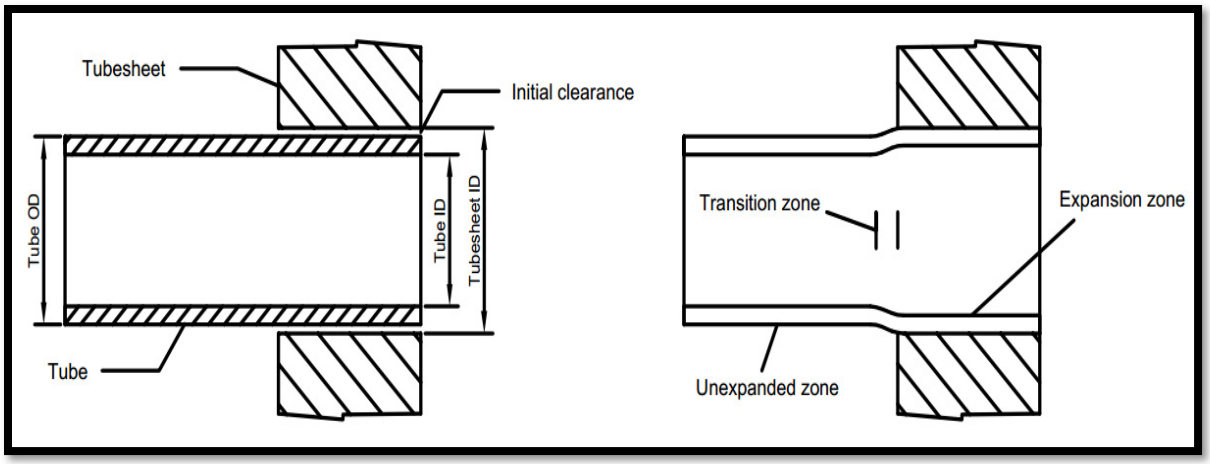

Figure 1.2 Tube expansion

1.4 Common expansion processes

The purpose of the tube expansion process is to close the gap between tube and tubesheet and to produce the contact pressure at the interface. By doing this, the flow stream from the primary to second circuit and vice versa is blocked. In this process, based on the expansion pressure level, the tubesheet undergoes either elastic or partially plastic deformation. Therefore, the level of the expansion pressure should be monitored to avoid tube over expansion, which could cause a full plastic deformation of the tubesheet, over thinning of the tube or its extrusion along the tubesheet bore.

There are four common expansion processes in the industry:

1) Mechanical rolling,
2) Hydraulic expansion,
3) Hybrid expansion,
4) Explosive expansion.

1.4.1 Mechanical rolling

This process is the oldest and the most used method for the expansion of tubes. The required time for this process makes it a favorite of manufacturers. The tube expander consists of three major parts, shown in Figure 1.3:

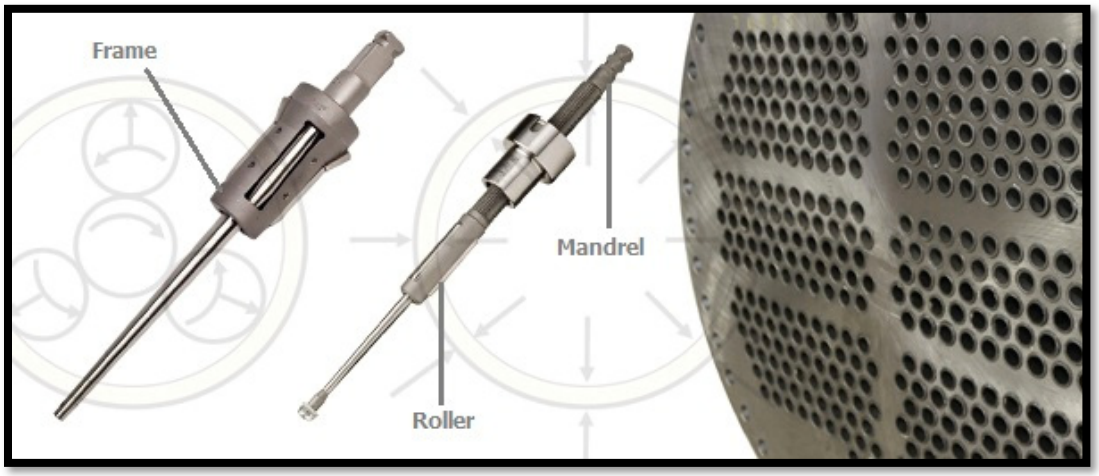

Figure 1.3 Mechanical rollers
(www.elliott-tool.com)

1) Roller: This part is used to expand the tube's inside diameter by applying an imposed displacement by the roller to increase the tube diameter and produce expansion. The number of rollers can vary from 3 to 7 rollers placed at an equal distance around the periphery;
2) Frame: This part holds the rollers and keeps them fixed at an equal interval. Any misplaced rollers lead to a dent forming inside the tube;
3) Mandrel: This component guides the rollers and controls the radial displacement. The mandrel, tube and tubesheet bore axis are concentric. The mandrel roller system is designed to obtain a perfectly inner circular surface of the tube. The mandrel acts by an electrical or pneumatic actuator and can reach speeds up to 1100 rpm.

In mechanical rolling, after releasing the rollers, the tubesheet springs back, compressing the tube to produce a residual contact pressure. Likewise, using this expansion process, the strength of the connection is increased significantly while generating high residual stresses

and undesirable local deformations in the tube, resulting in stress corrosion cracking and stress concentrations. In addition, mechanical rolling results in a higher level of strain hardening in the tube material and a reduction in the contact pressure at the interface.
The biggest disadvantage of mechanical rolling rests in the fact that the residual stresses of the tube cannot be estimated, due to the irregularities of the process and the difficulty in controlling deformation making the effective life of tubes impossible to predict.

1.4.2 Hydraulic expansion

The hydraulic expansion process was proposed by Westinghouse in the mid 70's. As its name suggests, this method applies hydraulic pressure of water or other fluids to expand the tube.
The elements of the hydraulic process shown in Figure 1.4 are as follows:

1) Probe,
2) Pump,
3) Booster,
4) Pressure gauge,
5) Overflow valve,
6) Hydraulic fluid tank,
7) Control valve.

Prior to loading, the secondary section is filled with fluid and the booster is placed in its initial position. Then, the pressure pump increases the pressure to run the expander (primary pressure) and the booster intensifies this pressure to the required pressure for expansion of the tube. During unloading, the overflow valve discharges the fluid to the tank to relieve the pressure. Figure 1.5 shows a detailed view of hydraulic expansion, which achieves a homogeneous expansion pressure over the inner surface of the tube. According to Krips and Podhorsky (1976), the most important advantage of this process would be highlighted in the fact that the expansion pressure can be determined with high accuracy.
Like mechanical rolling, in this process, the tube undergoes plastic deformation prior to contact with the tubesheet. Also, both tube and tubesheet spring back during unloading, so

the gap might not be fully closed along the tubesheet thickness; this can provoke stress corrosion cracking from the shell side, resulting in internal leakage between two circuits.

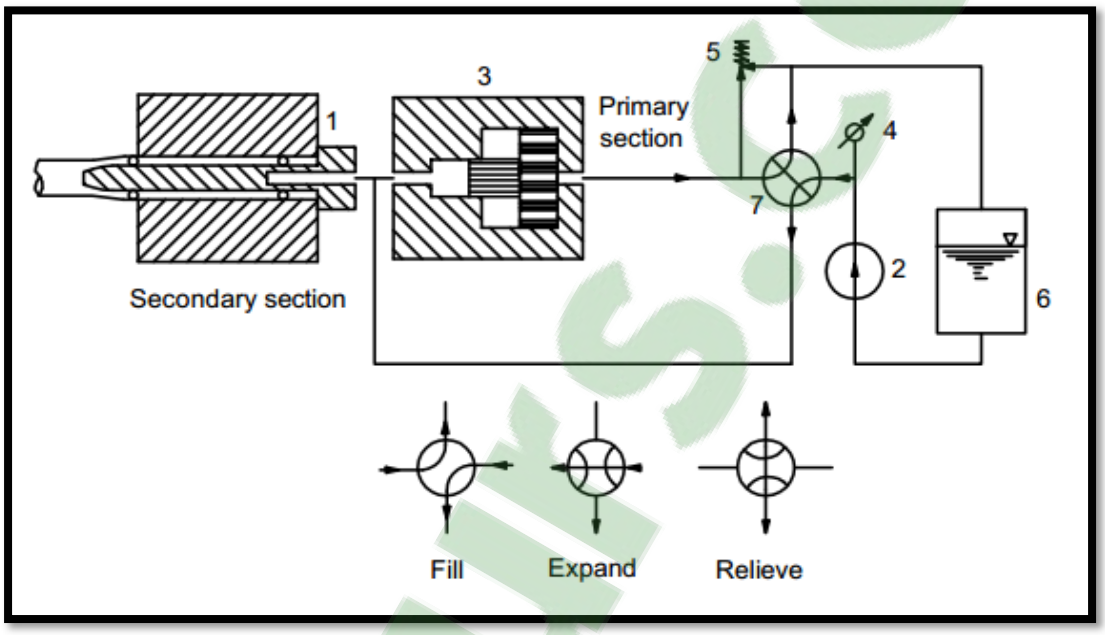

Figure 1.4 Diagram of the tube expansion installation
(Taken from Krips and Podhorsky, 1976)

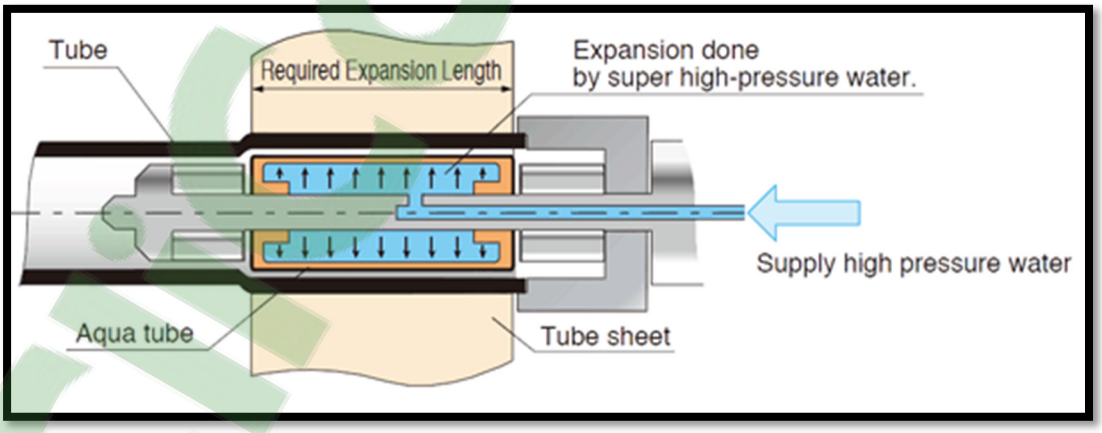

Figure 1.5 Schematic of hydraulic expansion process
(www.sugino.com)

1.4.3 Hybrid expansion

For the first time, hybrid expansion was proposed by Krips and Podhorsky in 1979, three years after the invention of hydraulic expansion. After being acquainted with some

weaknesses in the former method, the hybrid technique was invented to achieve an optimum design.

Hybrid expansion consists of hydraulic and mechanical rolling processes in succession. This method is able to expand the tubes with high strength materials or combined with multiple materials. The process starts with hydraulic expansion to close the clearance between the tube and tubesheet. Then, mechanical rolling is performed to remove the dents and undesired deformations over the inside surface of the tube in order for the joint to reach higher strength. In fact, after releasing the hydraulic pressure, the tube has enough time to return partially to its initial position, and this leads to the relief the residual stresses.

However, while hybrid expansion achieves superior quality in contrast with the two preceding processes applied individually, the required time for preparation and process is much longer. Therefore, the application of such a process is limited to high-sealed services.

1.4.4 Explosive expansion

Tube expansion by explosion was initially invented by Berman Irwin et al. in 1966. In this process, explosive plugs are placed inside the tube, and an explosion takes place to cause the tube expansion (Figure 1.6). The minimum required preparation time makes this process more desirable. However, explosion impact must be predetermined to have the least damage and unwanted deformation in the joint. In fact, in this process, any damage will lead to the tube plugging from both sides.

After detonation, the outer contact edge of the tube and tubesheet will be seal welded to reduce the possibility of leakage from shell side to head side and vice versa. In addition, mechanical rolling can be applied as a supplement to get a perfectly circular inner surface of the tube.

1.5 Hydraulic expansion principles

The hydraulic expansion process can be divided into two main steps:

1) Loading step, in which the expander is applied to expand the tube;
2) Unloading step, in which the expander is released.

Figure 1.6 Plug installation in explosive expansion
(www.tei.co.uk)

As is manifested in Figure 1.7, by applying the expander, the tube expands radially in the elastic range until it reaches point B. In step 2, the tube begins to deform plastically in the tube's inside diameter, deforming plastically until the outer surface of the tube touches the inner surface of the tubesheet in step of 3. This point is shown as point D in the graph. In this work, it is assumed that the tube undergoes full plastic deformation before it comes into contact with the tubesheet. After that, any increase in the expansion pressure would cause elastic deformation at the tubesheet's inner surface up to point E, producing a contact pressure at the interface.

It is worthy to note that the slope of line 4 represents the combined rigidity of the assembly, including both the tube and the tubesheet. Up to point E, the expansion pressure P_e is lower than the pressure to cause yield in the tubesheet P_{ys} and the tubesheet never suffers plastic deformation. Then, in step 7, the tubesheet deforms elasto-plastically starting at the tubesheet's inner surface. Finally, step 5 is the unloading phase, during which the tube and tubesheet spring back. The greatest slope of line 5 corresponds to the full elastic rigidity contribution of both the tube and tubesheet and pressure resistance by the whole assembly.

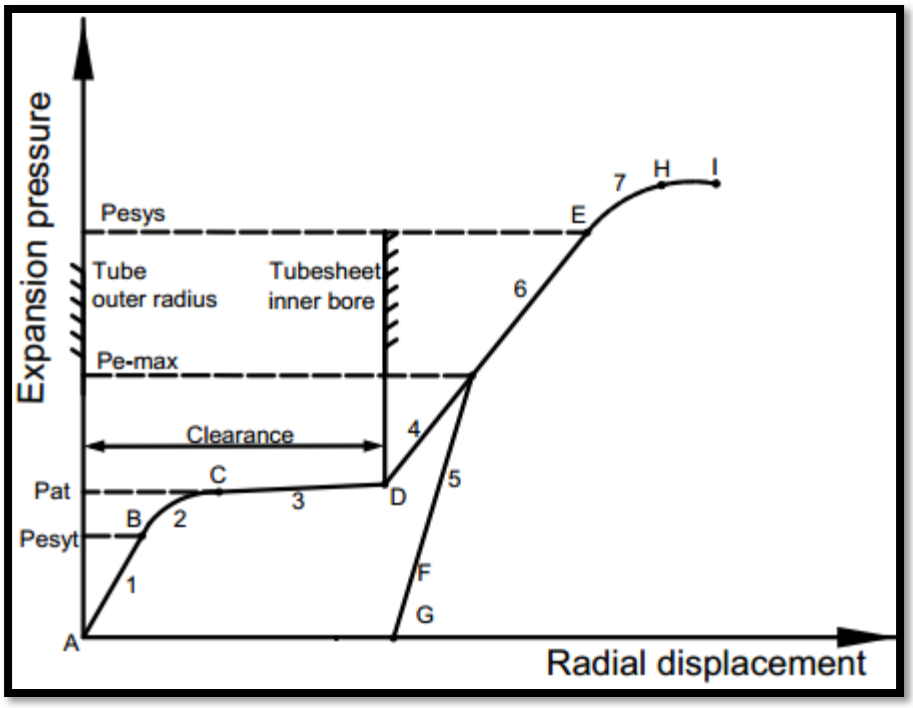

Figure 1.7 Hydraulic expansion steps

1.6 Factors influencing the rigidity of tube to tubesheet connection

In order to reach an optimum design of the tube to tubesheet connection, one should consider the following parameters to reduce the risk of leakage:

1) Expansion pressure,
2) Initial clearance,
3) Residual stresses produced by the expansion process,
4) Final contact pressure between tube and tubesheet,
5) Material properties of tube and tubesheet,
6) Friction at the interface,
7) Tube layout and expansion sequence,
8) Operating conditions.

However, the effect of every single factor may vary, depending on the rigidity of the joint. A comprehensive work requires taking into account the entire engaged parameters, and it is the designer's responsibility to analyze these factors meticulously as much as possible.

According to the author, the factors mentioned above would be classified into three main sections:

1) Connection geometry, which includes initial clearance, tube and tubesheet inner and outer diameters and their thicknesses, etc.;
2) Mechanical properties of the tube and tubesheet. In this section, elastic modulus, yield stress, plasticity constants, etc. can be considered influence factors;
3) Service conditions, which consider the effect of operational parameters on the performance of shell and tube heat exchangers. These effects are described as below:
    a. Thermal stresses produced by temperature gradients between two circuits,
    b. Differential pressure between two circuits,
    c. Equipment vibration due to the misalignment or hydraulic shock,
    d. Stress corrosion cracking,
    e. Fatigue.

1.6.1 Expansion pressure

In the hydraulic expansion method, two O-rings are within a specific distance. This distance is usually the same length as the tubesheet thickness. Therefore, the area between these O-rings will expand. As is mentioned in the foregoing, the accurate determination of the expansion pressure in the hydraulic process can be considered an advantage of this technique. The level of expansion pressure dictates the deformation in the tubesheet. Since such pressure is limited to the one that produces yield stress in tubesheet P_{sy}, the tubesheet just bears the load to remain in the elastic range and, undoubtedly, any increase in expansion pressure above P_{sy} would result in partial or full plastic deformation of the tubesheet.

There are two limits to define the expansion pressure according to Updike (1989); the lower limit, in which the expansion pressure allows the tube to close the gap with no contact pressure at the interface of tube and the tubesheet, and the upper limit, which is known as the pressure that causes plastic axial extrusion of the tube through the tubesheet bore.

Through the years, several methods were proposed in order to determine the optimum degree of expansion and the “percentage of tube wall thickness reduction” showed the highest reliability and effectiveness. In fact, this method measures the tube wall thinning at the end

of the process. According to Yokel (1992), if the wall reduction reaches 12%, the joint should be rejected.

In addition, over expansion might lead to either higher residual stresses in the assembly or higher strain hardening in both parts, and it reduces the integrity of the joint notably.

1.6.2 Initial clearance

Initial clearance must give enough room to the tube to go under plastic deformation before it comes into contact with the tubesheet. Otherwise, the tube springs back and won't allow the generation of the interface contact pressure. As a result, fluid can pass through the gap from one side to the opposite side.

The standard of the Tubular Exchanger Manufacturers Association (TEMA) addresses the permissible tubesheet bore diameters and tolerances for each nominal tube OD in Table RCB 7.41. These dimensions prevent the risk of tube thinning, which takes place in the tube wall as a result of over expansion.

Several studies to determine the effect of initial clearance on the rigidity of the tube to tubesheet connection have been undertaken by researchers through the years. Allam et al. (1998) and Merah et al. (2003) performed Finite Element Analyses, and they concluded that for low strain hardening, the effect of initial clearance is negligible. However, with strain hardened materials, the residual contact pressure has been found to decrease linearly when increasing initial clearance [Merah et al., 2003].

1.6.3 Residual stresses produced by the expansion process

Residual stresses are the stresses that remain in the joint at the end of expansion process. However, both the tube and tubesheet should bear a lower level of residual stresses in the hydraulic process. The effect of high residual stresses is considered in this analysis due to its destructive outcome.

Tensile residual stresses are found at the inner and outer surface of expanded tubes and, in the case of micro-crack existence, they accelerate their propagation, which can be accelerated by the presence of corrosion. It is worthy to note that in mechanical rolling, tensile residual stresses on the inner surface of the tube in the transition zone can reach yield stress (Updike

and Kalnins, 1988). Therefore, this zone requires special attention due to the high risk of stress corrosion cracking, since the joint is very often exposed to corrosive services.

In addition, residual stresses affect the mechanical properties of the materials. In fact, these stresses weaken the rigidity of the joint by reducing the yield strength of the material and induce lower corrosion resistance.

In hydraulic expansion, after the loading step, residual stresses reach their peak, but during unloading the tube and tubesheet spring back, which allows the stresses to be relieved and reduced to a certain extent. The advantage of hybrid expansion is to lower strain hardening, which reduces the residual stresses by the quick application of mechanical rolling when the gap is already closed by hydraulic expansion. Therefore, residual stresses are extremely lower in this process.

1.6.4 Contact pressure

The contact pressure produced at the interface of the tube and tubesheet is optimum when the tubesheet is more rigid than the tube. In fact, this facilitates the tube expansion process and reduces undesirable deformation in the tubesheet (Grimison and Lee, 1943).

Two limits are taken into account for contact pressure. The lower limit is represented by cases when the tube's outer surface touches the tubesheet bore and it leaves no contact pressure at the interface. The upper limit is reached when no tube extrusion occurs along the tubesheet bore. However, the unloading step reduces the residual contact pressure, while the final contact pressure will be generated according to these two limits.

The contact pressure is highly affected by initial clearance and the tube expansion sequences for different tube layouts. In fact, the residual contact pressure is reduced at the interface when adjacent tubes are expanded (Chaaban, 1989). As a result, the number of tubes surrounding a specific tube could have a significant effect on contact pressure (Bouzid, 2016).

1.6.5 Material properties of tube and tubesheet

As it is explained previously, manufacturers of shell and tube exchangers prefer tubesheets with higher strengths than that of the tubes in order to facilitate the expansion process, due to the lower expansion pressure needed to close the gap and produce a rigid connection.

In joint analysis, it is likely to assume for both parts exhibiting isotropic behavior, homogenous materials and free of dislocations and cracks. In addition, the materials do not exhibit strain hardening behavior. The other desired assumption is that the tube undergoes plastic deformation prior to contact with the tubesheet.

The behavior of materials in plastic regime could be another crucial factor in the analysis of tube to tubesheet. Actually, all research conducted on this subject is assumed to obey one of the following plastic behaviors:

1) Elastic Perfectly Plastic (EPP): In fact, EPP is a simplification by considering the tangent modulus equal to zero;
2) Multi-Linear Kinematic Hardening.

The level of the expansion pressure dictates tubesheet behavior. When the maximum expansion pressure P_{em} is lower than the tubesheet yield pressure P_{ys}, the tubesheet is in the elastic range. However, any increase in expansion pressure beyond P_{ys} results in plastic deformation of the tubesheet starting at the inner bore surface.

1.6.6 Friction at the interface

The highest integrity of the joint is obtained once the tube extrusion is prevented through the tubesheet bore (Grimison and Lee, 1943). This could be acquired by higher friction at the interface, although greater friction could cause higher strain hardening in tube material, which can reduce the residual interfacial contact pressure. Therefore, friction has a key role in obtaining a rigid joint.

According to Al-Aboodi et al. (2010), a friction coefficient greater than 0.2 has an insignificant effect on the residual contact stress for metal to metal contact, and this value should be considered a turning point. This point is demonstrated in Figure 1.8. Furthermore,

the author investigated the effect of friction on strain hardening and its relation to higher residual stresses at the interface.

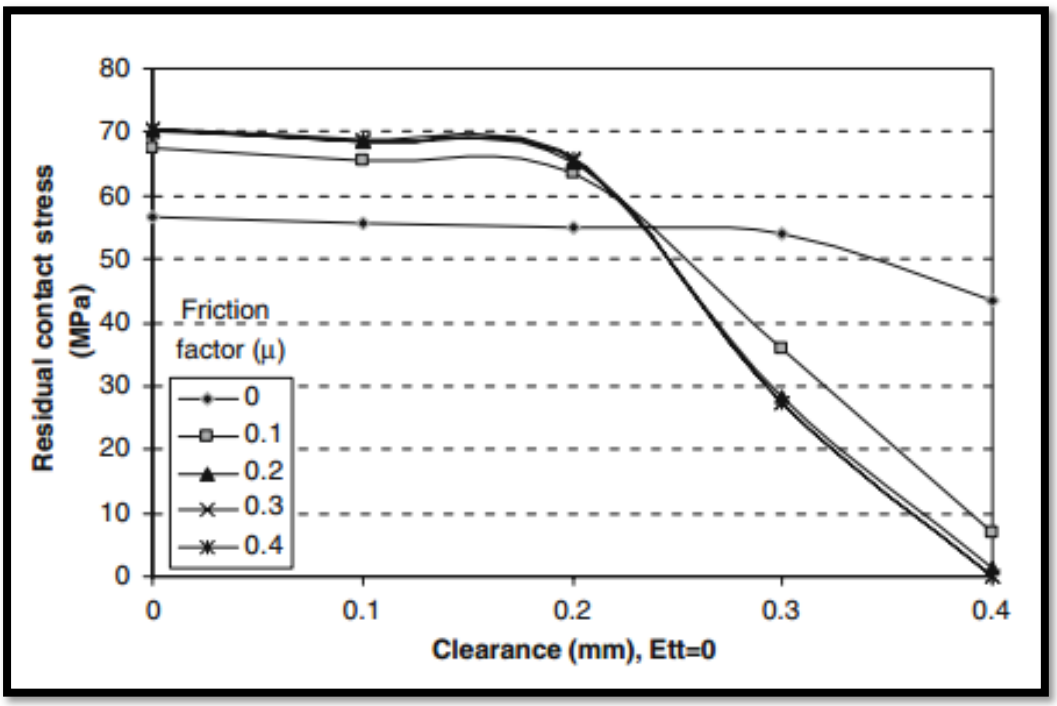

Figure 1.8 Influence of friction and radial clearance on interfacial contact stress (Taken from Al-Aboodi et al. 2010)

1.6.7 Tube layout and expansion sequence

The arrangement of tubes and their order of expansion is another dominant factor which should be considered in joint analysis. The most practiced arrangement is surrounding every single tube with at least six adjacent tubes, to place as many tubes as possible in order to increase the heat transfer between the two circuits. The two popular patterns, the square and triangular layouts of tubes, used by the industry are shown in Figure 1.9.

The research devoted to this factor revealed a reduction in the contact pressure of a tube when adjacent tubes are expanded. Therefore, the expansion of tubes needs a particular attention to account for this effect.

In 1993, Huang et al. did a finite element analysis to compare square and triangular arrangements of tubes. He concluded that the average residual contact pressure in the central tube in a triangular layout was 100% greater than that of the square pattern. In fact, the

triangular pattern, due to the number of tubes which surround the central tube, would result in higher rigidity of the joint.

The triangular pattern, in comparison with the square pattern, affords a higher level of heat transfer; however, due to the number of tubes placed in the triangular model, the access to the tube bundle on the shell side is limited and operation requirements for dirty services should be forecasted.

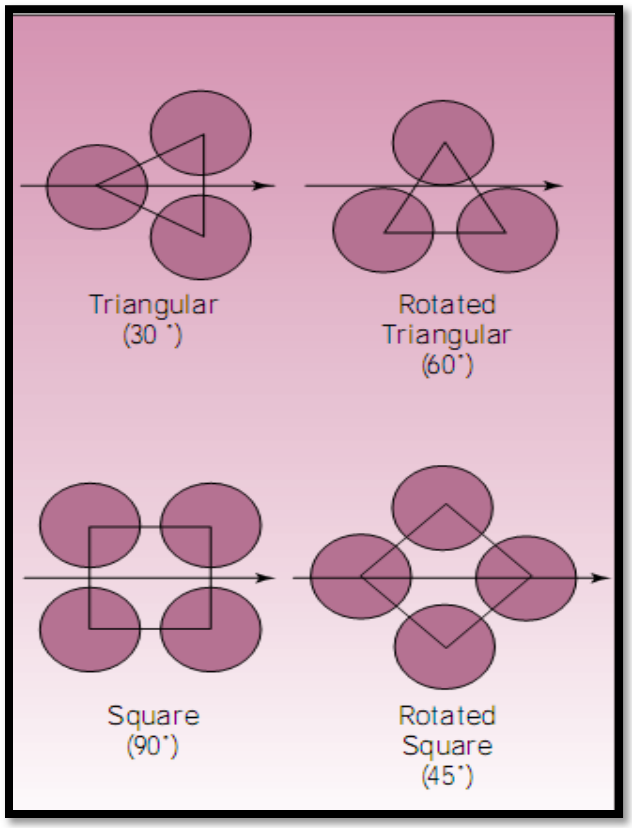

Figure 1.9 Tube square and triangular layouts
(http://chemical-eng-world.blogspot.ca)

1.6.8 Operating conditions

Heat exchangers are usually used in elevated temperature services, and this can cause thermal loading in both the tube and the tubesheet and weaken the connection tightness. The generated circumferential thermal gradient can be important depending on the number of passes. In this case, high temperature fluid enters the top section of the head side and leaves at the bottom section of the head side with a much lower temperature. As a result, the

temperature distribution in the tubesheet (Figure. 1.10) leads to thermal loading, which results in either an undesirable distortion of parts or joint loosening.

1.7 Failure mechanisms in tube to tubesheet connection

Recall from the preceding sections that the tube to tubesheet connection plays a significant role in the integrity of heat exchangers. Rigid joints are preferred because they prevent leakage from primary to secondary circuits.

Any failure in a joint may result in total plant shutdown and expensive maintenance. Therefore, periodic inspections of tube to tubesheet connections should be performed in order to detect early stage failure and conduct tube plugging or replacement.

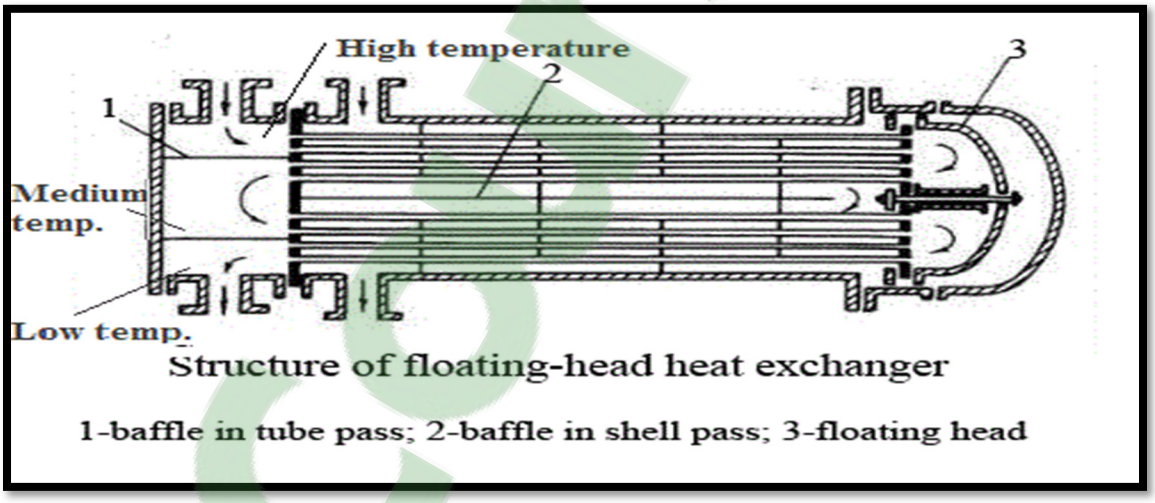

Figure 1.10 Tubesheet different thermal zones
(www.china-ogpe.com)

This connection experiences several types of failure mechanisms, which are seen in Figure 1.11 and can be described as following:

1) High residual stresses,
2) Intergranular attack (IGA),
3) Stress Corrosion Cracking (SCC),
4) Fatigue.

1.7.1 Residual stresses

Refer to 1.6.3.

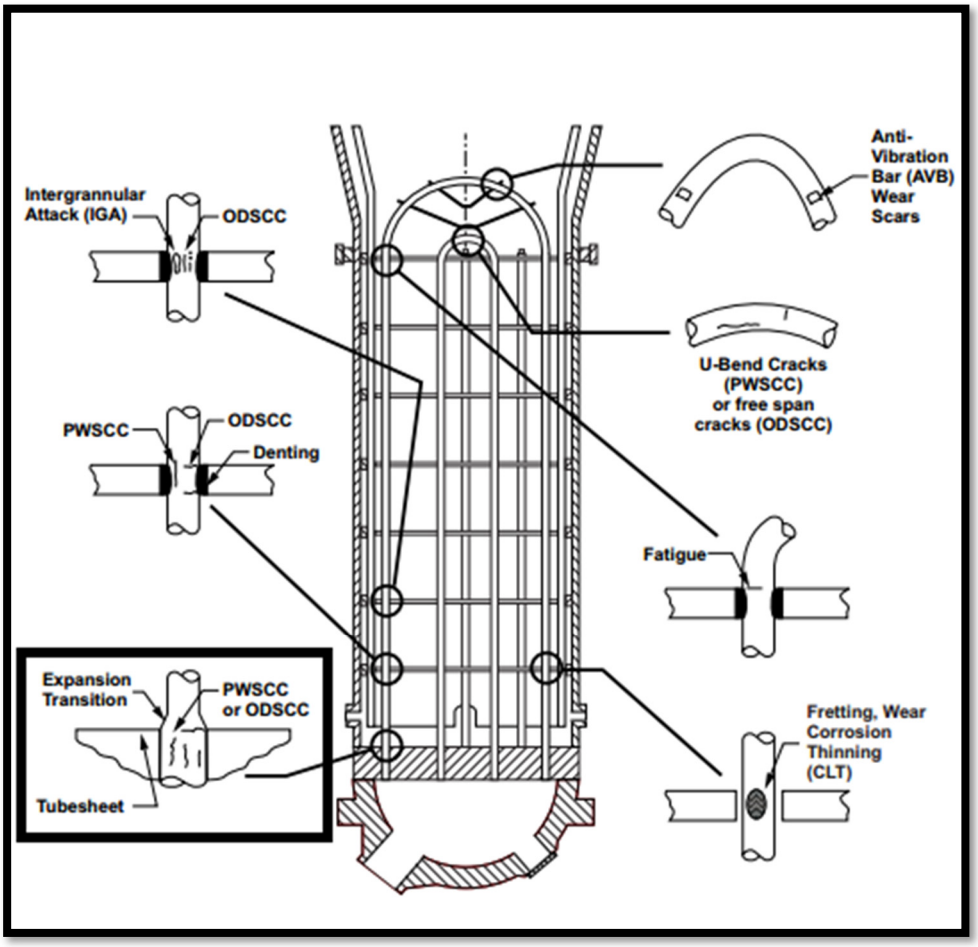

Figure 1.11 Example of degradation mechanisms of tube (www.cpuc.ca.gov)

1.7.2 Intergranular attack (IGA)

As the name of this mechanism suggests, this phenomenon takes place along the grain boundaries in the presence of tensile residual stresses, as is demonstrated in Figure 1.12. The main cause of this phenomenon is heterogeneity in local composition (impurities or precipitation), which usually appears during the heating or cooling of the process in the presence of chromium carbides and sulfur formation at the grain boundaries in Alloy 600

tubes of steam generators (Do Haeng Hur et al. 2008). Sulfur reduces the corrosion resistance of the tube material; however, the grain bulk remains initially unaffected.

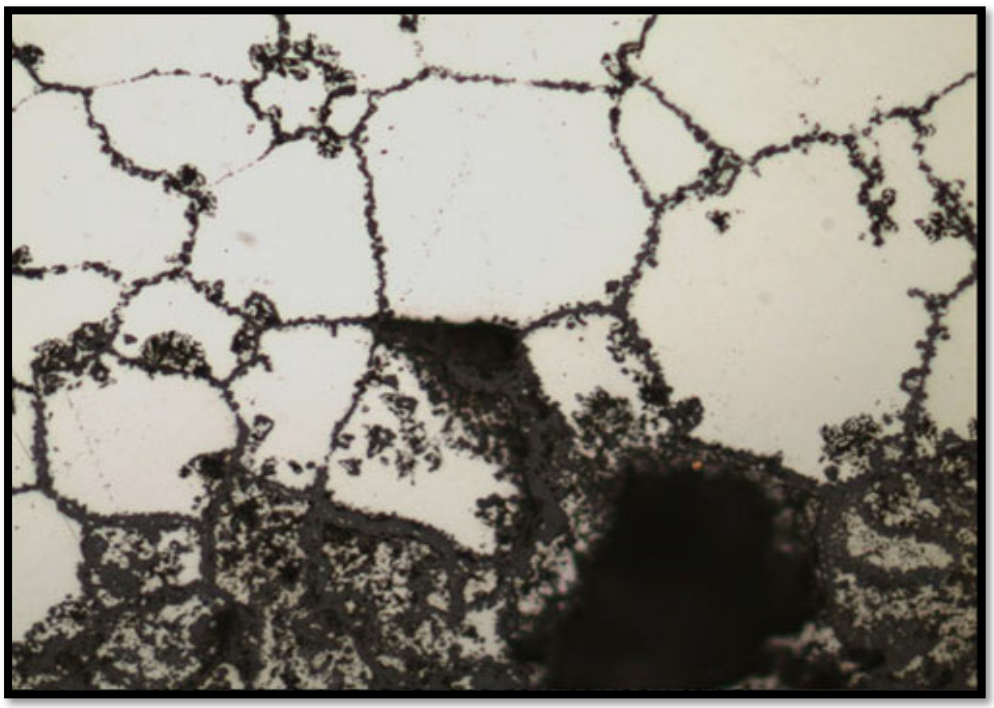

Figure 1.12 Intergranular attack at tube ID
(Photo 2MA0270, Mag: 500X, unetched)
(met-tech.com)

As a result, an intergranular attack seriously affects the mechanical properties of the material by means of full deterioration of grain boundaries. To prevent the intergranular attack, heat treatment and modifications in either the operation or manufacturing processes are proposed by Green S.J. (1986), which can be summarized as follows:

1) Heat treatment at 740°C for 15 hours for Alloy 600 to reduce the residual stresses and to minimize the intergranular attack,
2) Decrease in service temperature and removal of debris and corrosives by tube purge out or water jet washing,
3) Reduce the crevice depth exposed to the secondary circuit on the shell side by the expansion process and dispose of chemical residues, which can be concentrated at this area.

1.7.3 Stress corrosion cracking (SCC)

Stress corrosion cracking is typically produced by corrosion and the influence of tensile stresses, which can be in the form of applied or residual stresses. However, these stresses are usually much lower than the yield stress of the material. Welding, heat treatments and cold forming are examples of residual stresses built up in the material.

In addition to the intergranular paths, the cracks in SCC might progress in transgranular paths. Material, subjected loading and the type of corrosion environment would determine the crack propagation. Figure 1.11 shows several local SCC in a steam generator.

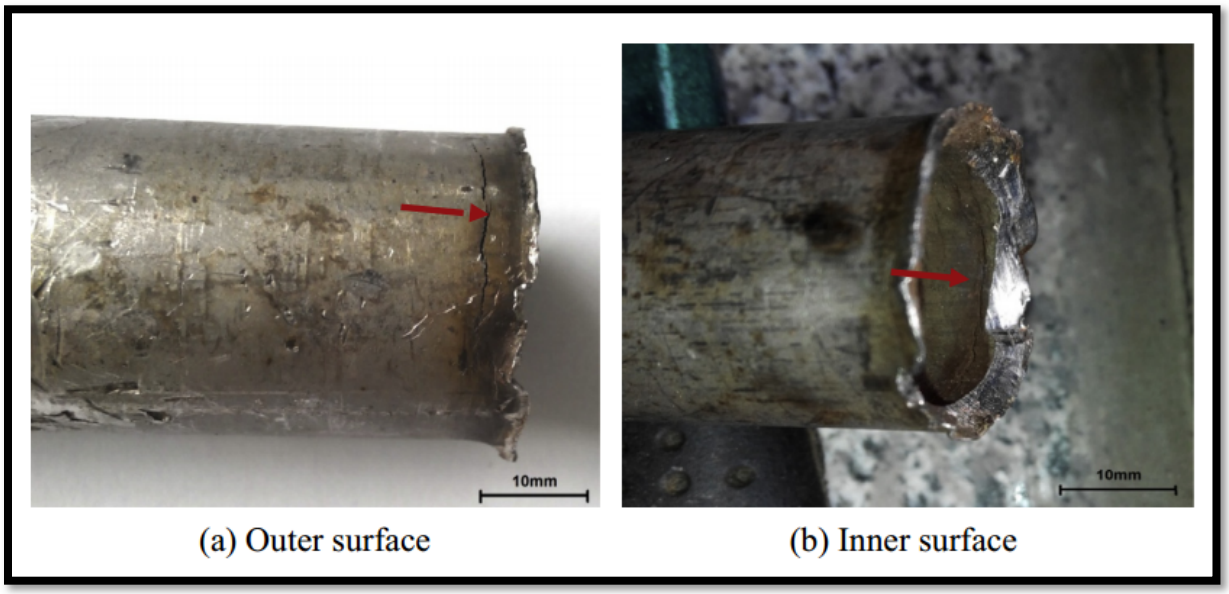

Figure 1.13 Cracks in tube in the immediate vicinity of transition zone
(Taken from Shugen Xu et al., 2015)

The crack in the tube-to-tubesheet joint could initiate at the inner or outer surface of the tube, and/ or even at the tubesheet inner bore from the shell side. These cracks are shown in Figure 1.13. As this figure demonstrates, the most susceptible area for crack initiation is the transition zone, where the tensile stresses are concentrated. The transition zone is subjected to the corrosive service of the shell side, which accelerates SCC.

In order to specify the crack type and improve the SCC behavior, metallurgical examinations and corrective interventions should be performed. Such actions must result in a reduction of tensile stresses and corrosion effects. The interventions are described as below:

1) Control the operating temperature;
2) Change the material to avoid chemical reaction to service fluid;
3) Reduce the tensile stresses by means of introducing compressive stresses;
4) Control of service loading.

1.7.4 Fatigue or cyclic stresses

The definition of fatigue by ASTM E1823-97 is: "The process of progressive localized permanent structural change occurring in a material subjected to conditions which produce fluctuating stresses and strains at some points and which may culminate in cracks or complete fracture after a sufficient number of fluctuations."

In the tube to tubesheet connection, fluctuating stresses may occur due to the mechanical or thermal loading combined with corrosion. Piping vibration and cyclic temperature are two examples of cyclic loading in heat exchangers.

Mechanical fatigue in exchangers usually takes place in stress concentrated areas, such as: tube to tubesheet assembly, baffle connection or welded joints. In fact, these areas, due to their geometry, introduce the tensile stresses, which raises the possibility of the crack propagation and reduce the effective life of the connection. Thermal loading in addition to cyclical stresses can cause crack initiation and in corrosive services results in the exposure of the tube base metal to cyclical corrosion.

The fatigue failure analysis is composed of the following stages of the so-called crack propagation approach:

1) Crack initiation or low speed crack propagation;
2) Steady-state crack growth;
3) High-speed crack propagation leading to ultimate fracture.

In this approach, the required number of cycles from initial crack length to a critical length will be computed based on Paris-Erdogan's power law, in order to obtain the safe life of parts in the presence of cracks (Fig. 1.14).

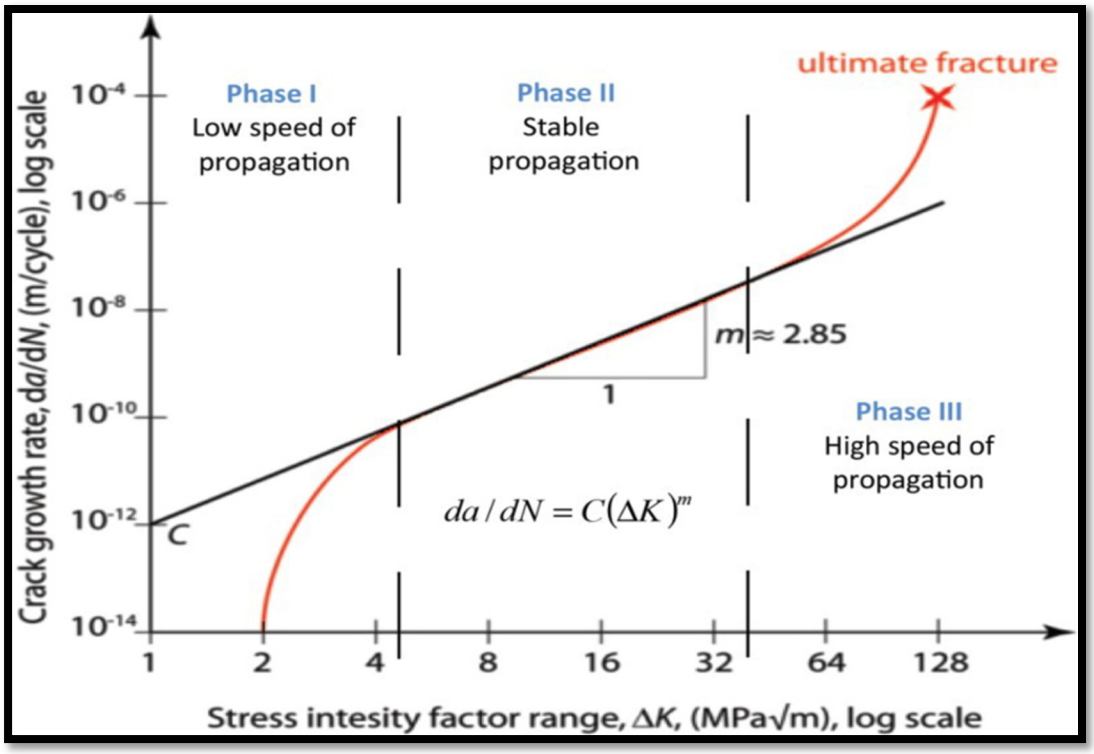

Figure 1.14 Three phases of crack growth, Paris–Erdogan's law (www.researchgate.net)

1.8 Determination of residual stresses in transition zone

Due to the complex deformation of the transition zone after the expansion process, the methods used to determine residual stresses at this zone should be meticulous. Effects of expansion pressure through loading and unloading steps must be analyzed separately to obtain the most accurate results.

In this work, analytical and Finite Element Analysis is performed to calculate the expansion process's residual stresses in the transition zone. Several formulas for different steps of loading and unloading are proposed and, finally, the results are compared to those obtained from the literature. It is worthy to note that Updike in 1988 and Allam in 1998 have undertaken investigations on the evaluation of the residual stresses at the transition zone. The former used an analytical approach based on the incremental plastic theory and FEM, while the latter's FEA results to determine these stresses at the maximum expansion pressure level have been employed, and the lack of an analytical model presenting stresses at maximum expansion pressure is felt in their studies.

1.8.1 Analytical approach

In the developed analytical model, three main theories have been applied to analyze the expansion process and residual stresses:

1) Thick cylinders,
2) Rigid-plastic cylindrical shell subjected to axial symmetric loading,
3) Beams on elastic foundation.

The thick cylinders theory is used to determine the residual stresses during the loading step by calling the equilibrium equations. In addition, it is assumed that the materials of the tube and tubesheet obey the Von Mises yield criterion of maximum distortion and the materials follow an elastic perfectly plastic behavior. The equations proposed by Laghzale and Bouzid (2009) are taken into account to determine radial displacement of the tube and tubesheet and residual contact pressure at the interface of the expanded zone. Since the tube begins deforming plastically at the junction between the expanded and transition zones, the equations of cylinders under symmetrically axial loading proposed by Sawczuk (1960) are applied to the transition zone.

Two cases, one considering the effect of reverse yielding in the expanded zone on residual stresses during the unloading, are investigated. In the first case, it is assumed that the tube expanded zone and the tubesheet suffer no reverse yielding and their spring back is purely elastic. In this case, the beam of elastic foundation theory is applied to determine the residual stresses during the unloading and, finally, to determine the ultimate residual stresses in the transition zone. In the second case, the expanded zone experiences reverse yielding during unloading, and its effect on residual stresses is studied. It is assumed that the transition zone is not subjected to reverse yielding.

1.8.2 Finite element analysis

To validate the analytical model, Finite Element Analysis using ANSYS Workbench 16.2 is used. A 3-D portion of the tube-to-tubesheet connection is modeled using geometry tools (Figure 1.15) and the static structural analysis module is used to simulate the hydraulic expansion process, including the loading and unloading steps.

In the numerical model, it is assumed that the material follows an elastic perfectly plastic behavior obtained by considering a bilinear isotropic hardening option with a small value of the tangent modulus of less than 0.01 GPa.

It is worthwhile to note that the expansion pressure is restricted to produce elastic deformation in the tubesheet. In addition, the initial clearance is large enough for the tube to go to plasticity prior to contact with the tubesheet.

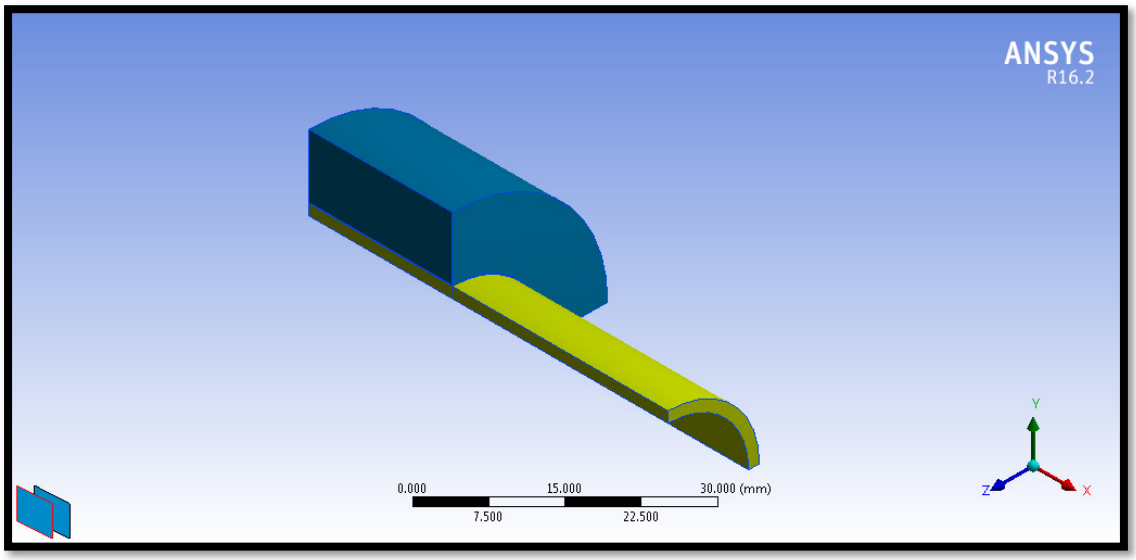

Figure 1.15 ANSYS 3D model of tube to tubesheet connection

CHAPTER 2

LITERATURE REVIEW

2.1 Introduction

Oppenheimer (1921) could be named as the first researcher who brought a published scientific contribution to the tube-to-tubesheet connection. Tube expansion has been employed since the 1840s. It wasn't until 1921 that some experiments devoted to the subject and applied by manufacturers resulted in obtaining acceptable connection rigidity. Therefore, the lack of scientific knowledge was extremely felt then. At the time, the sole process used was mechanical rolling. In 1921, Oppenheimer focused on this method by considering the required electrical power for the different steps of expansion and the effect of holding force on the ultimate rigidity of the joint.

Several research concentrating on the tube to tubesheet connection has been conducted by others since then. In fact, optimization of geometry, expansion pressure and combination of tube and tubesheet materials were the main objectives of these investigations at the time, with no attention to the operating conditions. The operation conditions, for the first time, were considered by the Japanese researcher, Toba (1966). The author undertook an experimental study on the residual stresses and stress corrosion cracking in the vicinity of the expanded joint of aluminum brass tube condensers. The study disclosed the crucial role of residual stresses in connection analysis, which can simply accelerate joint failure.

The weaknesses of the mechanical rolling process and several failures of heat exchangers have compelled researchers to focus more meticulously on the fundamentals of this process and their effects on joint tightness. As a result, Krips and Podhorsky (1976) ended studying the alternative proposed method of tube expansion, which was called hydraulic expansion, both analytically and experimentally. According to the author, the advantage of such a process rests in the accurate determination of the expansion pressure, which is achieved by the hydraulic pressure of water or other fluids.

In 1978, Wilson conducted the first finite element analysis (FEA) of a hydraulically expanded tube to tubesheet connection. In fact, FEA is a cost- and time-effective method used to evaluate the joint parameters as compared to the experimental approach.
In this chapter, an attempt is made to rigorously review the various literature written about tube-to-tubesheet joint expansion by dividing it into experimental, analytical and finite element approaches. The dominant findings of each approach will be discussed in detail in its own section.

2.2 Experimental approach

As was mentioned previously, Oppenheimer (1927) carried out the first study on the rolling of tubes into boiler plates to determine the final contact pressure at the interface after unloading. The author concluded that the holding force of shrinking is directly related to the following parameters:

1) The friction coefficient between the tube and tubesheet,
2) The thickness of the tubesheet (Figure 2.1),
3) The amount that the tubesheet bore springs back after withdrawing the expansion pressure, diminished by the amount that the tube springs back, which in turn is directly proportional to the clearance,
4) The ratio of the tube's outer radius to its wall thickness after rolling,
5) The ratio of pitch to diameter of holes after rolling,
6) Tube and tubesheet materials.

Furthermore, a couple of tests have been elaborated by placing one or several circular grooves in the surface of the tubesheet bore and forcing the tube material to thrust into these grooves. As a result, an increase of 12 times in pure contact pressure since the groove was fully filled with tube material has been observed. Nevertheless, this process requires higher rolling power and grows the strain hardening in comparison with plain rolling.
In 1935, Cassidy (1935) conducted research to investigate the effect of grooves rolling in the plate hole. The results disclosed an increase of 39% and 53% in the contact pressure of one and two grooves respectively, in contrast with the plain drilled bore.

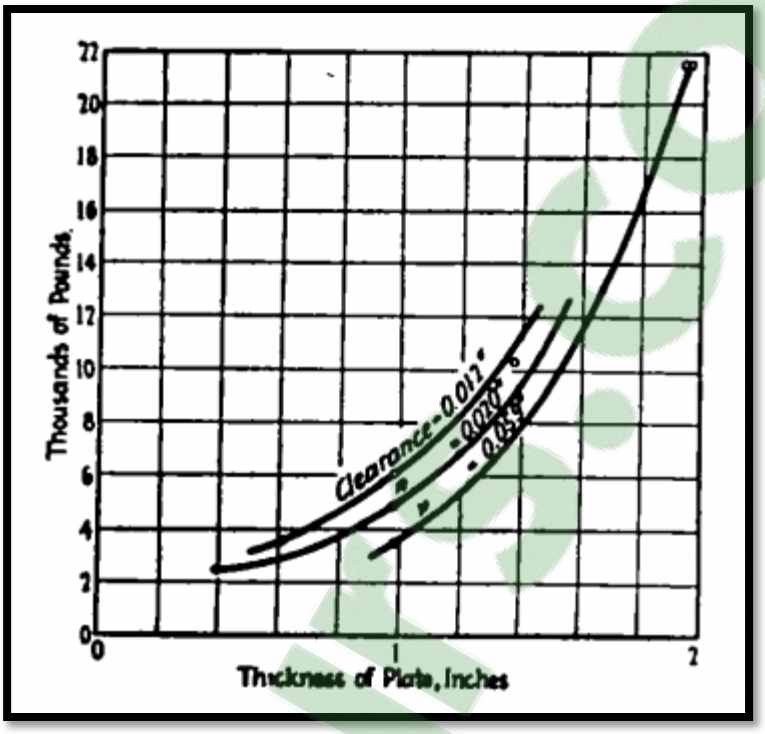

Figure 2.1 Holding force due to shrink fit alone
in relation to plate thickness
(Taken from Oppenheimer P.H. 1927)

In 1943, Grimison and Lee undertook an experimental investigation for the Babcock & Wilcox Company to determine the fundamentals of tube expansion, the optimum degree of expansion and various methods of measuring the degree of expansion. The authors concluded that, indeed, the slipping of the tube beyond the limit of expansion reduces the resistance to the extrusion and, to achieve the highest contact pressure, prevention of the tube from extrusion seems to be necessary. In addition, the results showed that the seat pressure increases with tube thickness and hardness of either the tube or tubesheet. According to the author's observations, in hard plates, pre-rolling gives the maximum seat pressure, with a smaller increase in tube inside diameter. Consequently, less cold working and tube wall thinning are required.

In the same year, Fisher and Cope (1943) proposed a new technique of tube rolling in which small tubes could be expanded automatically to produce a uniform and stable connection. By employing this method, the need for highly skilled and pre-trained operators would be diminished without sacrificing joint quality.

Again, in 1943, Maxwell suggested some modifications in tube expansion using mechanical rollers for the sake of process optimization and a tighter connection. The author recommends using tapered rolls in parallel expansion, which leads to different speeds from end to end of rolls, where it is greater at the large end than the small one. Also, he suggests that the slipping of the roll through the tube's inner surface begins at a pressure beyond the tube yield point; therefore, the friction should be reduced in order to avoid early local yield starting in the tube material and the build-up of surface irregularity in either the tube or the roll. According to the author, this process could be accomplished either by removing the irregularities and mill scales from the interface or supplying a lubricant which facilitates the roll slipping along the tube's inner surface.

Furthermore, according to the author, since in heavy tubes, differential temperature occurs during the rolling expansion, which reduces the contact pressure considerably after loading, the multi-stage method could be considered a remedy.

In 1954, Fisher and Brown conducted a comprehensive review of the tube to tubesheet connection by employing years of experience. Their study covers the majority of parameters associated with tube expansion. Some of the dominant conclusions can be summarized as follows:

1) Parallel axis rollers provide a more rigid connection than tapered rollers due to the uniform loading on the tube and tubesheet. Nevertheless, the elastic limit of the joint should be considered a turning point in order to obtain a tight connection;
2) In tube rolling, rollers with sharp ends should be replaced by rollers having a radius of 5 in. in order to avoid scratching the tube's inner surface;
3) The higher rigidity is achieved since the tube hardness is slightly less than that of the tubesheet material. In this case, a rougher finish has been proposed by authors to increase the sliding resistance of the tube at a higher pressure;
4) Rectangular grooves machined at the tubesheet bore increase the rigidity of the joint by 100% and act as reinforcement. Placing these grooves near the center reduces the potential of shearing the tube metal extruded into the grooves;
5) The clearance should be held as small as possible between 0.005 and 0.008 in. for small seamless drawn tubes. However, for large size tubes, the gap can reach 0.01 in.

In 1956, Alexander and Ford (1956) constructed an apparatus that allows the measurement of strain radially and circumferentially at selected points at the back and front of the tubesheet. The location of these strain gauges is shown in Figure 2.2.

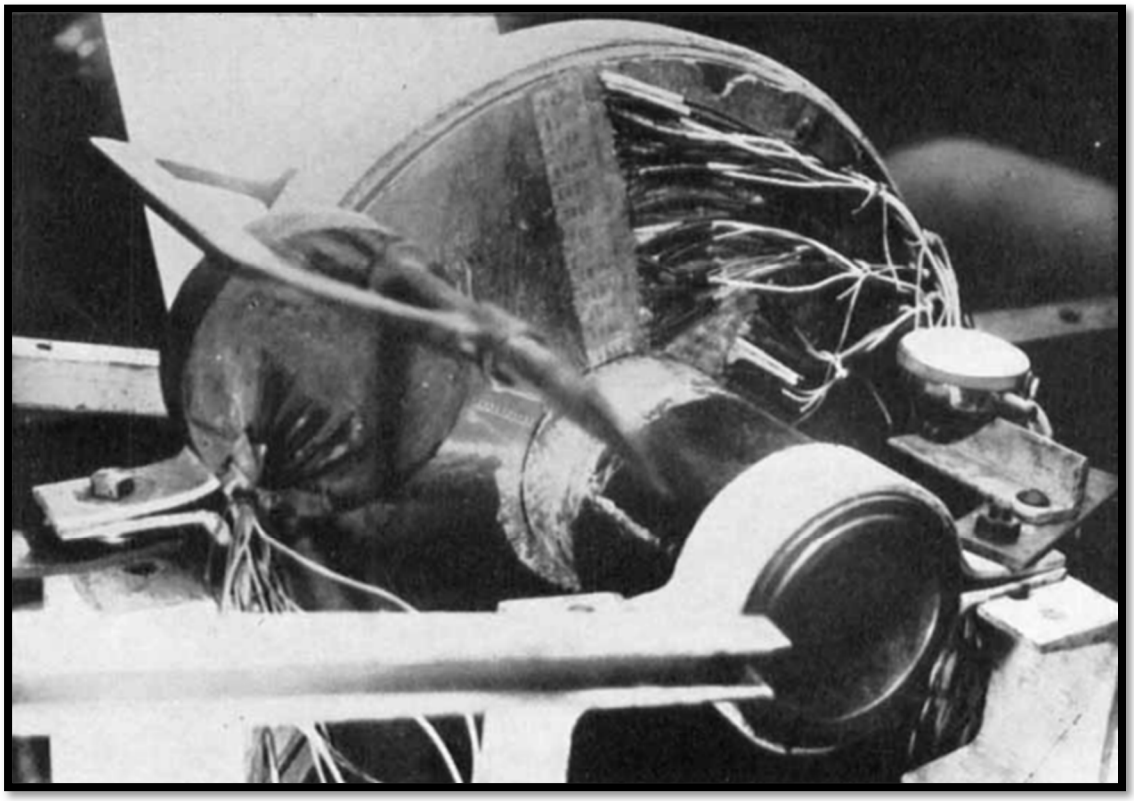

Figure 2.2 Specimen 5 (back) after expanding
(Taken from J. M. Alexander, 1956)

The detailed observation of the authors and their conclusions can be explained briefly as follows:

1) The plastic zone in the tubesheet would not pass a ratio of 2.5, which is defined by the plastic radius of the plate to the initial tube radius.
2) The elastic body of the tube at the transition zone constrains the axial extrusion of the tube at the back of the plate. As a result, the strains at the back of the plate are greater than that of the front.
3) The push-out or pull-out load is dependent upon the contact pressure and surface finish of the joint components.

4) By restricting the axial extrusion, higher circumferential strains are allowed, resulting in higher seat pressure. Such restrictions are obtained either by adding the grooves or increasing the surface roughness.
5) During unloading, tube inward radial displacement is less than that of seat, which produces the contact pressure at the interface.
6) Finally, the authors criticize the concept of parallel rolling previously mentioned by Fisher and Cope (1954) by means of showing the higher performance of a conical mandrel with three rollers, which is in agreement with the method used by Maxwell (1943).

In 1959, Culver and Ford investigated the effect of retubing, the starting position of the mandrel within the tube and initial clearance on the connection rigidity. The authors concluded that the seat pressure can reach its maximum theoretical value after retubing. In addition, an extra pass, which causes the work hardened seat, can make a stronger joint than that of the first expansion. Also, test results showed that much higher rigidity is obtained if the rollers start at certain points close to the plate back surface, because it provides expansion uniformity along the seat length. The study of the effect of initial clearance revealed that there is no significant effect of an initial gap of 0 to 0.02 in. on the joint strength.

In 1966, the Japanese researcher, Atsushi Toba, observed large tensile residual stresses on the inner surface of the transition zone of an Aluminum Brass condenser tube, which represents the main source of stress corrosion cracking in expanded tubes. The author investigated the effect of greater initial clearance on residual stresses by conducting stress corrosion cracking tests using aqueous ammonia.

In the 70's, Westinghouse proposed a new method called hydraulic expansion, which could diminish the inherent weaknesses of mechanical rolling. In this process, as long as the hydraulic pressure of liquid is employed to expand the tube, the expansion pressure and residual stresses can be precisely determined. In fact, the uniform internal pressure through the connection provided by this method reduces the irregularities at the inner surface and the risk of tube shearing.

In addition, this new process leaves a much lower level of residual stresses in the tube, which makes the tube less susceptible to stress corrosion cracking. The gap between the tube and

tubesheet is fully closed due to the consistency of the process. Likewise, the risk of leakage from shell side to the head is reduced and tube plugging is avoided. Therefore, hydraulic expansion meets higher quality and requirements, which mechanical rolling could never reach.

In 1982, Uragami compared the hybrid and hydraulic expansion processes in terms of resistance to fatigue. The tube and tubesheet materials used were Inconel 600 and SA.508, respectively. The test results showed 12 to 15 times higher fatigue resistance in hybrid expansion. Also, the author concluded that the effect of residual stresses in the tube transition zone in hybrid expansion can be ignored.

Haslinger et al. (1983) conducted several tests in order to determine the effect of cyclic loading on joint tightness once the loading exceeds the allowable stresses proposed by HEI. The effect of rolling coupling and rolling amplitude was investigated as well in the tests. The author concluded that tightness improves with higher coupling as long as the deformation is not significant. The author recommended considering rolling amplitude as an evaluator for connection quality, rather than electromotor coupling.

In the same year, Druez et al. (1983) developed an experimental technique for determining residual stress distribution through the tube thickness in straight and bent tubes by means of strain gauges after machining, after exposition to a corrosive environment. The investigation showed that axial and tangential stresses in both tubes could get as far as tube yield stress and, as a result, the residual contact pressure reduces from 30 to 50%. In addition, the test disclosed that the most critical area is found at the tube's outer surface, located at the edge of rollers.

In 1984, Scott conducted an experimental study to find a method in which the residual stresses at the transition zone are held as small as possible. In order to measure such stresses in the presence of corrosion cracking, X-ray diffraction and strain gauging techniques were employed. The test results indicated that residual stresses are notably fewer in hydraulic expansion versus mechanical rolling. However, the pull-out strength of hydraulic expansion is considerably less than tube rolling.

Furthermore, the author concluded that thermal cycling tends to weaken the joint and, to avoid this, placing the grooves in the tubesheet bore can increase the rigidity of expanded joints by 13 times.

In 1993, Flesch et al. carried out research to evaluate the operating stresses in the transition zone of 900-MWe PWR steam generator tubes and analyze the direction of cracks. In this study, residual and operating stresses have been classified as indicated in table 2.1:

Beside the experimental approach, the author ran a Finite Element Analysis in order to create a model which acts as an aging prediction tool for steam generators. The main findings of this study can be summarized as follows:

1) Circumferential cracks initiate in the central part of the tubesheet, where deposits of sludge accumulate. The presence of sludge may cause prevailing stress conditions to switch from circumferential to longitudinal.
2) The presence of sludge externally associated with the increase in tube wall temperature could result in circumferential cracks on the inner surface of the tube.
3) Circumferential cracks due to the unpredictability in terms of propagation kinetics and concept of Leak Before Risk of Break (LBRB) are more difficult to manipulate than longitudinal cracks.

Three years later, Sang (1996) conducted several tests to evaluate the reliability factors f_r presented in table A-2 of Appendix A of Section VIII, Division 1 of the boilers and pressure vessel codes (ASME, 1986). Samples were made with and without grooves on the tubesheet bores as specified in the ASME code. Figure 2.3 demonstrates the comparison between the test results and Table A-2 ASME for bared, one, two and three groove tubesheet bore.

Furthermore, the author concluded that the reliability factor is dependent on the degree of expansion, expansion length, material properties and residual interface force. Therefore, such factors should be considered for establishing allowable loads for tube to tubesheet connection.

In 1999, Reinhardt et al. performed an experimental evaluation of residual stresses in the transition zone of a hydraulically expanded tube. In this study, a mock up joint has been designed due to the fact that the tube to tubesheet connection is notably dependent upon the geometry, material properties and process of fabrication. Nevertheless, the tube was

expanded into an equivalent sleeve, and the external diameter was evaluated using a formula proposed by Chaaban et al. (1992).

Table 2.1 Origin and type of stresses in the transition zone
(Taken from B. Flesch and others, 1993)

	PERMANENT	**DUE TO THE OPERATION**

ELASTIC	• TUBE BUNDLE ASSEMBLY	• STEADY STATE OPERATION
		  • Pressures
		  • Temperatures
		  • Interaction with TPS, TS
		• OPERATING TRANSIENTS

ELASTOPLASTIC	• TUBE MANUFACTURING • TUBE ROLLING / KISS ROLLING	• OPERATING TRANSIENTS • DENTING

The study revealed that the hoop stress reaches its maximum value roughly at the middle of the transition zone. It is worthwhile to note that this location coincides with the back face of the sleeve of the tested specimen. This is near the expansion probe o-ring, where the application of the expansion pressure ends. Also, the results showed that the peak of axial stress occurs at the intersection of the transition zone with the expansion zone, where the highest bending moment would be expected.

Bazergui and Allam, in 2002, conducted research on the axial strength of hydraulically expanded tube to tubesheet joints. An experimental apparatus was designed to determine the accurate interface friction between Inconel-690 tubes and SA-508 Class 3 tubesheet steel (Figure 2.4). This study aims at reducing the discrepancy between the experimental and FE pull out test results.

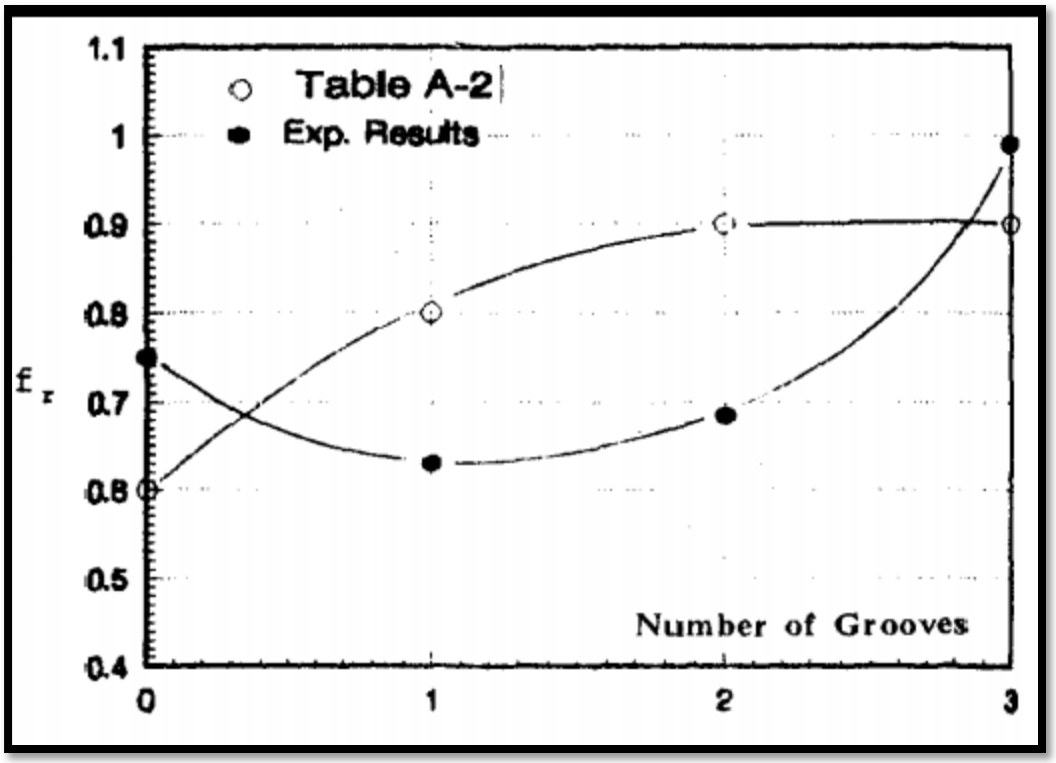

Figure 2.3 Comparison between test results and Table A-2
(Taken from J. M. Alexander 1956)

The simple study does not represent real operating conditions, since the specimens were subjected to neither in-service mechanical and/or thermal loading nor heat treatment. Nevertheless, due to the limited number of specimens, only expansion pressure and initial clearance were considered. The major conclusion of this research work is that the coefficient of friction is not significantly affected by normal interference stress. Also, for the mentioned material combination, the tangential load-displacement frictional curve is nonlinear, with a small displacement of up to 10 μm prior to the maximum resistance load occurrence.

A steam generator tubing leakage in a Korean nuclear power plant due to stress corrosion cracking occurred in 1999 and consequently resulted in a plant shutdown. Hwang et al. (2005) fostered cooperation with the US nuclear regulatory commission to conduct an experimental investigation to develop appropriate repair procedures for either tube plugging or tube sleeving. Pressure and leak tests were conducted at the ambient and PWR operating temperature of 282°C. The authors concluded that, in all specimens, the crack propagated fully through the thickness of a tube under a pressure of 20.7 MPa, but no water leakage was

reported. In addition, the reported length of the tube's outside crack was 17 times longer than that of the tube's inside.

During the same year, Wang et al. (2005) carried out an investigation which was focused on the effect of the geometry of grooves on the strength of hydraulically expanded tube-to-tubesheet joints. Several specimens with different groove width, depth, spacing and location were tested. In all cases, one groove had been placed in the tubesheet bore, except for the investigation of spacing effect, where two grooves with an interval of 6mm were located symmetrically about the center plane of the tubesheet thickness. The pull out force was the main strength criteria measured by a MTS 880 testing machine. Results disclosed that groove width has a dominant effect on connection rigidity and groove depth; spacing and location should be given lower credit.

2.2.1 Comments and conclusion

- The very first investigations of tube to tubesheet joints were focused on optimum geometrical design and degree of expansion. Adding grooves, reducing the initial clearance and changing the length and type of rolls projected into the tube were in the area of interests. Also, surface finish effect and restraining the tube axial extrusion through the tubesheet hole were significantly notable.
- Tube roller expansion with the same length as the tubesheet thickness builds up a uniform and stable joint along the seat, which reduces the risk of stress corrosion cracking from the secondary side.
- The effect of residual stresses and stress corrosion cracking in tube transition zone came into consideration for the first time in 1966 by Toba. His study disclosed the effect of operative factors which could notably affect the effective life of the joint and, consequently, the equipment. In addition, results showed that due to their higher residual stresses, transition zones deserve closer attention in the analysis of the joint.

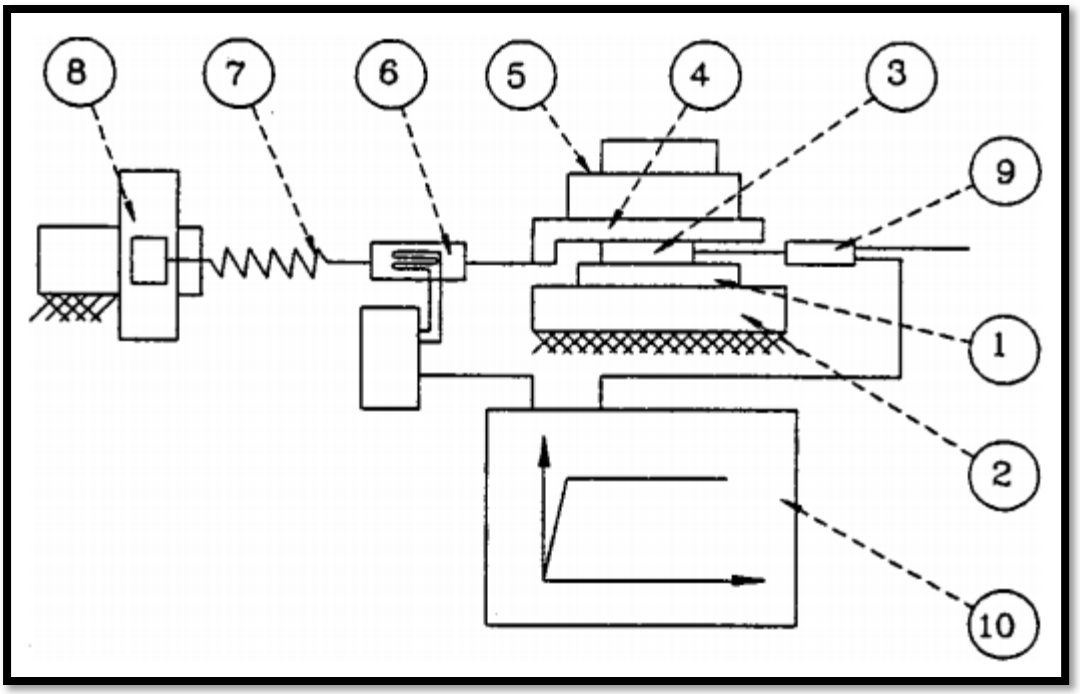

Figure 2.4 Experimental friction test set-up, 1) two tube specimens, 2) apparatus support, 3) two tubesheet specimens, 4) movable frame, 5) known weight, 6) load gauging cell, 7) linear spring, 8) 3D arm, 9) displacement transducer, 10) X-Y plotter
(Taken from A. Bazergui and others 2002)

2.3 Analytical approach

In 1929, Jantscha conducted the first analytical study of the tube to tubesheet joint, which consists of an elasto-plastic expansion behavior of materials.

In 1943, Goodier and Schoessow presented a theoretical method to determine the frictional holding power (pull out and push out forces) at the common surface.

$$P_{pull-out} = p_c \frac{2\pi R_i}{r_i}\left(1 - e^{-r_i f l}\right) \tag{2.1}$$

$$P_{push-out} = p_c \frac{2\pi R_i}{\beta}\left(e^{\beta f l} - 1\right) \tag{2.2}$$

Where β is:

$$\beta = \frac{\nu\left(R_o^2 - R_i^2\right)}{R_i(R_o^2 - r_i^2)}$$

In fact, their study was used to compare the results with experimental data in order to develop an analytical model capable of predicting the residual contact pressure in the mechanical rolling process.

Later, in 1947, Sachs carried out a theoretical evaluation of the condition in which the maximum tightness of connection is achieved. The expansion pressure is assumed to be uniform and the average flow resistance of materials is 1.1 times of yield stress. In this work, various combinations of materials have been studied, and the conclusion is briefly discussed below:

1) If the tube and tubesheet are made of the same material, maximum tightness is obtained once the ratio of the outside to inside diameter of the tube increases to 1.4.
2) If the tube material is harder, this ratio should be increased to 1.65 to accomplish highest tightness.
3) Finally, once the yield strength of the tube is two times greater than that of the tubesheet, the contact pressure reaches its maximum value. However, this statement does not agree with recent studies and findings, where other researchers would recommend harder tubesheet material.

In 1963, Denton and Alexander developed an experimental technique to evaluate the axial and circumferential residual stresses in the tube. The method is based on the removal of the material layer containing residual stress while measuring the change of tube diameter. This method is known as “bending deflection.” Finally, the authors examined the technique previously proposed by Davidenkov et al. to measure residual stresses and demonstrated that, under certain circumstances, their method is inaccurate.

In 1976, Krips and Podhorsky proposed a plane stress model based on autofrettaged thick cylinder theory with an elastic perfectly plastic material using Tresca yield criteria to calculate the residual contact pressure after loading and given by:

$$P_c = \frac{1}{K}(P_{em} - P_{e-min}) \tag{2.3}$$

$$\frac{P_{min}}{S_{yt}} = 2\left[\frac{E_s}{E_t}\right]\left[\frac{1}{1+2\overline{c}}\right]\frac{(Y_s^2-1)\ln(Y_t)}{(Y_t^2-1)(1-\nu+(1+\nu)Y_s^2)} + \ln Y_t \tag{2.4}$$

$$K = 1 + \frac{E_s}{E_t}\left[\frac{1}{1+2\overline{c}}\right]\left[\frac{Y_s^2-1}{Y_t^2-1}\right]\left[\frac{(1-\nu)Y_t^2+1+\nu}{1-\nu+(1+\nu)Y_s^2}\right] \tag{2.5}$$

Where P_c, P_{em}, $P_{e\text{-}min}$ and K represent contact pressure, maximum expansion pressure, the expansion pressure which leaves zero contact pressure and the constant based on geometry and material properties respectively. In fact, as shown above, the uniform expansion pressure can be taken into account as a measurable internal pressure, which guarantees the accuracy of calculations. Unfortunately, the compatibility of displacement during unloading is violated, which leads to big differences in most of the cases studied.

In 1988, Updike and Kalnins developed a theoretical model to determine residual stresses in the transition zone. This method is mainly a combination of a numerical and an analytical approach based on the incremental plasticity theory, which uses stored results in the KSHEL-PL program database to determine the expansion pressure and the residual stresses in the transition zone. The study indicated that both axial and hoop stresses on the tube's inner surface may be tensile and can reach up to 90% of tube yield stress. This method considers an elastic recovery when the pressure is released, based on the theory of beams on elastic foundation considering concentrated force and moment at the junction of the shell and tubesheet such that the unloading longitudinal and hoop stresses are obtained as follows:

$$\frac{\sigma_x}{S_{yt}} = \pm 1.816\left(\frac{E_t w}{S_{yt} r_m}\right)e^{-\beta x}(\cos\beta x - \sin\beta x) \tag{2.6}$$

$$\frac{\sigma_\theta}{S_{yt}} = 0.3\frac{\sigma_x}{S_{yt}} + \left(\frac{E_t w}{S_{yt} r_m}\right)e^{-\beta x}(\cos\beta x + \sin\beta x) \tag{2.7}$$

Where $\nu_t = 0.3$ and $\beta = 1.285/\sqrt{r_m t_t}$.

A year later, again, Updike and Kalnins (1989) carried out an analytical investigation by means of a theoretical model, which had been previously introduced by the same authors, to

demonstrate the effect of initial gap, reverse yielding and strain hardening of tube and tubesheet materials on the residual stresses on the inner surface of the tube transition zone. The authors concluded that, for the majority of tested cases, the maximum residual stresses are between 85 and 90% of the tube yield stress, except in the case of a loosely fitted tube, where the value of such stresses is above the yield stress.

In 1995, Allam et al. proposed an analytical solution to investigate the level of expansion to be applied to accomplish an optimum residual contact pressure between the tube and tubesheet based on the Krips and Podhorsky model. A finite element analysis was conducted to validate the results of the analytical model. The authors introduced two factors $\alpha = 1.15$ and $\beta = 0.85$ to correct for the Tresca and the violation of the compatibility during unloading in the equation (2.3):

$$P_c = \frac{\alpha}{K}(P_{em} - \beta P_{e-min}) \tag{2.8}$$

Furthermore, the authors concluded that a tighter joint is reached since the inner surface of the tubesheet goes under plastic deformation. Nevertheless, further expansion beyond 25% of tubesheet plastic deformation does not produce any significant increase in residual contact pressure.

In the same year, Kohlpaintner (1995) presented an elasto-plastic computational method to determine the residual contact pressure. A plane stress model that accounts for both the effect of different materials and elastic-plastic tubesheet deformation was analyzed, and conclusions were summarized as follows:

1) Tube material with low yield strength produces a higher contact pressure.
2) Better spring back is reached once Young's modulus of the tube is greater than that of the tubesheet.
3) Joint efficiency is highly dependent upon the initial clearance.

In 1998, M. Allam et al. developed a methodology based on a detailed parametric analysis using a finite element model to account for the effect of strain hardening of the tube material in the evaluation of the residual contact pressure. The authors introduced a correction factor "f" given by:

$$f = A + B\left(\frac{c}{2r_0}\right)\left(\frac{E_{tt}}{E_t}\right) + C\left(\frac{E_{tt}}{E_t}\right) \tag{2.9}$$

Where: $A = 0.91745,\ B = -5559, C = -1.48397.$

In the same year, Allam et al. (1998) presented a simplified theoretical model to determine maximum residual stresses introduced in the transition zone of an expanded tube to tubesheet joint. A standard deviation analysis was used to determine the tensile residual stresses and their axial locations. A finite element analysis was conducted to validate the proposed analytical model.

Finally, the authors concluded that the axial residual stress reaches approximately 86 to 109% of tube yield stress, and its location is almost at the end of the transition zone. For the hoop residual stress, its maximum value reaches 55 to 68% of tube yield stress at the beginning of the transition zone.

In 2009, Laghzale and Bouzid developed a new analytical model to predict the residual contact pressure of a hydraulically expanded joint. The tube and tubesheet follow the elastic perfectly plastic material behavior and obey Tresca's yield criterion. Three cases have been studied:

1) Expansion without tubesheet plastic deformation;
2) Expansion with elasto-plastic deformation of tubesheet;
3) Unloading phase with tube reverse yielding.

The authors proposed a new expression of the contact pressure in the case of tube reverse yielding and give the expansion pressure P_{ry} at which reverse yielding starts:

$$P_{ry} = P_{em} - \left(P_{em} - 2S_{yt}\right)\lambda \tag{2.10}$$

$$\lambda = \frac{(Y_t^2 - 1)}{\frac{4Y_t^2}{\frac{Y_t^2+1}{Y_t^2-1} - \nu_t + \frac{E_t}{E_s}\left(\frac{Y_s^2+1}{Y_s^2-1} + \nu_s\right)}} - (Y_t^4 - 1)$$

$$P_c = \frac{\left(\frac{E_t}{E_s}\left(\frac{Y_s^2+1}{Y_s^2-1}+\nu_s\right)+\frac{Y_t^2+1}{Y_t^2-1}-\nu_t\right)P_{cm}+\frac{2P'}{Y_{ry}^2-1}-\frac{2P_{em}}{Y_t^2-1}}{\left[\frac{Y_{ry}^2+1}{Y_{ry}^2-1}-\nu_t+\frac{E_t}{E_s}\left(\frac{Y_s^2+1}{Y_s^2-1}+\nu_s\right)\right]} \quad (2.11)$$

Where P' and Y_{ry} represent the tube autofrettaged pressure and the ratio of outer diameter to plastic diameter during reverse yielding, respectively. The authors analyzed the effect of initial clearance, material strain hardening and creep on the residual contact pressure. The results demonstrated a significant effect of the initial gap on the connection rigidity. However, it is worthy to note that, according to the authors, the tubesheet strain hardening has low or no effect on the contact pressure. In addition, it was concluded that creep causes a reduction of 16.5% and 84.6% with respect to the initial residual contact pressure only a few hours after load withdrawal.

Two years later, Huang and Xie (2011) introduced an analytical model based on kinematic hardening, which incorporates Von-Mises yield criterion, incompressible material and plane strain assumption. The strain hardening of both the tube and tubesheet were taken into account. According to the author, the developed model is able to analyze the effect of material strain hardening, initial clearance, Young's modulus, Poisson ratio, etc.

In 2015, Bouzid and Kazeminia conducted an analytical study to investigate the effect of reverse yielding on the contact pressure of hydraulically expanded tube-to-tubesheet joints. The model is based on the Henckey deformation theory and the Von-Mises yield criterion. Results disclosed that reverse yielding, which is present during unloading, makes the joint less rigid by reducing the residual contact pressure depending upon material properties and initial clearance. Ignoring reverse yielding may result in a 100% overestimation of the contact pressure.

2.3.1 Comments and conclusion

- All analytical models devoted to the mechanical rolling process were assumed to be expanded by a uniform internal pressure as a simplification. However, this assumption ignores several fundamentals of tube rolling. In addition, except recent research, it is assumed that the unloading is purely elastic, with no reverse yielding.

- No analytical model has been proposed to predict residual stresses in the transition zone of the expanded tube. In fact, Updike et al. (1972) developed a numerical program based on the incremental theory of plasticity without giving the detailed equations, and Allam et al. (1998) and other researchers applied the FEM to determine residual stresses.
- Numerical studies revealed that maximum axial and hoop stresses take place at the inner surface of the tube in the transition zone. It is worthwhile to note that axial stresses can exceed tube yield stress.
- Initial clearance possesses a significant effect on residual contact pressure due to the strain hardening of the tube material. However, tubesheet strain hardening could be ignored in the stress analysis of the tube to tubesheet joint.
- Any increase in expansion pressure produces a notable increase in residual contact pressure, up to the point where 25% of the tubesheet goes under plastic deformation. Beyond this point, no significant increase in contact pressure is obtained.

2.4 Finite element (numerical) approach

As is mentioned in the foregoing, one of the first finite element analyses of the tube to tubesheet connection was conducted by Wilson in 1978. The objective of his study was to determine the residual stresses and radial displacement of the tube during expansion at the transition zone, and to evaluate the results in the context of actual operating conditions with attention to stress corrosion cracking. An idealized tube rolling model subjected to uniform internal pressure has been employed, and its length was equal to the tubesheet thickness. An axisymmetric isoparametric quadrilateral element was used to model both the tube and the tubesheet. The ratio of the tubesheet's outer diameter to the tube's inner diameter was three.
The results indicated a slight increase in radial residual stresses, which leads to higher rigidity of the joint as the expansion pressure is increased. In addition, the results disclosed the effect of the coefficient of thermal expansion and yield point on the distribution of residual stresses. Finally, the authors proposed an extension of the pressure or expansion zone beyond the tubesheet thickness in order to complete the closure of the crevice by applying a lower expansion pressure.

In 1983, Kasriae B. et al. performed an Elastic-Plastic finite element analysis to establish conditions in which the tube is rolled into the tubesheet with low ligament efficiency. A triangular tube pattern was designed, and the expansion sequence effect of tubes is considered as well. The analyzed model defines a tube wall thinning of 2 to 3% in order to obtain a reliable connection.

Furthermore, the author concluded that the joint efficiency decreases by making use of low ligament efficiency and higher yield strength of the tube rather than the tubesheet material. In fact, once the tube is more rigid, the joint tends to loosen during unloading due to the decrease in residual contact pressure.

Ramuet al. (1987) developed a finite element model to investigate the distribution of residual stresses in rolled joints used in the nuclear industry. An axisymmetric pattern of tube and tubesheet with uniform expansion pressure was modeled. The final results included just the deformation of the tube, and no more details were published by the authors.

One year later, Wang and Soler (1988) conducted a numerical study of the tube to tubesheet connection by finite element to highlight the effect of adjacent holes for various geometries in order to determine the upper limit of the expansion of adjacent tubes. The finite element model was under a plane stress state with seven tubes. Finally, the residual contact pressures were compared to those presented by Soler in 1984 and 1985 in order to determine the equivalent tubesheet diameter that gives the same results.

In 1984, Scot et al. performed a finite element analysis using a MARC general purpose program to determine residual stresses in the transition zone. The model was assumed to be a static non-linear elastic-plastic problem by creating a circular axisymmetric steel sleeve around a single tube. The study showed that the hydraulically expanded connection is weakened by thermal loading, but still has a 15 times stronger performance at reactor operating temperature than at room temperature.

In 1989, Chaaban et al. carried out a finite element analysis to reach an optimum design at which the maximum contact pressure is obtained while the residual stresses in the transition zone would be as low as possible. Ligament thickness, strain hardening of the material, initial gap, expansion sequence of tubes and the level of applied expansion pressure were studied in order to investigate their effects on residual interface pressure.

The model consisting of a single tube surrounded by an annular sleeve was used in most cases except for expansion sequence analysis, where a seven-tube plane stress model was preferred. Isoparametric-axisymmetric 8-noded elements (CAX8) for the single tube model and isoparametric 8-noded plain stress elements (CPS8) for the seven-tube model were used to perform the elastic perfectly plastic analysis. The authors concluded that the single tube model overestimates the residual contact pressure in comparison with the seven-tube model. Furthermore, the results indicated that there is a small effect of material strain hardening and ligament thickness on the residual contact pressure.

Again, in 1992, Chaaban and others proposed an empirical equation to determine the equivalent external sleeve diameter, which can be employed in the single tube model to determine the contact pressure of a tube-to-tubesheet connection.

In 1993, Middlebrooks et al., with the companionship of the steam generator services engineering of Westinghouse Electrical Corporation, presented results of two different finite element codes to calculate the residual stresses and strains in the hydraulic expansion of tube-to-tubesheet joints. The Westinghouse WECAN finite element computer code was employed using the Von Mises yield criterion and the Prandtl-Reuss flow rule to obtain results for both plain-stress and plain-strain conditions. Finally, the authors concluded that hydraulic expansion causes a 1.5% tube wall thinning and a 0.9% tube length shrinking.

In the same year, Huang (1993) simulated two finite element models of triangular and square tube patterns by applying the plane stress analysis. The objective of his study was to evaluate the residual contact pressure in two patterns, and final results showed a 100% higher contact pressure in the triangular pattern, in comparison with the square design.

In 1995, Metzeger (1995) developed a numerical model to simulate the mechanical rolling process in steam generator tubes surrounded by a triangular hole pattern tubesheet. Several techniques were used to model the geometry, and the process is below:

1) 3D finite deformation element,
2) Sliding contact surfaces with friction,
3) Kinematic hardening of roller motion,
4) General periodic symmetry.

The final model consisted of 19796 nodes and 12864 three dimensional isoparametric continuum elements and four geometric configurations were considered. The results showed clearly that the use of axisymmetric design is inaccurate for the tube rolling model.

Later in the same year, Kohlpaintner (1995) conducted a finite element analysis of hydraulically expanded tube to tubesheet joints in order to compare with analytical results. Two tube-to-tubesheet connections with identical material properties but different geometries were studied. A finite disk with 19 holes was designed with an equivalent diameter. As can be seen in figure 2.5, the analytical results are in a good agreement with the numerical ones.

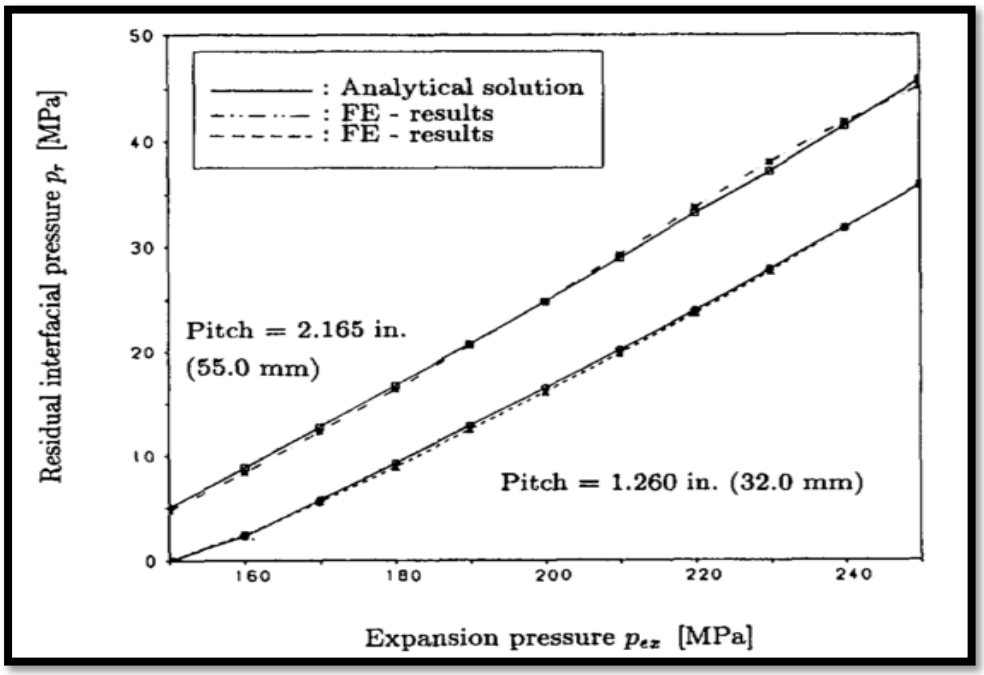

Figure 2.5 Comparison of numerical and analytical data
(Taken from W. R. Kohlpaintner, 1995)

In 1998, Allam et al. used the finite element method to investigate the effect of strain hardening of the tube material on contact pressure and maximum tensile residual stresses in hydraulically expanded tube-to-tubesheet joints. The joint was modeled by means of 2-D axisymmetric 8-noded quadrilateral isoparametric elements. An arbitrary coefficient of friction of 0.35 using Coulomb's friction law was considered. The finite element results demonstrated that the connection geometry and material properties have a significant effect on the contact pressure, but have less importance on maximum tensile residual stresses

normalized by tube yield stress. Also, the effect of the initial clearance is more significant with a strain hardening material than elastic perfectly plastic material behavior.

In 2001, Kyu et al. simulated a corrosion crack inside a steam generator rolled tube by using ANSYS (V 5.3). It was assumed that this semi-elliptical surface crack is located at the point where the residual stresses reach their maximum value. In addition, a crack growth equation based on stress intensity factor, formerly proposed by Scott (1991), was employed. A schematic diagram of the model is shown in figure 2.6.

Several cases of measured residual stress distributions were simulated, and it was concluded that:

1) Any increase in crack length under residual stresses will develop the growth rate of the crack depth; however, it reduces the growth rate of the crack length.
2) According to the variation curve of the crack aspect ratio, a constant crack aspect ratio during the initial crack growth stage had occurred.
3) The required time for the simulated crack to pass through the entire wall was estimated from 2.2 to 5 years and this range is highly dependent upon the residual stresses.

In 2002, a finite element model was proposed by Allam et al. (2002) to determine the axial strength of the tube to tubesheet connection. Two finite element designs, 3D and axisymmetric based meshes, were modeled using ABAQUS FE code. A 19-hole tubesheet previously presented by Kohlpaintner (1995) was simulated in 3D design. In the axisymmetric model, an equivalent single tube made up of 2D axisymmetric 8-noded quadrilateral isoparametric elements was designed.

Rigid body motion of the tube in the axial direction was considered as an upper limit for the expansion. At the last increment step of loading, the shearing and traction at the interface were examined, and a comparison between the results of the 3D and axisymmetric models indicated a good agreement in predicting the joint axial strength.

In 2003, Merah et al. conducted a finite element evaluation of the effect of initial clearance on the contact pressure and tube wall thinning. In fact, the study was performed to complement an experimental investigation on the effect of over-tolerance in connection rigidity.

The tubesheet material was carbon steel SA-516 G.70 (σ_{ys}= 261 MPa) and standard tubes of ¾ in. were expanded to plate bores (Figure 2.7). All nine tubes were cut from seamless cold-drawn low carbon steel tubes SA-179 (σ_{ys}= 248 MPa).

Furthermore, a single-hole planar design was developed using the same dimensions to analyze both the plain stress and plain strain conditions, and the results can be summarized as follows:

1) For high strain hardening materials, the residual contact pressure is highly affected by initial clearance. However, there is no practical effect of initial clearance on the contact pressure for low strain hardening material.
2) A reduction factor accounting for initial clearance and strain hardening behavior in available solutions of residual contact pressure was proposed by the numerical model.
3) Tube wall reduction increases linearly with increasing initial clearance and tube strain hardening.

In 2004, Xiaotian and Shuyan (2004) conducted a finite element analysis in order to determine the distribution of thermal and mechanical stresses in a steam generator erected in a 10MW nuclear plant. It was assumed that the generator had been started up after a few hours of casual shut down and, consequently, temperatures in two circuits were 430°C and 100° C respectively. This high range of temperature gradient provokes thermal stresses, which led to generator degradation. 12Mo Cr V material was taken into account for the tube and tubesheet. This study disclosed the effect of a high level of thermal stresses on joint failure by provoking local cracks.

In 2005, Wang and Sang simulated a non-linear finite element method based on a 2D axisymmetric model of a hydraulically expanded tube-to-tubesheet joint in order to analyze the effect of the geometry of grooves on the connection strength. This model enabled the authors to determine the residual stresses and deformations at the interface.

Two different models with one and two grooves located on the inner surface of the tubesheet have been analyzed, and the equivalent sleeve diameter previously developed by Chaaban (1992) and Kohlpaintner (1995), was used. The results indicated a good agreement with experiments in disclosing the significant effect of groove width.

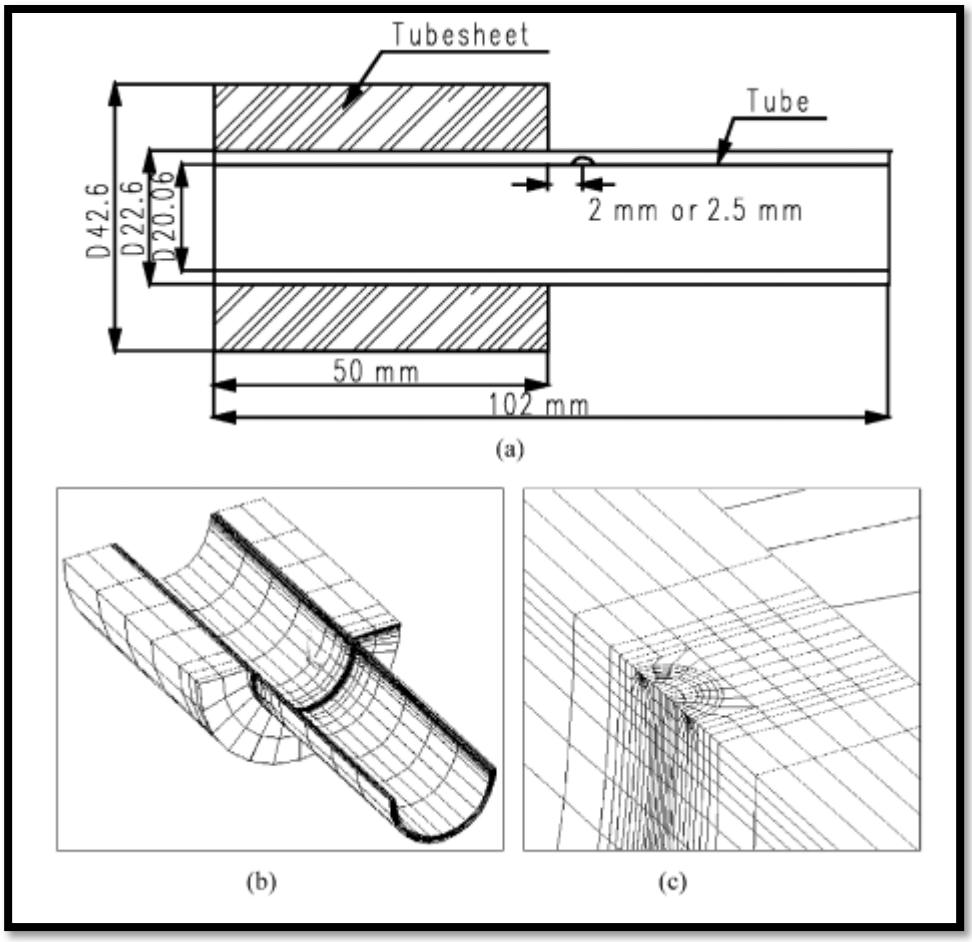

Figure 2.6 Schematic diagram and finite element mesh configurations of a tube with an inner surface crack: (a) a schematic diagram of a S/G tube; (b) global mesh of a tube; (c) detail mesh near the crack. (Taken from Kyu I. S. and others, 2001)

In 2009, Laghzale and Bouzid validated the results of a developed analytical model based on bilinear isotropic material behavior in comparison with plain strain finite element modeling. Two cases corresponding to elastic and partial plastic deformation of the tubesheet were considered, while tube reverse yielding during unloading was ignored.

Due to the symmetry of geometry and loading, a 90-degree portion of the joint was modeled for simplicity. The friction at the interface was not considered, because a previous study by Merah et al. (2003) showed a negligible effect on the residual contact pressure. Finally, the comparison of the two approaches showed that the proposed analytical model is able to tackle a parametric study quickly.

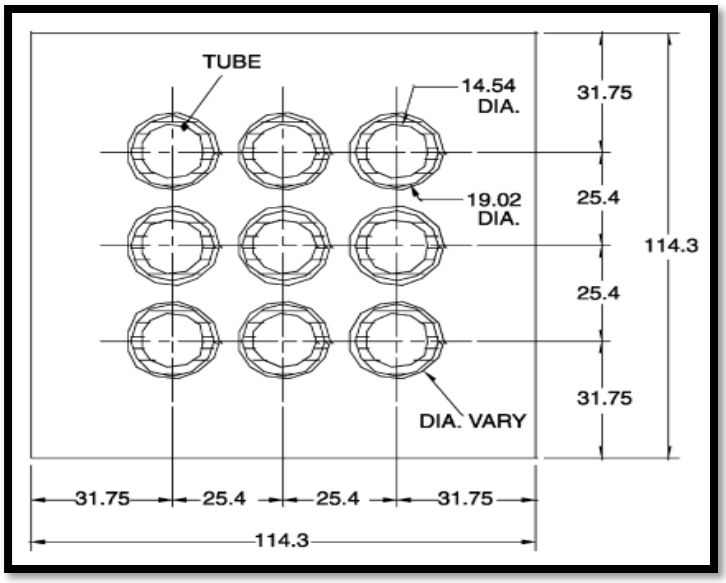

Figure 2.7 Model geometry and dimensions in mm
(Taken from N. Merah and others, 2003)

One year later, Al-Aboodi et al. (2010) used an axisymmetric finite element model to evaluate the combined effects of friction, initial clearance and material strain hardening on the joint strength of rolling expansion. 2-D VISCO108, CONTA 172 and TARGE169 elements were employed to simulate nonlinearities under ANSYS modeling. Also, the elastic perfectly plastic behavior of material was defined by bilinear curves having a tangent modulus equal to 733 MPa. Nevertheless, the study investigated the strain hardening effect of the material by varying the tangent modulus from 0 to 1.2 GPa to cover most steel materials of tubes and tubesheets.

The results of the FE model revealed that the introduction of friction at the interface results in higher residual interfacial stress and lower critical clearance, due to the higher axial stresses restraining the tube from expanding in the longitudinal direction.

In 2011, Shuaib et al. studied the effect of large initial clearance and grooves on the radial deformation and residual stresses in the expansion and transition zones by employing a 2D nonlinear axisymmetric finite element model. In order to model a loose joint, an over-enlarged tubesheet bore with over tolerances which exceeds the values prescribed by TEMA, were used (Figure 2.8).

A tube wall reduction of 5% was taken into account, as the upper limit of loading and an elastic perfectly plastic material behavior was assumed. Several parameters have been covered, and conclusions were drawn as below:

1) The coefficient of friction has a considerable effect to determine the maximum level of initial clearance beyond the point where contact pressure begins to reduce.
2) A 15% increase in residual contact pressure is attainable by locating the grooves in the tubesheet hole.
3) A difference of 25% to 70% in residual stresses between the inner and outer surfaces of the tube in the transition zone would make the outer surface less prone to stress corrosion cracking.
4) Joints with grooves develop slight tensile residual axial stress in the grooved area, but no residual stresses of importance are found at the inner surface of the tube in this area.

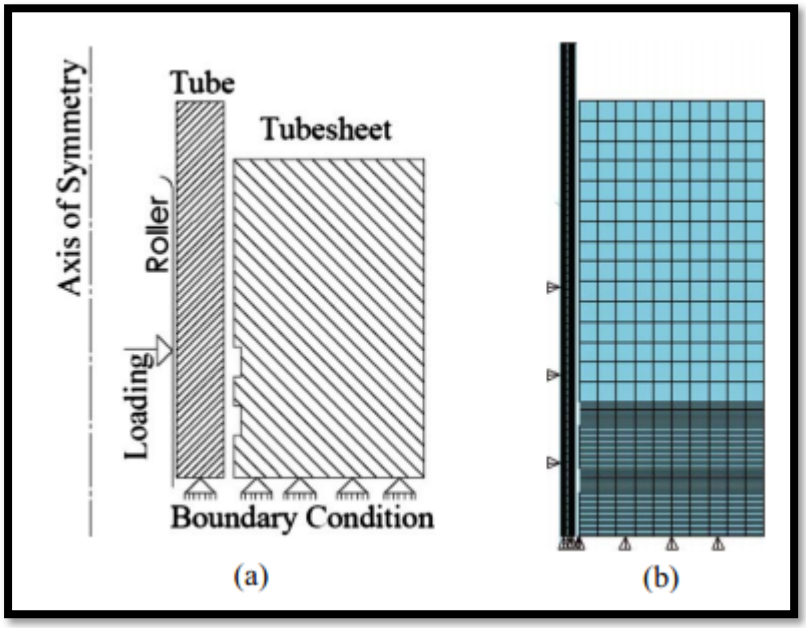

Figure 2.8 a) Equivalent sleeve joint model and
b) FE mesh for the grooved joint
(Taken from A. N. Shuaib and others 2011)

2.4.1 Finite element (numerical) approach

- Recent studies demonstrated the acceptable performance of axisymmetric design for the hydraulic expansion of tubes. This is why, in this process, the applied internal pressure is assumed to create a uniform outward radial displacement over most of the expanded zone. Nevertheless, the fundamental of the rolling process together with the 3D finite element results show that a correction factor is required if axisymmetric modeling is used.
- Various nonlinearities should be considered in tube to tubesheet joint analysis:
    1) Tube and tubesheet plastic deformations,
    2) Elasto-plastic material behavior,
    3) Contact at the interface.
- In elastic perfectly plastic analysis, tangent modulus E_{tt} and E_{ts} are required, but should be kept as small as possible to avoid singularity.

2.5 Objective of the research work

In this work, in order to analyze residual stresses in the transition zone of the tube, an analytical model to predict these stresses will be developed. In the best interest of the analysis, the two steps of loading and unloading will be considered separately in order to evaluate the level of stresses at the two most critical phases of the expansion process. The results will be compared to those of finite element modeling in order to validate the analytical model.

This study begins by tracking the radial displacement of the tube and residual contact pressure during loading at the expansion zone of the tube. These parameters are necessary to calculate the stresses in the transition zone, since it is assumed that the radial displacement of the junction point represents the displacement of the transition zone edge, and they are monitored until the expansion pressure reaches its maximum level. At this pressure, the contact pressure and radial displacement are at their peaks; therefore, the determination of stresses is indispensable.

The next step of tube expansion occurs once the expansion pressure is released and the tube and tubesheet spring back. This stage lets the tube relieve a significant portion of these

stresses. Superposing the stresses at maximum expansion pressure and during unloading gives the residual stresses in expanded tube.

In order to validate the analytical data, two FE models are designed to compare the results. In the first case, during unloading, the tube springs back elastically in both the expansion and transition zone, but in the second case, the reverse yielding takes place in the expansion zone. The main reason for selecting different models was investigating the performance of the model with and without the occurrence of reverse yielding; however, it is important to note that the transition zone never experiences reverse yielding.

CHAPTER 3

ANALYTICAL MODELING OF A HYDRAULICALLY EXPANDED TUBE TO TUBESHEET CONNECTION

3.1 Introduction

Through the years, several studies have been conducted around the tube to tubesheet joint, and the main objective of the preceding investigations was concentrated on the expansion zone. The transition zone owned a very small portion of such contributions, and due to the crucial role of this zone in joint failure, the treatment of the transition zone seems indispensable. In fact, the axial residual stresses in this zone reach their highest value on the inner surface of the tube and make this area prone to stress corrosion cracking and intergranular attacks.

In spite of the wide use of shell and tube heat exchangers in the industry, standards are limited to the fabrication process, and instructions are lacking for analyzing the suitability of the expansion processes; their optimum expansion level is obtained by trial and error. The Tubular Exchanger Manufacturers Association (TEMA) addresses the permissible tubesheet bore diameters and tolerances for each nominal tube OD in Table RCB 7.41. These dimensions prevent the risk of tube thinning that takes place in the expansion zone.

Therefore, researchers developed several models to simulate the connection in order to disclose the effect of different influence factors on the connection rigidity. The analytical investigation of the tube to tubesheet connection was initiated by Jantscha in 1929. The area of interest in the majority of studies was the expansion zone of the joint, and the transition zone was highlighted only in a few cases. Updike (1988) proposed an analytical model to calculate the residual stresses in the transition zone. The main contribution of the author was the introduction of new equations for the change in residual stresses during unloading in the transition zone by applying the beam on elastic foundation theory. Furthermore, the author used the same model to disclose the effect of the initial gap, reverse yielding and strain hardening on these stresses.

In 1998, M. Allam and his colleague conducted a valuable investigation about the stresses in the transition zone of hydraulically expanded tube-to-tubesheet joints. A standard deviation analysis was used to determine tensile residual stresses and their axial locations. Again, here, the unloading stress was calculated by means of discontinuity stress equations in a thin elastic shell, which had been proposed by Harvey in 1985. This study showed that the value of axial residual stresses approximately reaches 86 to 109% of tube yield stress, and its location is almost at the end of the transition zone. The hoop stresses reach a maximum value between 55 to 68% of tube yield stress at the beginning of the transition zone.

The main weakness of the methods used is that the stresses in the transition zone are evaluated using a combined analytical-numerical approach. During loading, the stresses are evaluated numerically using FEM, while during unloading, they are calculated using a model based on the theory of beam on elastic foundation of a semi-infinite cylinder subjected to edge loads.

3.2 Analytical model of the expansion zone

The analytical model consists of a single tube expanded into the tubesheet, which is represented by a sleeve with an equivalent outer diameter, as described by Chaaban et al. (1992). The process is assumed to be hydraulic expansion. Therefore, the tube is subjected to a consistent internal pressure. The clearance between the tube and tubesheet is large enough to give space to the tube to go under full plastic deformation before it comes into contact with the tubesheet.

Based on the amplitude of the expansion pressure, two main cases could be distinguished:

1) Expansion without tubesheet plastic deformation;
2) Expansion with tubesheet plastic deformation.

The main focus of this work will be on the case where the tubesheet simply bears elastic deformation.

3.2.1 Expansion without tubesheet plastic deformation

As is seen in figure 3.1, by applying the expansion pressure on the tube's inner surface, the tube begins to deform elastically in step 1. It is necessary to note that the axial length of the

band of pressure expanding the tube is considered to be equal to the length of the tubesheet. By starting the second step, the tube goes under plastic deformation until it touches the tubesheet. Recall from previous chapters that it is assumed that the tube material accounts for elastic perfectly plastic behavior, obeying Von Mises yield criterion. Therefore, the tangent modulus is taken as zero, and no increase in expansion pressure is needed to close the gap between the tube and tubesheet. This behavior is manifested by the flat line representing the step 3.

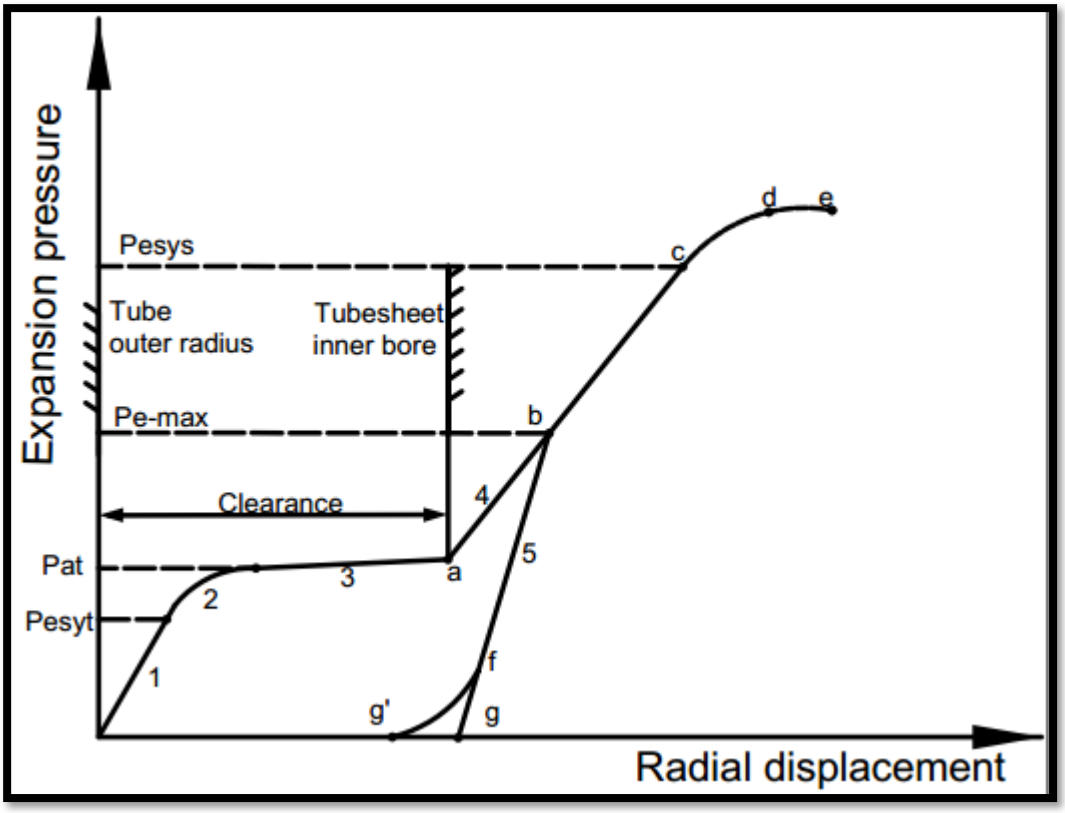

Figure 3.1 Expansion pressure diagram

At point a, the tube has already swept the radial clearance, and it is in full contact with the tubesheet. As it is mentioned in foregoing, at this point, no contact pressure is produced by the expansion pressure, and this level of expansion is considered as the lowest limit. In step 4, an increase in expansion pressure results in elastic deformation of tubesheet. Reminding that the tube in this step has no resistance to the pressure and it is only the tubesheet which

bears the expansion pressure, therefore, the slope of line 4 represents the rigidity of the tubesheet.

In current cases, the expansion pressure is increased to any level before point c and this point is shown as b in figure 3.1. Therefore, the tubesheet never experiences any plastic deformation.

3.2.1.1 Tube elastic deformation

Once the internal pressure is initially applied to the tube, the tube begins to deform elastically. The radial displacement of the tube's outer surface in the expansion zone is given by:

$$U_t(r_o) = 2r_o P_e \frac{1-\nu_t^2}{E_t(Y_t^2-1)} \tag{3.1}$$

The tube continues deforming elastically until it reaches to the yield; the pressure that causes the yield in the first fiber of tube is given by:

$$P_{yt} = \frac{S_{yt}}{\sqrt{3}} \frac{Y_t^2-1}{Y_t^2} \tag{3.2}$$

3.2.1.2 Tube elasto-plastic deformation

As is mentioned previously, any increase in expansion pressure beyond the P_{yt} leads to tube plastic deformation. Equation (3.1) is still valid for the elastic zone of the tube, and it gives the radial displacement of the tube's outside radius, which is a function of the elasto-plastic radius c_t. Therefore, replacing P_e by P_{yt} and Y_t by $Y_{tc} = r_o/c_t$ in the equation (3.1) gives:

$$U_t(r_o) = \frac{2r_o}{\sqrt{3}} \frac{S_{yt}(1-\nu_t^2)}{E_t Y_{tc}^2} \tag{3.3}$$

In addition, the pressure that causes full plasticity in the tube is given by:

$$P_{at} = \frac{S_{yt}}{\sqrt{3}} \frac{A_t . E_t (Y_t^2 - 1) + 2\ln(Y_t)}{1 + A_t . E_t} \tag{3.4}$$

Where A_t is a constant defined such that:

$$A_t = \frac{2(2 - \nu_t)}{3E_t}$$

3.2.1.3 Tubesheet elastic deformation

Once the tube comes into contact with the tubesheet, any increase in expansion pressure produces the contact pressure at the interface of the tube and tubesheet. This residual contact pressure reaches its maximum value P_{cm} at maximum expansion pressure.

Furthermore, since the first contact, the tube and tubesheet undergo the same displacement. This step has been manifested by line 4 in figure 3.1. In order to avoid the tubesheet yield, the maximum expansion pressure must remain lower than P_{ys}.

The geometrical compatibility equation of the displacement of the contact surface gives the tube total displacement:

$$U_t(r_o) = c + U_s(R_i) \tag{3.5}$$

The radial displacement of the tubesheet at inner surface is given by:

$$U_s(R_i) = \frac{(1 + \nu_s)R_i}{E_s(Y_s^2 - 1)} P_c(1 - 2\nu_s + Y_s^2) \tag{3.6}$$

Finally, the contact pressure at the interface of the tube and tubesheet is given by:

$$P_c = \frac{1}{\gamma}\left\{\frac{E_{tt}}{r_o}(Y_t^2 - 1)\left(U_t(r_o)|_{P_{at}} - c\right) + 2(1 - \bar{\nu}^2)(P_e - P_{at})\right\} \tag{3.7}$$

Where γ is defined as follows:

$$\gamma = (1+\bar{v})\left[1+(1-2\bar{v}){Y_t}^2\right] + \frac{E_{tt}\left({Y_t}^2-1\right)}{E_s\left({Y_s}^2-1\right)}(1+\nu_s)(1+Y_s^2-2\nu_s)$$

It is important to note that, as the elastic perfectly plastic behavior of the material is the assumption of this study, the tube tangent modulus must be zero.

3.2.1.4 Tubesheet plastic deformation

Recall from section 3.2.1.1, the contact pressure that causes yield in the tubesheet can be found by replacing S_{yt} by S_{ys} and Y_t by Y_s into equation (3.2):

$$P_{c\ ys} = \frac{S_{ys}}{\sqrt{3}}\frac{Y_s^2-1}{Y_s^2} \tag{3.8}$$

Also, the required expansion pressure to initiate tubesheet yield is given by:

$$P_{ys} = P_{at} + \frac{\gamma r_o P_{c\ ys} + \left(c - U_t(r_o)|_{P_{at}}\right)E_{tt}({Y_t}^2-1)}{2r_o(1-\bar{\nu}^2)} \tag{3.9}$$

Furthermore, the tubesheet inner surface displacement is given by Livier and Lazzarin (2002):

$$\begin{aligned} U_s(R_i) = \frac{(1+\nu_s)S_{ys}R_i}{E_s\sqrt{3}}\Bigg\{&\frac{c_s^2}{R_o^2}(1-2\nu_s)+1 \\ &+\frac{1}{1+A_s.\ E_s}\ \times\left[A_s\,.E_s\left(\frac{C_s^2}{R_i^2}-1\right)-2\ln\left(\frac{c_s}{R_i}\right)(1-2\nu_s)\right]\Bigg\} \end{aligned} \tag{3.10}$$

Where A_t is a constant defined such that:

$$A_s = \frac{2(2-\nu_s)}{3E_s}$$

Beyond the tubesheet yield pressure, the contact pressure at the interface is given again by Livier and Lazzarin (2002):

$$P_c = \frac{S_{ys}}{\sqrt{3}}\left\{1 - \frac{c_s^2}{R_o^2} + \frac{A_s \,.\, E_s\left(\frac{c_s^2}{R_i^2} - 1\right) + 2\ln\left(\frac{c_s}{R_i}\right)}{1 + A_s E_s}\right\} \tag{3.11}$$

3.2.2 Unloading of expansion zone

During the unloading, expansion pressure is released. As a result, the contact pressure is decreased from its maximum value at maximum expansion pressure to a lower state. The radial displacement at which the tube moves inward during unloading is given by Laghzale and Bouzid (2009):

$$\Delta U_t(r_o) = \frac{r_o(1+\nu_t)}{E_t(Y_t^2 - 1)}\{-2(1-\nu_t)P_{em} - (P_c - P_{cm})[1 + Y_t^2 \quad (1-2\nu_t)]\} \tag{3.12}$$

Where the contact pressure P_c is given by:

$$P_c = P_{cm} + \lambda(P_e - P_{em}) \tag{3.13}$$

$$\lambda = \frac{2(1-{\nu_t}^2)}{\frac{E_t({Y_t}^2-1)}{E_s({Y_s}^2-1)}\left({Y_s}^2 + 1 - 2\nu_s\right)(1+\nu_s) + (1+\nu_t)\left[1 + {Y_t}^2(1-2\nu_t)\right]}$$

3.3 Analytical model of the transition zone

3.3.1 Stresses during loading in the transition zone

The maximum expansion pressure represents the most crucial level of tube expansion, where the radial displacement, contact pressure and residual stresses reach their maximum values. Recall from section 3.1 that the residual tensile stresses at the transition zone could exceed the yield stress of the tube, and therefore makes it vulnerable to stress corrosion cracking and other in-service stresses.

As shown in Fig. 3.2, the transition zone is divided into three regions; the full plastic region, the partial plastic region and the elastic region. Assuming the partial region to be small, only the plastic and elastic regions are analyzed.

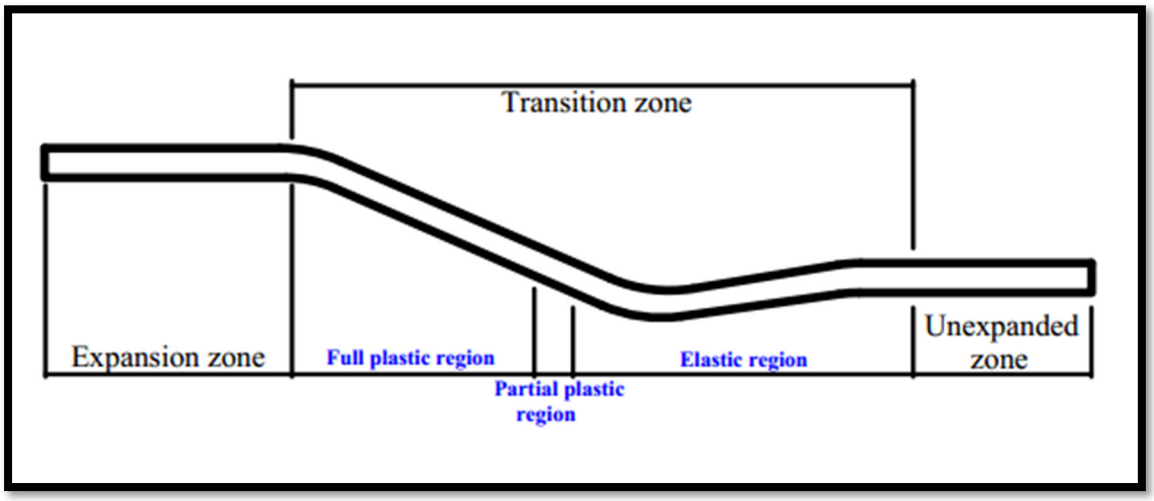

Figure 3.2 Schematic of different regions in transition zone

3.3.1.1 Stresses analysis of the full plastic region

In this work, in order to determine residual stresses in the full plastic region of the transition zone, the yield condition for a cylindrical shell subjected to axially symmetric loading proposed by Sawczuk and Hodge (1960) is applied. The tube shell is assumed to be homogeneous, having a rigid perfectly plastic behavior. Figure 3.3 shows the loading within a tube of infinite length. The pressure is assumed to act as a single force per unit circumference. Once the tube collapses under the applied force, a region delimited by X_1 from each side of the force is assumed to be fully plastic.

The problem is introduced by various parameters, which are well known as basic equations in the plastic analysis of cylindrical shells. The definitions of these parameters are in dimensionless form as follows:

$$n = \frac{N_\theta}{N_0} \tag{3.14}$$

$$m = \frac{M_x}{M_0} \tag{3.15}$$

$$q = \sqrt{\frac{R}{2M_0N_0}}Q \tag{3.16}$$

$$x = \sqrt{\frac{2N_0}{RM_0}}X \tag{3.17}$$

$$N_o = tS_{yt} \tag{3.18}$$

$$M_o = \frac{t^2S_{yt}}{4} \tag{3.19}$$

In the above equations, zero indexes stand for the limit between the expansion zone and the transition zone. The assumed rigid perfectly plastic tube shell behavior is defined by two equilibrium equations: an interaction curve (Figure 3.4) and a flow law. In case of no existence of distributed surface loads, the equilibrium equations are given as follows:

$$q' + n = 0 \tag{3.20}$$

$$m' = q \tag{3.21}$$

The plastic boundary conditions are given as below:

$$q = q_0 \qquad at \qquad x = 0 \tag{3.22}$$

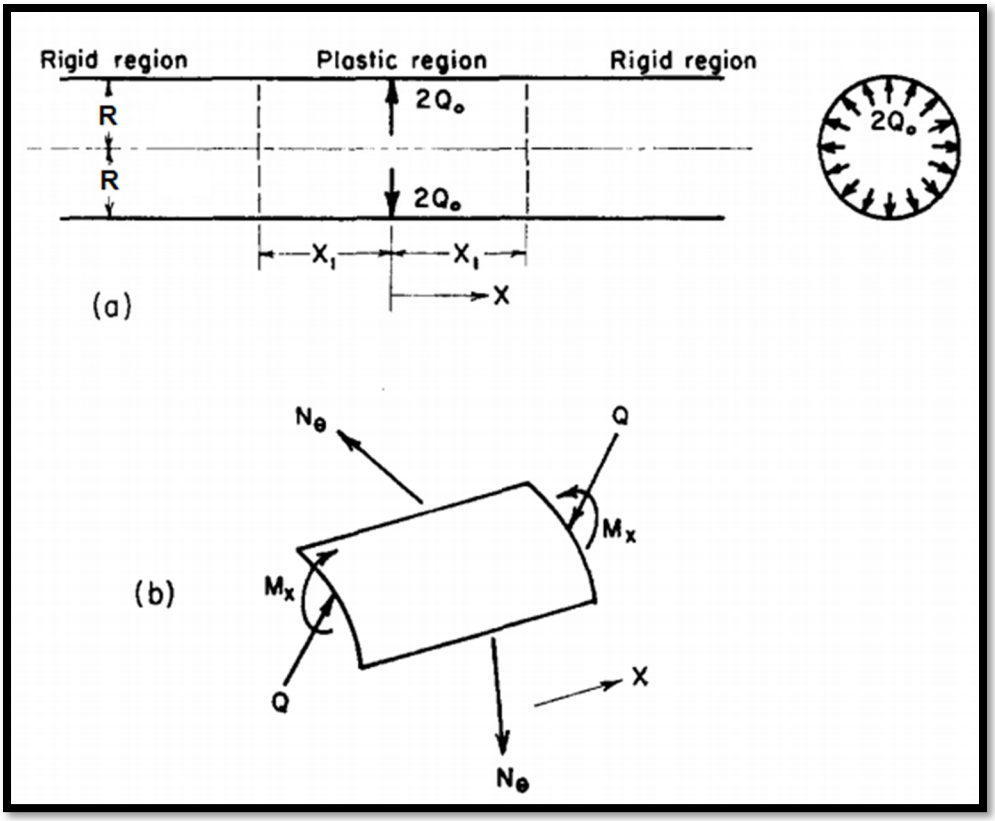

Figure 3.3 Cylindrical shell with ring load
a) Loaded shell, b) Stress resultants
(Taken from Sawczuk A. et al., 1960)

$$m = maximum \qquad at \qquad x = 0 \tag{3.23}$$

$$m = minimum \qquad at \qquad x = x_1 \tag{3.24}$$

$$w = 0 \qquad at \qquad x = x_1 \tag{3.25}$$

It is worthwhile to note that, for any particular value of x within the interaction curve, no plastic flow occurs and for the ideal rigid-plastic material, the rest of the shell remains rigid. However, if the stress point moves on to the curve, the plastic flow may take place according to the plastic potential flow law.

Also, it is assumed that the effect of shear force on plastic yielding is negligible. In fact, generally speaking, the radial stress in the transition zone is almost zero. Therefore, the description of the plastic behavior of the tube will be defined in terms of m and n for a Von Mises uniform shell, and introducing a new parameter p so that $dm/dp \geq 0$:

$$n = \pm \tan p \ \log \tan(p/2) \tag{3.26}$$

$$m = \pm\left(2/\sqrt{3}\right)[\tan^2 p \log \tan(p/2) + \sec p] \tag{3.27}$$

$$0 \leq p \ \leq \ \pi$$

Substituting equations 3.26 and 3.27 into equations 3.20 and 3.21 leads to an equation as below:

$$q^2 = q_0^2 - 2\int_{p_0}^{p} n(dm/dp)dp \tag{3.28}$$

With q known from equation 3.28, the equation can be written for x which lies within the length of plastic rigid boundary x_1:

$$x = \int_{p_0}^{p} (1/q)(dm/dp)dp \tag{3.29}$$

Since the material does not manifest any strain hardening behavior, which is the assumption of this work, the dimensionless stress point (m, n) is always on the interaction curve.

Knowing N_o and n from equations (3.18) and (3.26) and replacing into (3.14) gives the circumferential hoop stress and the hoop stress, as below:

$$\sigma_\theta = \pm \frac{N_\theta}{t} \tag{3.30}$$

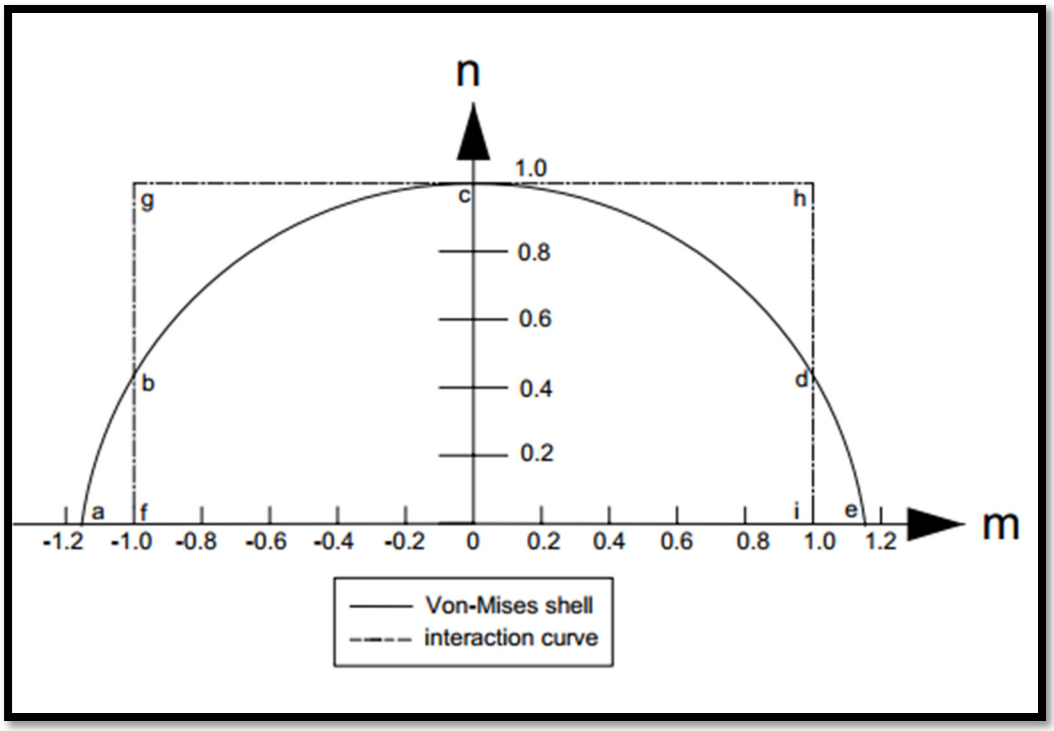

Figure 3.4 Interaction curves

Also, the axial stresses as well as equivalent stress for the tube material, assuming Von Mises yield criterion, are given as follows:

$$\sigma_x = (\sigma_\theta \pm \sqrt{\left(\sigma_\theta{}^2 - 4\left(\sigma_\theta{}^2 - S_{yt}{}^2\right)\right)})/2 \tag{3.31}$$

$$\sigma_e = \sqrt{(\sigma_x{}^2 + \sigma_\theta{}^2 - \sigma_x\sigma_\theta)} \tag{3.32}$$

3.3.1.2 Stresses analysis of the elastic region

The stresses within the perfectly plastic rigid region are known so far. However, in reality, the shell is not rigid. As shown in figure 3.2, the elastic region expands from point X_1 up to the unexpanded zone edge, and its corresponding stresses could be determined by applying discontinuity stress equations of a thin elastic shell (Harvey, 1985).

The Hoop and axial stresses based on the beam on elastic foundation theory can be written as follows:

$$\sigma_\theta = \pm\frac{Eu}{R} \pm \frac{6\nu M_x}{t^2} \tag{3.33}$$

$$\sigma_x = \pm\frac{6M_x}{t^2} \tag{3.34}$$

The positive and negative signs ($\pm$) correspond to the inner and outer surface of the tube. The displacement of a semi-infinite beam on elastic foundation at $x = 0$ is given by:

$$u_e = \frac{2P_{el}\,\beta}{k} - \frac{2M_{el}\beta^2}{k} \tag{3.35}$$

$$\beta = \frac{\sqrt[4]{3(1-\nu^2)}}{\sqrt{Rt}}$$

$$k = \frac{Et}{R^2}$$

Knowing that the displacement u_e at the plastic-elastic region is equal to zero, gives the shear force P_e:

$$P_{el} = \beta M_{el} \tag{3.36}$$

Noting that $\sigma_x = S_{yt}$, equation 3.34 gives the bending moment at the elastic-plastic edge:

$$M_x = \pm\frac{t^2 S_{yt}}{6} = M_{el} \tag{3.37}$$

Substituting equation (3.37) into (3.36) gives:

$$P_{el} = \frac{\beta t^2 S_{yt}}{6} \tag{3.38}$$

In order to calculate the stresses in the elastic region, the displacement and the bending moment of a semi-infinite shell as a function x are used (Figure 3.5).

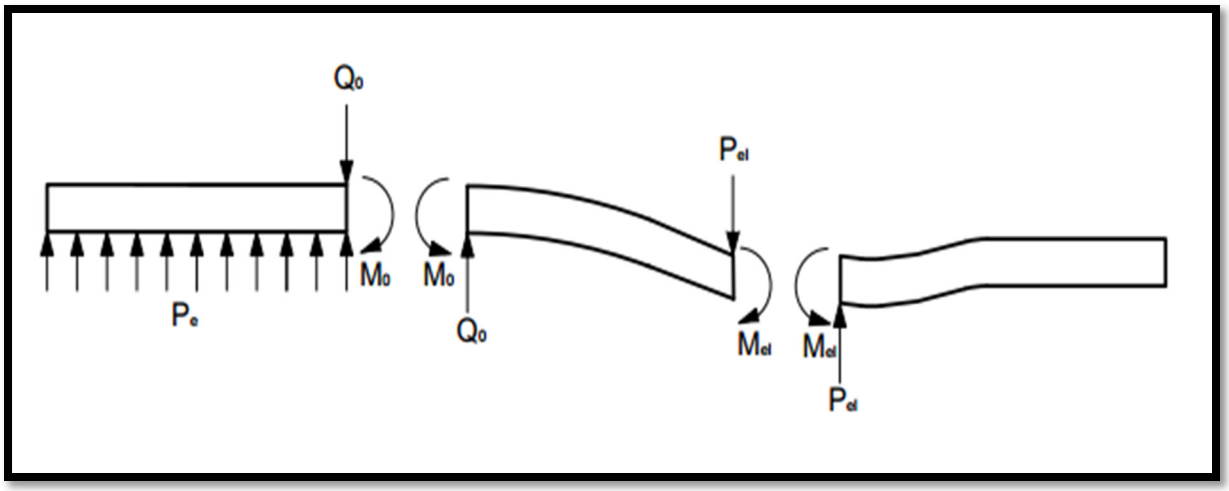

Figure 3.5 Semi-infinite beam with bending moment and force

The displacement is given by:

$$u_x = \frac{2P_{el}\,\beta}{k} D_{\beta x} - \frac{2M_{el}\,\beta^2}{k} C_{\beta x} \tag{3.39}$$

$$M_x = \frac{P_{el}}{\beta} B_{\beta x} - M_{el} A_{\beta x} \tag{3.40}$$

Where $A_{\beta x}, B_{\beta x}, C_{\beta x}$ and $D_{\beta x}$ are influence functions and are given as follows:

$$A_{\beta x} = e^{-\beta x}(\cos \beta x + \sin \beta x) \tag{3.41}$$

$$B_{\beta x} = e^{-\beta x} \sin \beta x \tag{3.42}$$

$$C_{\beta x} = e^{-\beta x}(\cos \beta x - \sin \beta x) \tag{3.43}$$

$$D_{\beta x} = e^{-\beta x} \cos \beta x \tag{3.44}$$

Substituting equations (3.41) to (3.44) into equations (3.39) and (3.40) and knowing that P_{el} and M_{el} from (3.37) and (3.38) lead to the following expressions for u_x and M_x:

$$u_x = \frac{S_{yt} t^2 \beta^2}{3k} e^{-\beta x} \sin \beta x \tag{3.45}$$

$$M_x = \frac{S_{yt}t^2}{6} e^{-\beta x} \cos \beta x \tag{3.46}$$

Substituting for equations (3.45) and (3.46) into equations (3.33) and (3.34) gives the stresses during loading in the elastic region of the transition zone:

$$\sigma_x = S_{yt} e^{-\beta x} \cos \beta x \tag{3.47}$$

$$\sigma_\theta = \frac{S_{yt}\sqrt{3(1-\nu^2)}}{3} e^{-\beta x} \sin \beta x \tag{3.48}$$

3.3.2 Unloading of plastic zone under elastic recovery

As manifested in figure 3.1, line 5 represents the unloading step, in which the expansion pressure drops down to zero. Assuming a pure elastic recovery of the tube with complete plastic zone and no reverse yielding, discontinuity stress equations for a long cylindrical shell under axisymmetric external band pressure can be employed in order to calculate residual stresses at the transition zone during unloading (Figure 3.6). The external pressure represents the contact pressure at the interface with the tubesheet.

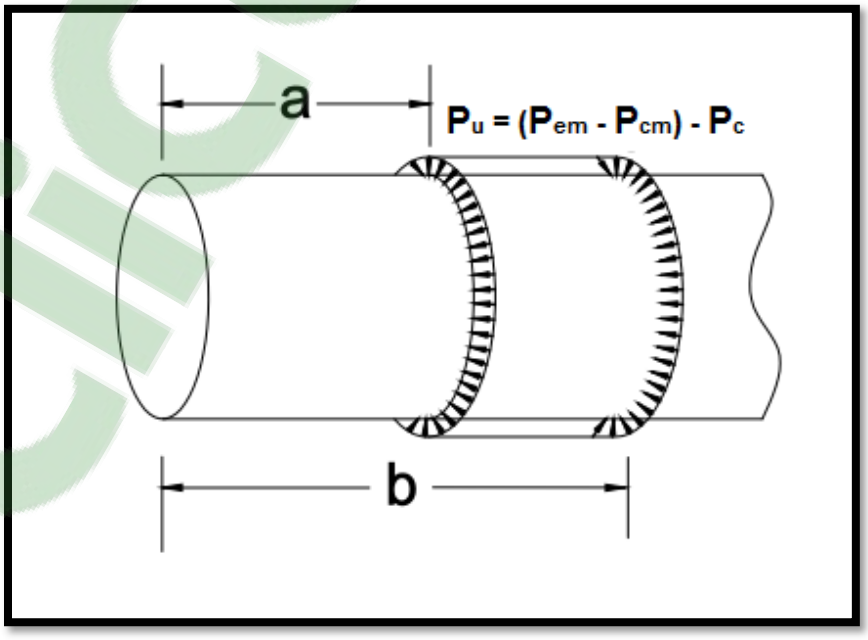

Figure 3.6 External pressure on long thin-walled cylindrical shell

The schema of stress distribution, rotation and radial displacement are manifested in figure 3.7. It is important to note that for long shells with free ends, $\beta l > 6$ must be valid, which covers both investigated cases in this study. The detailed theory is given by Young and Budynas (2002) for several circumstances of loading to any vessel that is a figure of revolution.

The following constants and functions are presented in this theory and are used in the determination of axial and hoop stresses.

$$A_1 = \frac{1}{2} e^{-\beta a} \cos \beta a \tag{3.49}$$

$$A_2 = \frac{1}{2} e^{-\beta a} (\sin \beta a - \cos \beta a) \tag{3.50}$$

$$A_3 = \frac{1}{2} e^{-\beta a} \sin \beta a \tag{3.51}$$

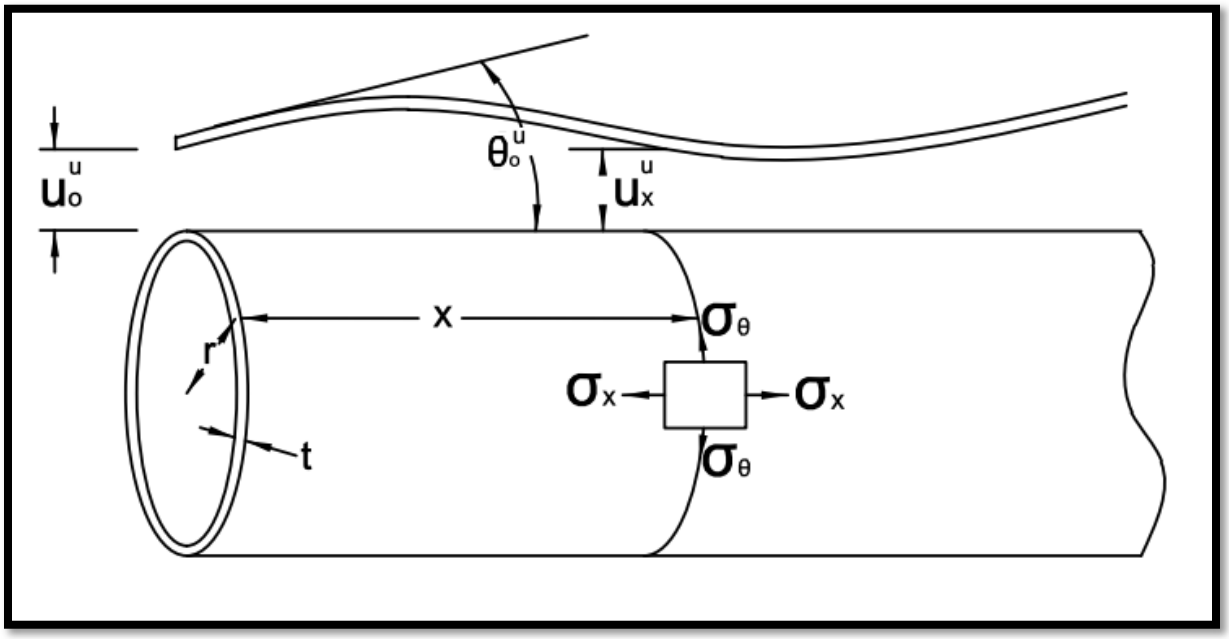

Figure 3.7 Stresses and displacement in a long thin-walled cylindrical shell subjected to a band pressure

$$A_4 = \frac{1}{2} e^{-\beta a} (\sin \beta a + \cos \beta a) \tag{3.52}$$

$$B_1 = \frac{1}{2} e^{-\beta b} \cos \beta b \tag{3.53}$$

$$B_2 = \frac{1}{2} e^{-\beta b} (\sin \beta b - \cos \beta b) \tag{3.54}$$

$$B_3 = \frac{1}{2} e^{-\beta b} \sin \beta b \tag{3.55}$$

$$B_4 = \frac{1}{2} e^{-\beta b} (\sin \beta b + \cos \beta b) \tag{3.56}$$

$$F_1 = \cosh \beta x \cos \beta x \tag{3.57}$$

$$F_2 = \cosh \beta x \sin \beta x + \sinh \beta x \cos \beta x \tag{3.58}$$

$$F_3 = \sinh \beta x \sin \beta x \tag{3.59}$$

$$F_4 = \cosh \beta x \sin \beta x - \sinh \beta x \cos \beta x \tag{3.60}$$

$$F_5 = 1 - \cosh \beta x \cos \beta x \tag{3.61}$$

$$F_6 = 2\beta x - (\cosh \beta x \sin \beta x + \sinh \beta x \cos \beta x) \tag{3.62}$$

$$F_{a1} = \langle x - a \rangle^0 \cosh \beta (x - a) \cos \beta (x - a) \tag{3.63}$$

$$F_{a2} = \cosh \beta (x - a) \sin \beta (x - a) + \sinh \beta (x - a) \cos \beta (x - a) \tag{3.64}$$

$$F_{a3} = \sinh \beta (x - a) \sin \beta (x - a) \tag{3.65}$$

$$F_{a4} = \cosh \beta (x - a) \sin \beta (x - a) - \sinh \beta (x - a) \cos \beta (x - a) \tag{3.66}$$

$$F_{a5} = \langle x - a \rangle^0 - F_{a1} \tag{3.67}$$

$$F_{a6} = 2\beta(x - a)\langle x - a \rangle^0 - F_{a2} \tag{3.68}$$

$$D = \frac{Et^3}{12(1 - \nu^2)} \tag{3.69}$$

The tube deformation and rotation at the free edge are given by:

$$\theta_o^u = \frac{-P_u}{D\beta^3}(B_3 - A_3) \tag{3.70}$$

$$u_o^u = \frac{-P_u}{2D\beta^4}(B_2 - A_2) \tag{3.71}$$

Also, load terms or load and deformation equations are calculated below:

$$LT_v = \frac{-P_u}{2\beta}(F_{a2} - F_{b2}) \tag{3.72}$$

$$LT_M = \frac{-P_u}{2\beta^2}(F_{a3} - F_{b3}) \tag{3.73}$$

$$LT_\theta = \frac{-P_u}{4D\beta^3}(F_{a4} - F_{b4}) \tag{3.74}$$

$$LT_u = \frac{-P_u}{4D\beta^4}(F_{a5} - F_{b5}) \tag{3.75}$$

In order to calculate $F_a$and F_b constants, a and b are substituted for x in equations (3.57) to (3.62). By knowing all unknowns from previous equations, the bending moment, shear force, rotation and radial displacement are given along the tube transition zone:

$$M_x^u = -2u_o^u D\beta^2 F_3 - \theta_o^u D\beta F_4 + LT_V \tag{3.77}$$

$$\theta_x^u = \theta_o^u F_1 - u_o^u \beta F_4 + LT_\theta \tag{3.78}$$

$$u_x^u = u_o^u F_1 + \frac{\theta_o^u}{2\beta} F_2 + LT_V \tag{3.79}$$

By substituting equations (3.76) and (3.77) into (3.33) and (3.34), the residual stresses during unloading can be found as follows:

$$\sigma_\theta = \pm \frac{E}{R} u_x^u \pm \frac{6\nu}{t^2} M_x^u \tag{3.80}$$

$$\sigma_x = \pm \frac{6}{t^2} M_x^u \tag{3.81}$$

Finally, by superimposing the loading and unloading stresses, the residual stresses along the transition zone of the expanded tube are calculated.

$$\sigma = \sigma_l + \sigma_u \tag{3.82}$$

CHAPTER 4

FINITE ELEMENT MODELING OF HYDRAULICALLY EXPANDED TUBE TO TUBESHEET JOINT

4.1 Introduction

Finite element analysis is a computerized method introduced in the 1950s that provides a precise prediction of how a structure reacts to the forces, stresses and other physical effects in the real world. This process is highly used in structural analysis, fluid mechanics and heat transfer. The method requires the creation of a model which represents perfectly the specifications of a structure. Therefore, the same geometry and material properties as the real structure must be afforded in order to reach the highest accuracy. The next step in finite element analysis is meshing the structure by means of various elements in the software. In fact, the structure is divided into an assembly of subdivisions with diverse shapes. From this point, the type of analysis specifies the typical range of elements, their combinations and number of nodes. Following this step, boundary conditions should be defined to simulate the supports and the loading on the structure. Finally, according to the desired analysis, the software provides algebric stiffness equations to solve the problem and to demonstrate the behavior of the structure.

As mentioned in the literature, the finite element analysis of the tube to tubesheet connection was first conducted by R. M. Wilson in 1978. The objective of his study was to determine the residual stresses and radial displacement of the tube during expansion at the transition zone of the tube and to evaluate the results in the context of actual operating conditions with attention to stress corrosion cracking. Since 1978, many other researchers employed finite element analysis in their studies due to the time and cost effectiveness of this method. These investigations led to valuable achievements in tube to tubesheet joint analysis without having to conduct complex experimentation on hard instrument samples, which let researchers advance their knowledge in this field.

4.2 FE Tube to tubesheet joint model

In this study, the analytical model has been validated using finite element modeling, using the general-purpose program ANSYS workbench 16.2. A symmetric 3D pattern of tube to tubesheet connection was modeled (Figure 4.1) by means of hexahedral mesh elements. Only a 90-degree portion of the joint is modeled for simplicity. In parallel to the 3D modeling, a 2D axisymmetric model of the joint was built as well in order to compare the residual stresses predicted by the analytical model. The final results showed higher precision with the 3D model, which is in agreement with the Metzeger D. R. (1995) work and, therefore, the 3D model will be adopted hereafter.

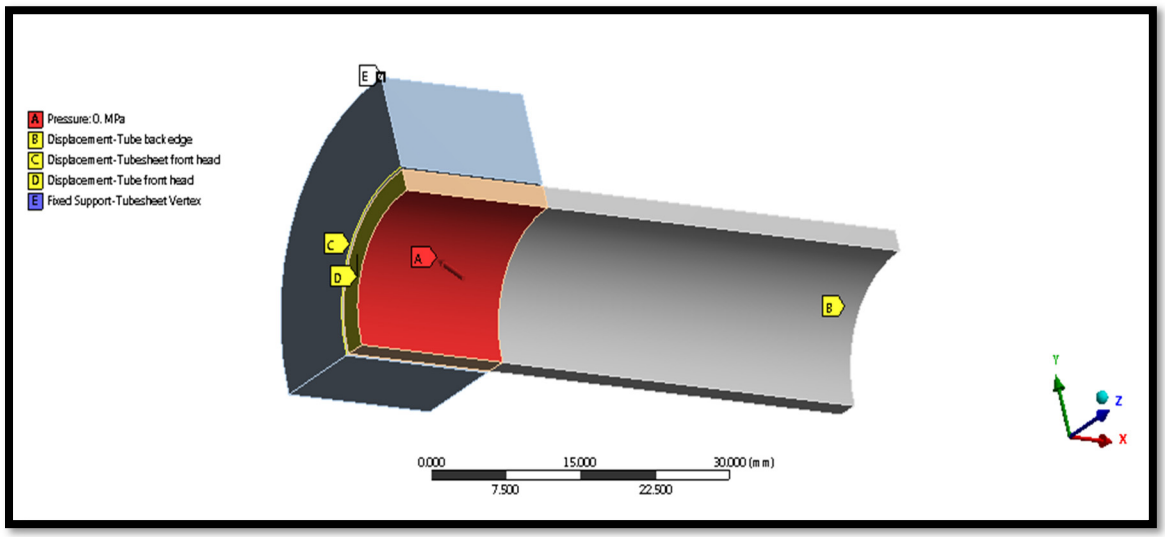

Figure 4.1 Symmetric 3D model of tube to tubesheet connection

In accordance with the analytical model, and to assure the accuracy of the theory used, the expansion process is treated in two separate steps explained earlier: loading sequence and unloading sequence. In fact, this technique allows the author to concentrate on each step of the process and to validate the theory used by comparing the analytical results with the numerical ones. The maximum level of expansion pressure is limited to avoid tubesheet yielding. In addition, the amplitude of the maximum expansion pressure is high enough to produce plastic deformation through the entire expansion zone while keeping the stresses as low as possible in the transition zone, to avoid the risk of stress corrosion cracking. The expansion pressure beyond the level that causes tubesheet yielding is not part of this study.

However, it is acknowledged that the effect of strain hardening can have a significant effect on the final residual stresses. Table 4.1 shows the geometrical and mechanical properties of the two investigated joint cases as well as their material types. In the first case, the expansion zone experiences full elastic recovery during unloading, while in the second case, this zone undergoes reverse yielding. Also, in both cases the selected tubesheet material has higher strength than tube material which is often the case in the industry. Nevertheless, the effect of reverse yielding on the residual stresses in the transition zone of the expanded tube is not considered.

Table 4.1

Geometry and mechanical properties

	Case 1		**Case 2**	
	Tube Alloy 690	**Tubesheet SA-533**	**Tube SA-240**	**Tubesheet SA-556M**
r_o, R_o (mm)	8.725	21.12	12.5	21.5
r_i, R_i (mm)	7.709	8.852	10.5	12.8
E_t, E_s (GPa)	211	201	209	199.6
E_{tt}, E_{ts} (GPa)	0.1	0.1	0.1	0.1
S_{yt}, S_{ys} (MPa)	345	414	238	375
ν_t, ν_s	0.3	0.3	0.3	0.3
L_t, L_{ts}	70	20	70	20
$P_{e\text{-}max}$ (MPa)	228		240	
C (mm)	0.127		0.3	
F	0.15		0.15	

4.2.1 Nonlinearities associated with joint analysis

Recall from chapter 2, three material and geometrical nonlinearities are involved in a tube expansion analysis, which make the treatment of the problem more complex. These nonlinearities are as follows:

1) Tube and tubesheet large deformations,

2) Material elasto-plastic behavior,
3) Contact surface.

Tube and tubesheet large deformations are a geometrical non-linearity that takes place in this process due to the large displacement of the tube and tubesheet geometries. In addition to the large strain occurring in the expansion zone, the transition zone experiences elasto-plastic behavior, which is a nonlinear behavior of material. In this work, the elastic-perfectly-plastic assumption is taken as a simplification to solve the problem and, by doing so, the kinematic hardening behavior of the material which may take place in hardened materials is neglected (Figure 4.2).

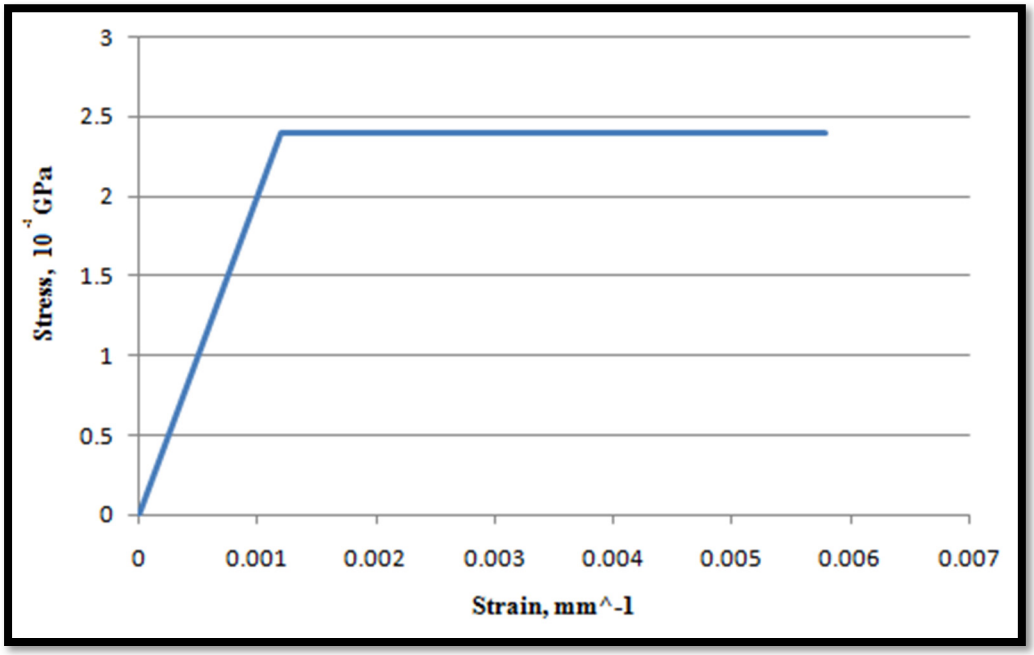

Figure 4.2 Tube material stress-strain curve (case 2)

The last nonlinearity in connection with tube-to-tubesheet joint analysis begins at the lowest pressure limit, once the tube comes into contact with the tubesheet. This nonlinearity is essentially of a geometrical type, because the contact area between the tube and tubesheet is a function of deformation. In this study, the rolling friction and mesh refinement in the contact area are taken into account in the modeling to simulate the real behavior taking place in the expansion zone of the tube.

In order to overcome the divergence associated with the above nonlinearities, the expansion pressure was gradually applied to the joint and, in particular, when tube yield pressure is reached. All phases related to plasticity and contact involved during loading will be discussed later in this chapter.

4.2.2 Elements and mesh

In ANSYS Workbench, the tube and tubesheet are modeled by SOLID186 elements, which are 3D 20-node elements and exhibit quadratic displacement behavior. SOLID186 is defined by three degrees of freedom per node; these are the translations in the nodal x, y and z directions. The element supports plasticity, large deflection and high strain capabilities (Figure 4.3). While the tube is represented by a cylinder, the tubesheet is modeled with a circular ring with an equivalent outside diameter, defined by Chaaban et al. in 1992.

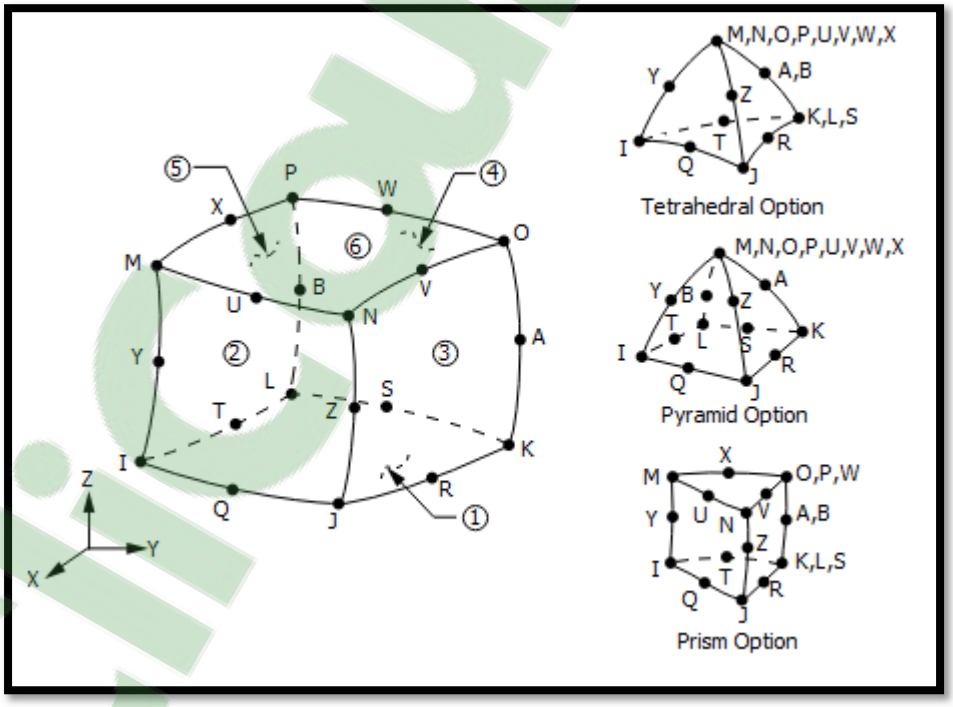

Figure 4.3 SOLID186 Homogeneous Structural Solid Geometry
(Taken from ANSYS Workbench 16.2)

The contact surface between the tube and the tubesheet is very important in the connection analysis, due to the need for accurate evaluation of the residual contact pressure at the

interface. Therefore, the correct elements should be employed to reproduce the real behavior. In ANSYS workbench, CONTA174 is applied to represent the contact surface and sliding friction between the 3D target interface elements (Figure 4.4). This element is located at the surface of the tube and tubesheet with mid-side nodes. The element owns the same geometric characteristics as SOLID186 and is defined by 8 nodes, where the underlying solid element has mid-side nodes as well.

The element associated with CONTA174 to model the contact surface is TARGE170, which is employed in analysis and can simulate 3D target surfaces correctly.

The next step is to proceed with the model mesh generation, which allows the program to build the global stiffness matrix that produces the force displacement relationship and produces the interactions between the parts. Five main structural meshes of the model are elaborated for the following segments:

1) Tube expansion zone,
2) Tube transition zone,
3) Tubesheet,
4) Contact surface,
5) Tube unexpanded zone.

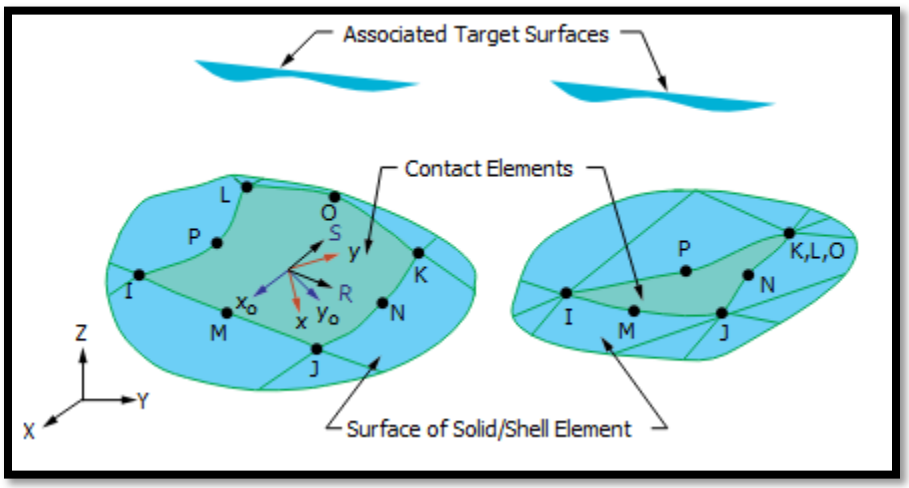

Figure 4.4 CONTA174 Geometry
(Taken from ANSYS Workbench 16.2)

As is well-known, the finite element is only an approximation. However, the discretization, the meshing and the assumptions of the simulated model carry high importance in reaching an accurate analysis of the problem. Therefore, in this study, in order to obtain an optimum mesh pattern, two designs of mesh have been compared. The first design is the automatic mesh pattern introduced by the program, and the second refinement is performed by the author due to the prior knowledge of stress concentration in the transition zone, which is the area of interest in the current investigation (Figure. 4.5).

In addition, a convergence analysis was conducted on the model based on the basis of the variation of residual stresses. The mesh refinement convergence criterion of less than 1% was adopted.

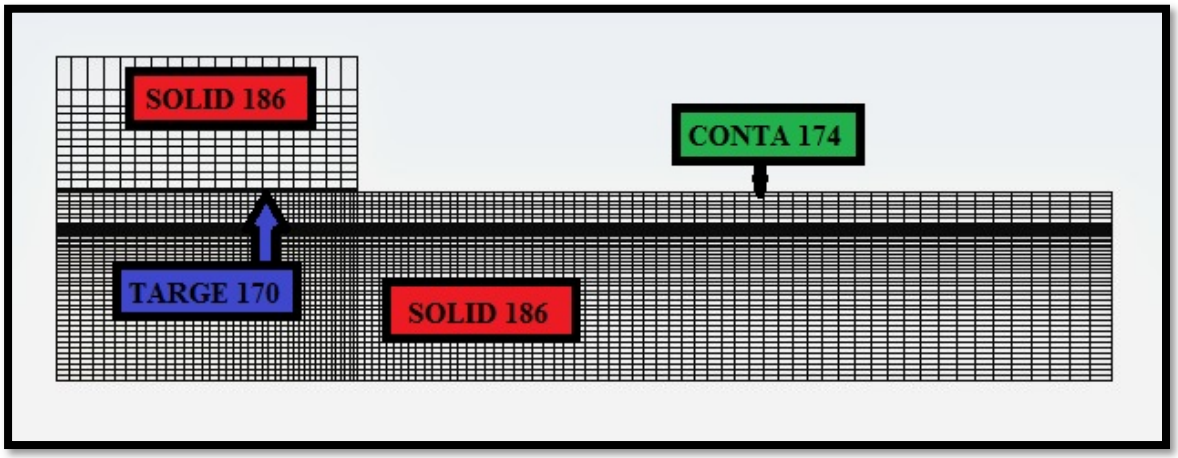

Figure 4.5 Mesh pattern of model

4.2.3 Contact surface and friction modeling

The interaction of the tube and the tubesheet is characterized through their contact surfaces. Two main influence factors for the selection of the friction coefficient are considered; these are tube extrusion and material strain hardening. As is well established, joint integrity is dependent on these two parameters. Therefore, an astute selection of friction coefficient seems necessary for the interface. After a detailed review of the literature, a friction coefficient of 0.15 was adopted in this analysis.

Although ANSYS Workbench supports a large selection of contact options to define interaction between the surfaces in the explicit analysis, the automatic node to surface

algorithm is used to simulate the contact surface. The entire outer surface of the tube is considered as contact surface in order to monitor the cases where tube extrusion takes place.

4.2.4 Constraints and loading

In the numerical simulation, the tube edge of the unexpanded zone experiences no rotation; however, it is free to displace in longitudinal and radial directions. The length of the unexpended zone is much greater than $2.45(Rt)^{½}$. In order to avoid singularity in the longitudinal direction, the opposite edge of the tube is fixed in the longitudinal direction. This constraint is also applied to the tubesheet to integrate the parts while deforming in the radial direction during the loading and unloading steps. Furthermore, a fixed support with no translation and rotation is applied to the tubesheet to avoid singularity through the analysis.

The simulation of the expansion process is performed by applying the pressure loading option in ANSYS Workbench. The tube length on which the pressure loading is applied is equal to the tubesheet length (20 mm). This length is very common in most applications. Nevertheless, in TEMA, the recommended length of loading is equal to tubesheet length minus 1/8 of inch. The magnitude of pressure in every step is tabulated in the software, and the maximum expansion pressure is taken lower than the one that produces tubesheet yielding. This is to ensure that the tubesheet never experiences plastic deformation.

CHAPTER 5

RESULTS AND DISCUSSIONS

5.1 Introduction

To validate the analytical developed model, the stresses and displacements during the loading and unloading along the tube length are compared to those obtained with the numerical FE model. The two important stresses are the hoop and axial stresses generated in the transition zone of the expanded tube. In comparison with other stresses, the radial and shear stresses are relatively small and are ignored in analysis. In order to monitor the elastic-perfectly plastic behavior of the three tube zones during loading and unloading, the equivalent stresses are also presented.

5.2 Case without reverse yielding of expansion zone

The rigorous analysis of the tube-to-tubesheet of the first case revealed that at 38.4 MPa, the tube began to deform plastically. The tube comes into contact with the tubesheet inner bore at 40.7 MPa, and at this pressure, only 15.5 mm of the tube expansion zone length from the free end is in partial plasticity (Figure 5.1). Recall from the preceding chapters that, at this level, no contact pressure is produced at the interface, and it can be considered as the expansion lower limit mentioned in the literature.

5.2.1 Pressure loading

One of the points of interest in tube expansion analysis occurs once the expansion pressure reaches its maximum value. This value must be restricted to an upper limit in order to avoid extrusion of the tube along the tubesheet bore. Therefore, in respect to this upper limit, the expansion pressure is 228 MPa in this case, which is much lower than the tube yield stress. Therefore, during unloading, the tube expansion zone experiences an elastic recovery with no reverse yielding.

Three different regions at the transition zone could be identified due to the distribution of the equivalent stresses obtained, considering the elastic perfectly plastic behavior of the tube. These regions are the full plastic region, the partial plastic region and the elastic region, as already pointed out in Figure 3.2.

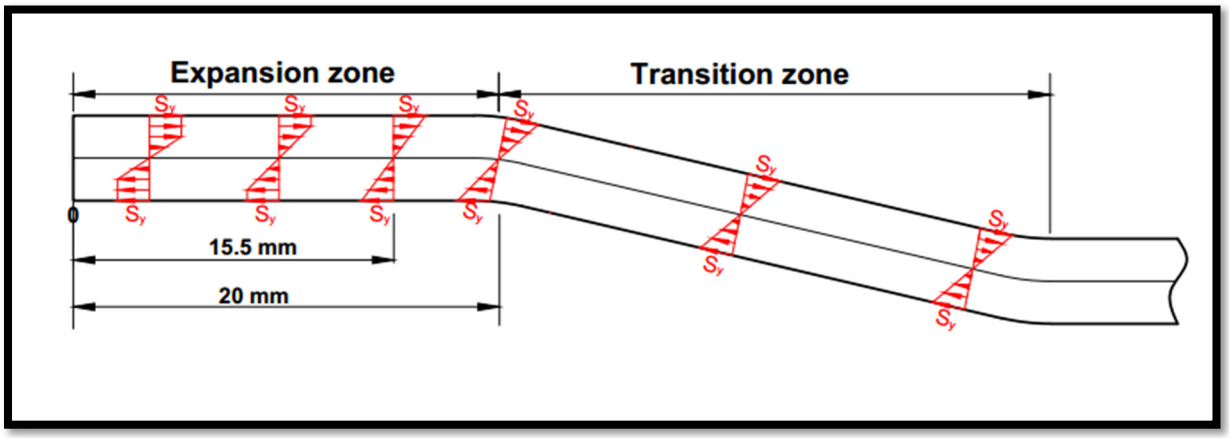

Figure 5.1 Schematic of plasticity in tube when tube touches the tubesheet

According to the geometry and mechanical properties of the numerical model, the length of these regions along the transition zone at maximum expansion pressure are 4, 1 and 11 mm respectively (Figure 5.2). These values are 4.1, 0 and 12 mm respectively as predicted by the analytical model. It is worth noting that because the partial plastic region is small and, for simplicity, the transition from full plasticity to full elastic behavior is not considered by the analytical model.

The axial stress on the inner surface, as a result of bending, is at its maximum positive value reaching yield at the elastic-plastic region interface of the transition zone and drops down abruptly to a minimum negative value, reaching yield at the expansion transition zone interface passing by zero. In addition, at this elastic-plastic region interface point, the hoop stress and the radial displacement of the tube are almost zero. Figure 5.3 compares the stresses of the tube's inner surface in the transition zone at maximum expansion pressure of both models. The stresses of the expansion zone obtained from FEM only are also shown for reference. The conditions mentioned earlier are clearly seen at specified locations. The curves of Figure 5.3 show a 4% difference in the value of inner surface axial stresses between the two models at the junction between the expansion and transition zones. The

difference for hoop stresses at this junction is about 5%. However, at the junction between the elastic-plastic regions, the axial stress difference is 12% while the hoop stress difference is 8%.

Furthermore, the axial and hoop stresses at the tube's outer surface are shown to be of the same magnitude, but with opposite signs for the hoop stress as compared to that of the inner surface, as shown in figure 5.4. It is worthy to note that the hoop stress is almost zero at the end of the plastic collapse region of the tube transition zone, while the axial stress reaches yield. The deviation in the location of the maximum point of the graphs rests in the fact that, in reality, the length of the transition zone is stretched into the expansion zone by 1.5 mm. Also, it is important to note that the axial stress is higher than the hoop stress in the transition zone of the expanded tube, which is in good agreement with the literature. The analytical and numerical models are in good agreement and, in particular, in the elastic region of the transition region. Nonetheless, in the full plastic region, although the general trend of axial and hoop stresses are similar, the distributions show a slight shift. There is a 14% difference in the axial stress between the two models at the junction between the expansion and transition zones.

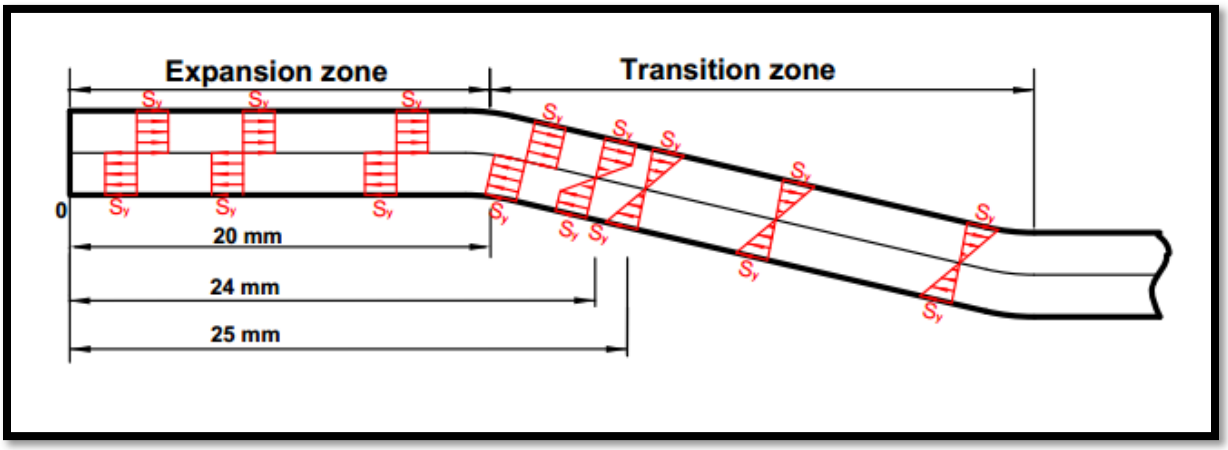

Figure 5.2 Schematic of plasticity in tube at maximum expansion pressure

5.2.2 Pressure unloading

The second step in tube analysis is dedicated to the unloading, with no reverse yielding taking place. In fact, it is assumed that when the expansion pressure is released, a significant portion of the residual stresses remains in the tube.

The residual stress distributions at the inner and outer tube surfaces after unloading are presented in figures 5.5 and 5.6. Once again, while the analytical and numerical stresses in the elastic region agree with each other at both the inner and outer tube surfaces, those of the plastic region show a difference, but the general trend is similar. The difference for maximum hoop stress between the two models is 17%, while the axial stress demonstrates better agreement with only an 8% maximum difference in the plastic region. The comparison of the hoop stress of the analytical and FE models at the tube outer surface during unloading discloses the most significant difference, which should be treated meticulously in order to find the cause. In fact, it is suspected that this difference is due to the simplified case of a ring load instead of a band pressure during loading when considering plastic collapse of the transition zone.

In addition to the distribution of stresses at inner and outer surfaces, the radial displacement of tube mid-thickness is also an area of interest, especially at the junction of the expansion and transition zones. Recall from the literature that the highest displacement occurs at this junction, while the joint analysis is unable to locate it exactly. Therefore, it is often assumed that the transition zone merges to the expansion zone that has exactly the length of the tubesheet thickness, where the rotation of tube is considered to be zero. This simplification simplifies the study and helps conduct the tube stress analysis (Figure 5.7).

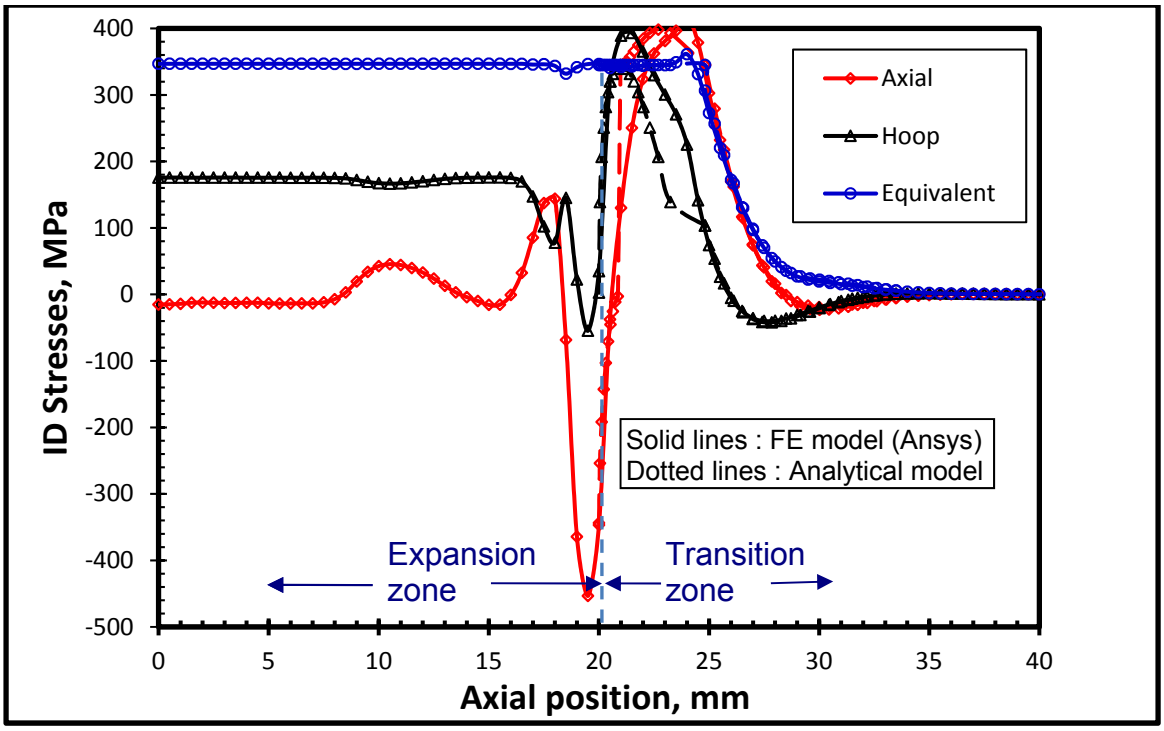

Figure 5.3 Comparison of stresses at tube inner surface at maximum expansion pressure

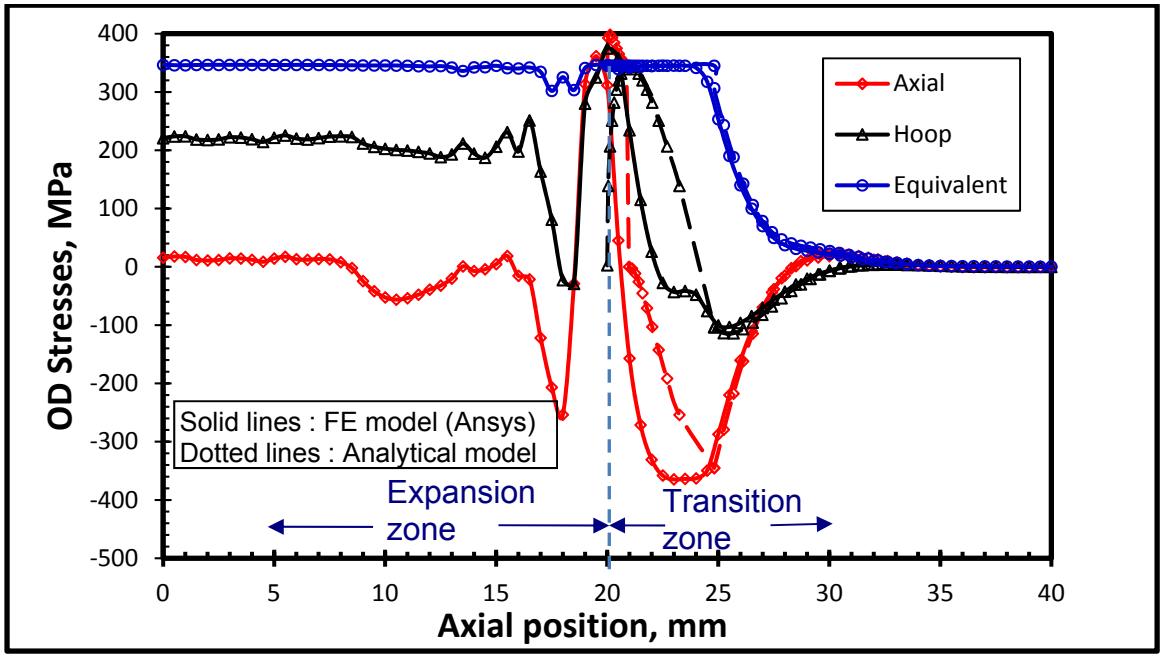

Figure 5.4 Comparison of stresses at tube outer surface at maximum expansion pressure

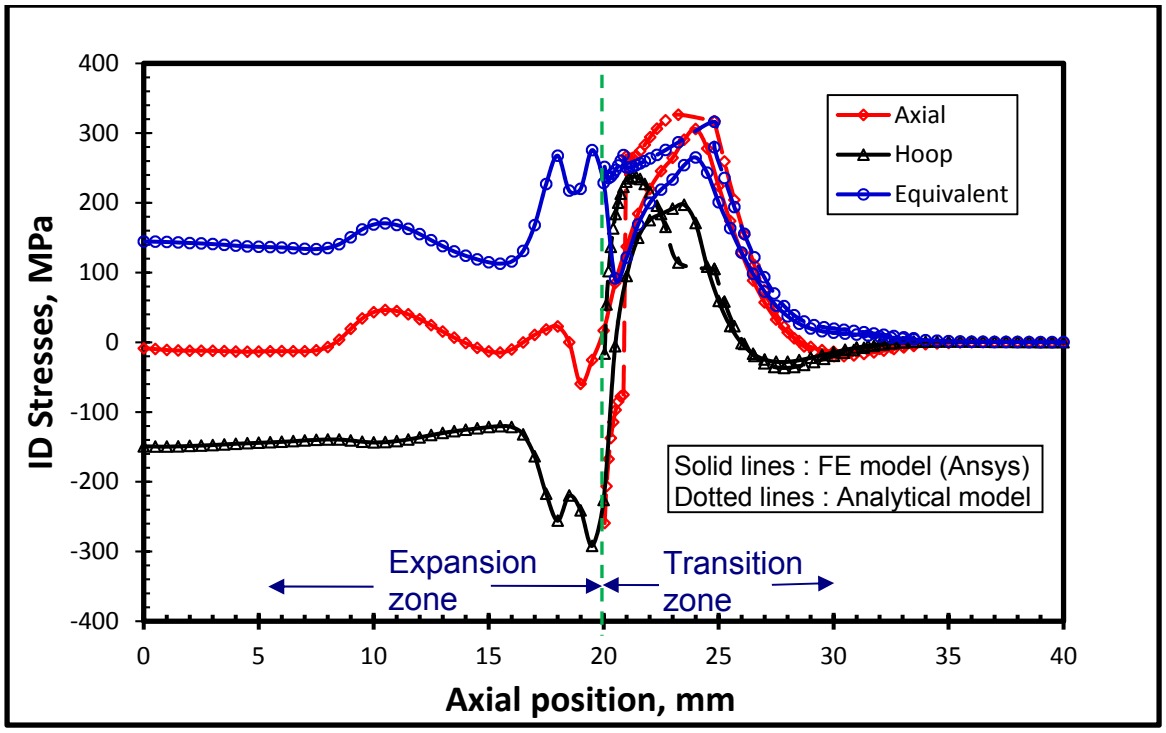

Figure 5.5 Comparison of stresses at tube inner surface during unloading

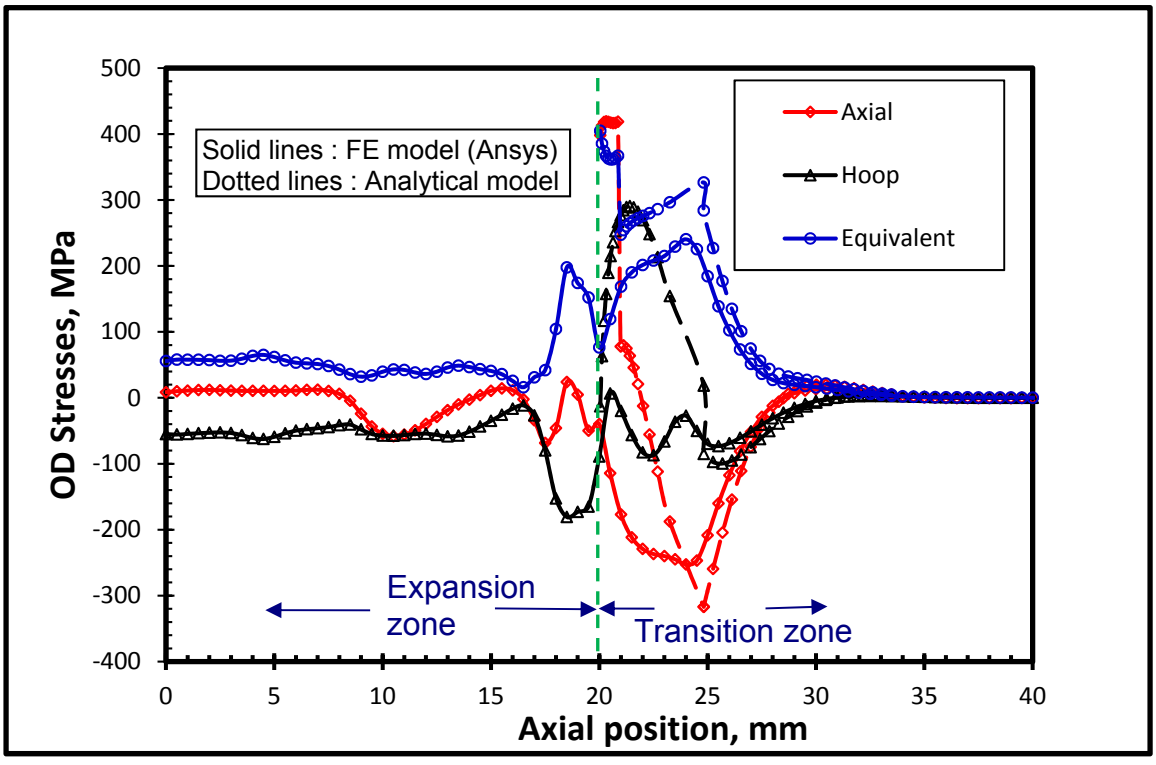

Figure 5.6 Comparison of stresses at tube outer surface during unloading

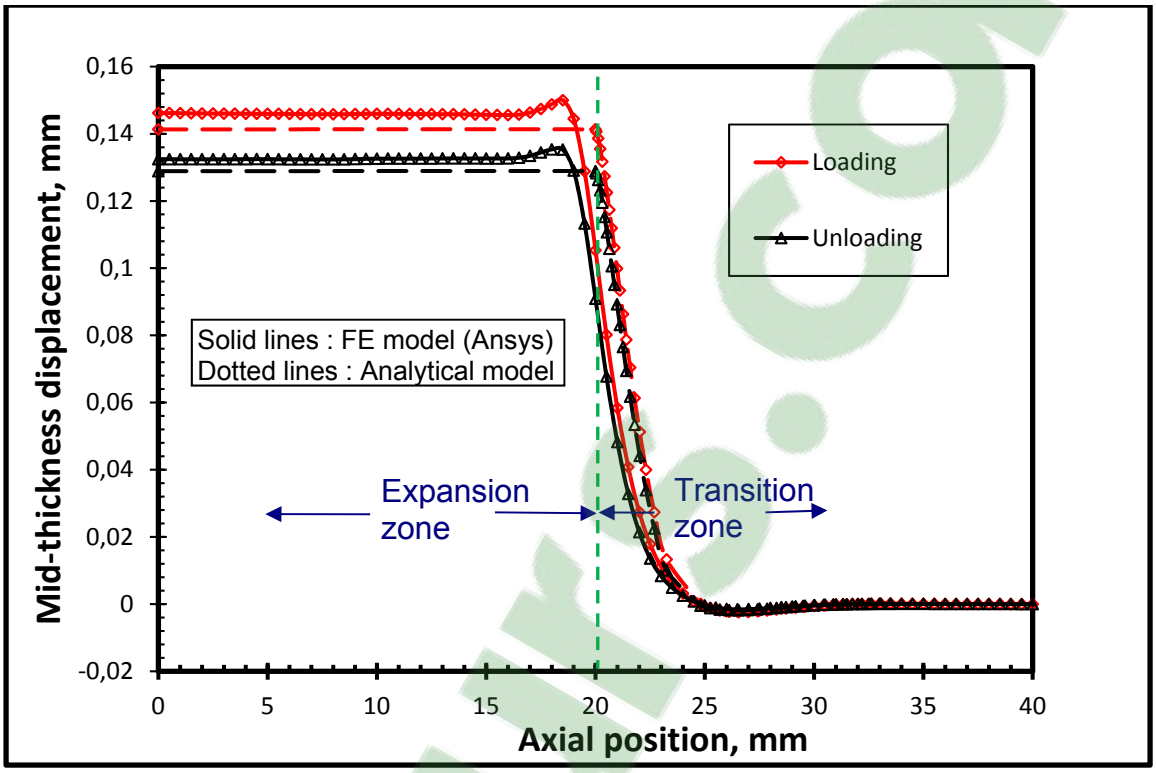

Figure 5.7 Radial displacement at tube mid-thickness

5.3 Pressure loading with reverse yielding case

In this case, a consistent monitoring of the FE model showed that plastic deformation of the tube starts at an expansion pressure of 40.7 MPa. The tube outer surface comes into contact with the tubesheet inner bore surface at 50 MPa, and at this pressure only 23 mm of the tube length from the free end is in full plasticity. The tube transition zone experiences partial plasticity over 1.5 mm of its length (Figure 5.8).

5.3.1 Pressure loading

In the current case, the applied expansion pressure is slightly above the tube yield stress of 240 MPa. This, combined with the clearance value produces reverse yielding during unloading. The different regions of the transition zone at maximum expansion pressure are shown in Figure 5.9.

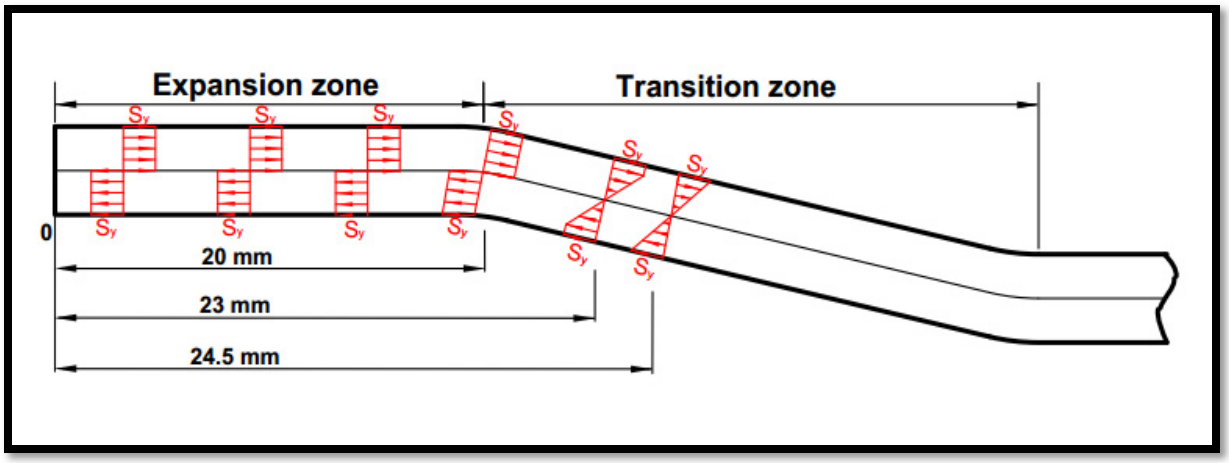

Figure 5.8 Schematic of plasticity in tube when tube touches the tubesheet

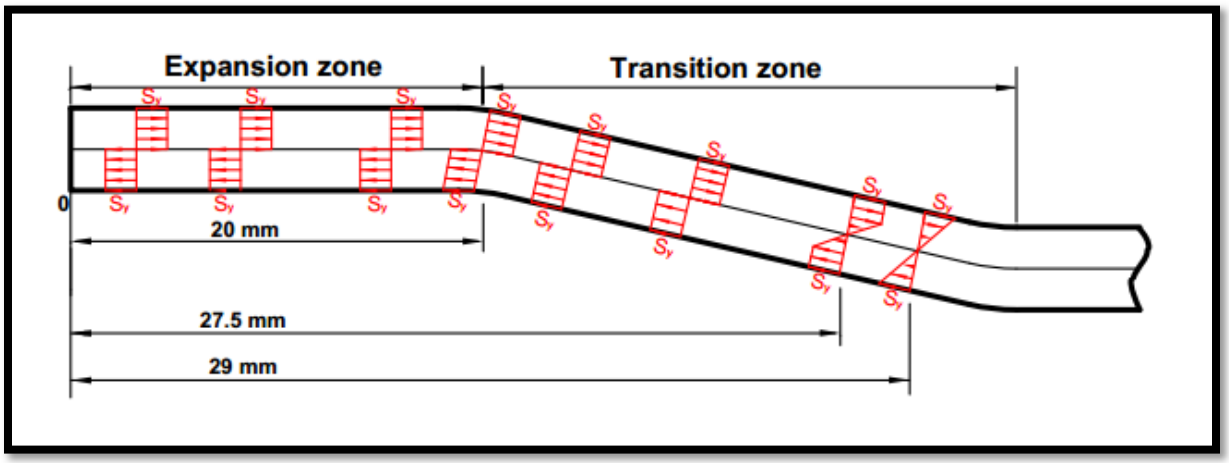

Figure 5.9 Schematic of plasticity in tube at maximum expansion pressure

The axial stress changes from a negative to a positive yield near the expansion to transition zone interface before it reduces gradually in the elastic region, as indicated in Figure 5.10. As in the previous case, the hoop stress and radial displacement of the tube are almost zero at this point of interface. Again, the analytical results are in agreement with the numerical FE model. The comparison of axial stresses on the inner surface shows only a 3% difference located at the junction between the expansion and transition zones. This difference in the hoop stress is about 3.5%. Also, at the elastic plastic interface, the axial stress difference is 11%, while the hoop stress difference is 8%.

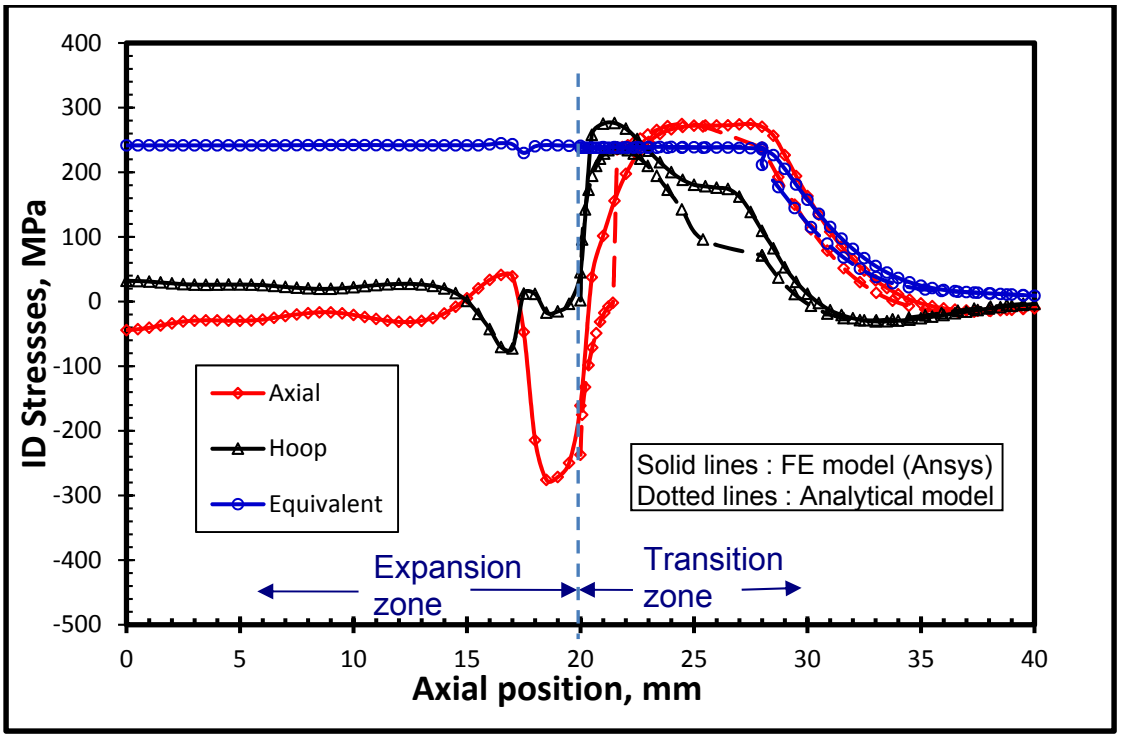

Figure 5.10 Comparison of stresses at tube inner surface at maximum expansion pressure

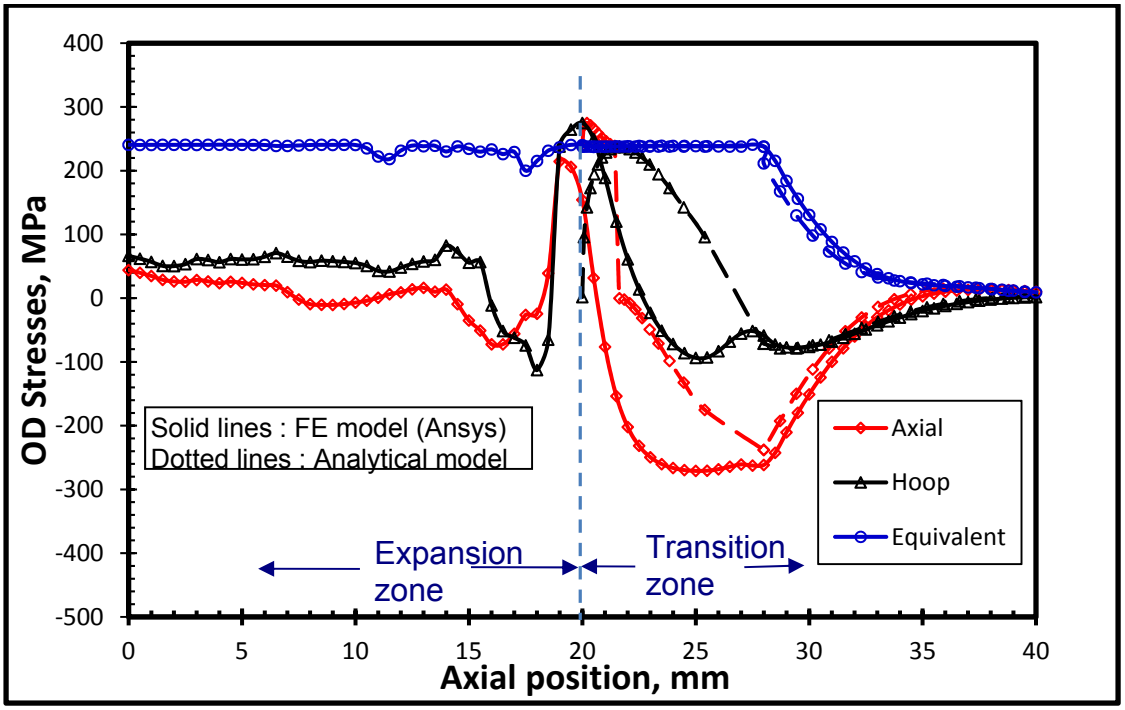

Figure 5.11 Comparison of stresses at tube outer surface at maximum expansion pressure

At the tube's outer surface, the axial stress difference is 24%. As is shown by the distributions of Figure 5.11, the maximum axial stress takes place at 18.5 mm from the start of the tube, which represents the end of the expansion zone and the beginning of the transition zone as indicated by the FE results. The hoop stresses obtained from the FE model at the tube's outer surface show a near zero value at the junction between the plastic and elastic regions, as assumed by the analytical model.

5.3.2 Pressure unloading

The current case involves reverse yielding during unloading. In fact, as is seen in figures 5.12 and 5.13, the equivalent stress during unloading reaches tube yielding in compression, which indicates the occurrence of reverse yielding in the tube expansion zone. Therefore, a significant change in stresses at the junction during unloading once the expansion zone experiences the reverse yielding is observed in this case.

As in the previous case, the spike in the displacement of the expansion transition junction is also present, and this location bears the largest displacement, which causes a sudden change of sign in the axial stress (Figure 5.14).

It can be said that the analytical model is in general agreement with what is observed with the more precise numerical FE model. A confirmation of peak stresses in the transition zone, which is divided into a full plastic region where the axial stresses reach yield at and an elastic region where the stresses are attenuated. There is a focal location that limits the transition zone and the expansion zone where there is a sudden change of axial stress from positive to negative yield, which is worth investigating in greater detail in future work, as it is a source of stress concentration and is prone to crack initiation due to stress corrosion cracking.

The residual stress distributions of the equivalent stress at the inner surface are very similar. However, the axial and hoop stresses show different trends. Nevertheless, at specific points, such as the junction point, this stress exhibits very good agreement between the two models.

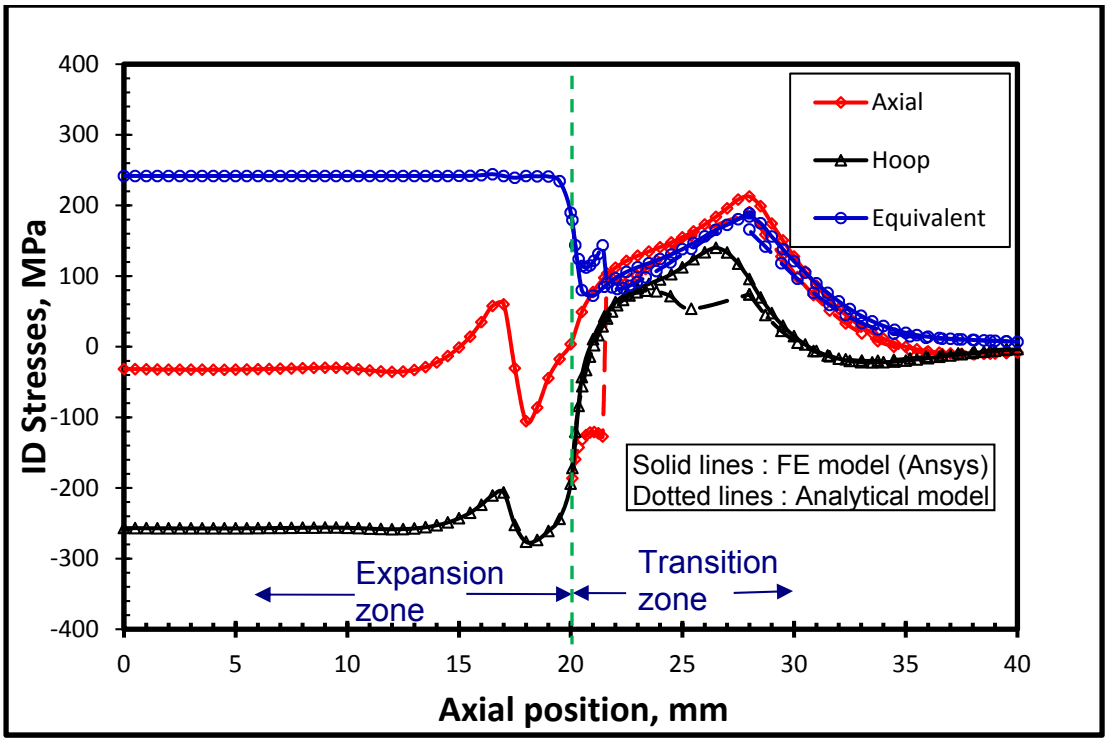

Figure 5.12 Comparison of stresses at tube inner surface during unloading

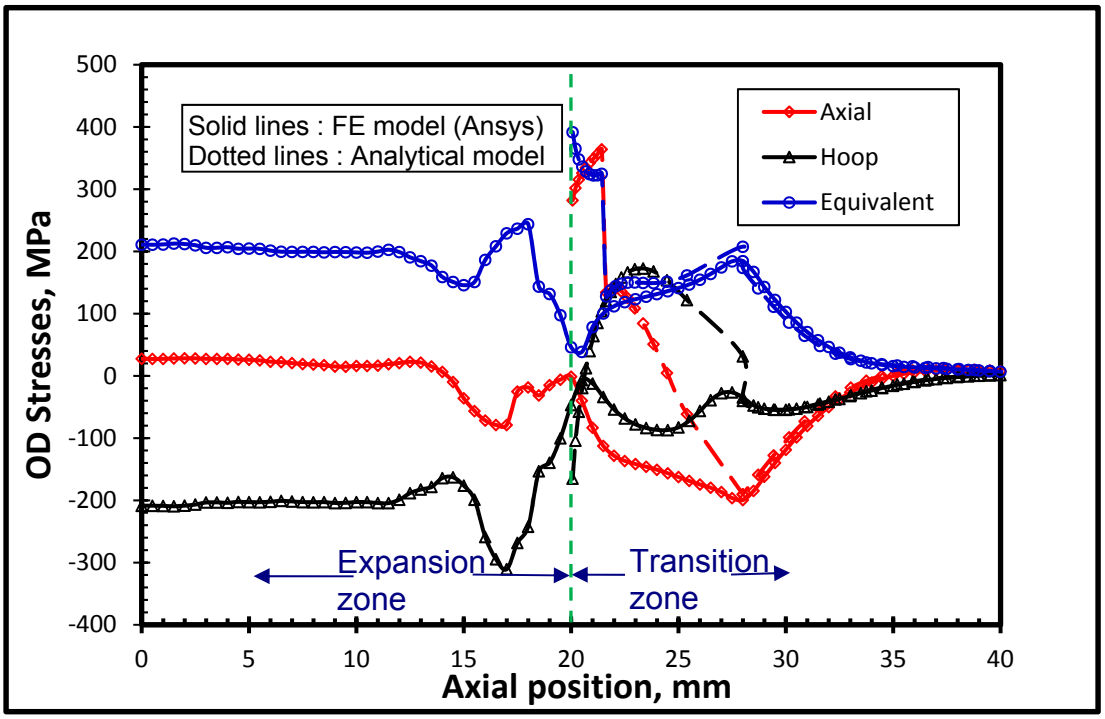

Figure 5.13 Comparison of stresses at tube outer surface during unloading

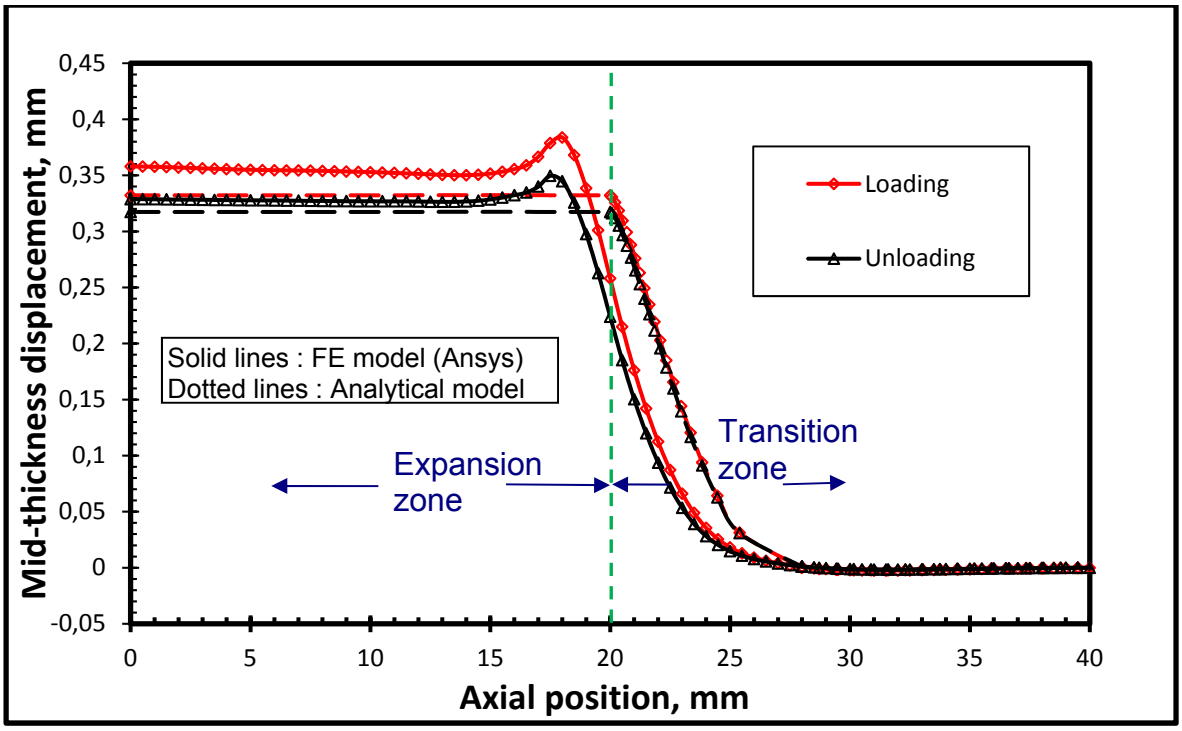

Figure 5.14 Radial displacement at tube mid-thickness

CONCLUSION

In this work, an analytical model has been developed to evaluate the distribution of axial and hoop stresses in the transition zone of hydraulically expanded tube-to-tubesheet joints. The analytical model analyses two regions of the transition zone, the full plastic region and the elastic region, while it neglects the very small partially plastic region that exists between the first two. In addition to the stresses the model gives the radial displacement along the tube transition zone.

Based on the literature and final results, the radial and shear stresses were neglected in the analysis in comparison with other stresses. The hydraulic expansion process is treated separately for loading and unloading and, basically, the model is based on two theories used to predict residual stresses at the end of process. During the loading, the theory of cylinders under symmetrically axial loading proposed by Sawczuk (1960) was employed. In fact, it is assumed that the tube obeys the Von-Mises yield criterion under the elastic perfectly plastic material behavior. In addition to this theory, the elastic region of the transition zone was treated using the beam on elastic foundation theory. Finally, the unloading of the complete transition zone stress analysis was tackled using the equations for a semi-infinite cylindrical shell under axisymmetric external band pressure, to determine the superposed stresses to obtain the finial residual stresses in this zone.

Two cases have been studied and, in either case, the maximum expansion pressure is limited to avoid tubesheet yielding while producing full plastic deformation of the tube expansion and transition zone. The main focus of the study was the tube transition zone. The effect of tubesheet plastic deformation on residual stresses in the transition zone is not investigated, as it is not the aim of this work. In the first case, it is assumed that, during unloading, the tube recovers elastically with no reverse yielding. The effect of the latter on residual stresses was investigated in the second case. It is concluded that reverse yielding in the expansion zone during unloading has a negligible effect on the evaluation of the residual stresses in the transition zone.

The stress comparison between the analytical and the numerical finite element models showed a relatively good agreement in the axial and hoop stresses in addition to the radial

displacements in the transition zone. In fact, the comparison of axial and hoop stresses at maximum expansion pressure in both models and the variations of these stresses throughout the transition zone justifies applying the simpler theory of yield condition for a cylindrical shell subjected to axially symmetric loading in which a ring of force is used instead of band of pressure to simulate the bending moment and shear force at transition zone edge.

The model can be used to limit the maximum expansion pressure and the maximum clearance in order to avoid the high stresses in the transition zone, which makes the joint susceptible to stress corrosion cracking and intergranular attacks at this zone. Limiting the expansion pressure reduces the risk of strain hardening in either the tube or tubesheet and leads to a higher integrity of connection.

A meticulous analysis of the first case results shows that, at maximum expansion pressure, the proposed theory for loading predicts an axial stress with a 4 to 12% difference in the plastic region. The developed model predicts better results for the hoop stress within 5 to 8%. During unloading, this difference reaches 17% for the hoop stress, while the axial stress agreement is within 8% along the transition zone.

In the second case, the comparison of the axial stresses on the inner surface shows only a 3% difference in the expansion-transition zone junction. This difference for hoop stresses is about 3.5%. In the plastic region, the axial and hoop stress differences are 11% and 8% respectively. Finally, during unloading, the residual stress distributions for both axial and hoop stresses on the inner surface show the same trend; however, the hoop stresses of the analytical model deviates significantly from those of the FE model. Nevertheless, at the interface regions, the agreement between the two models is acceptable.

In addition, as is reported in the literature, the tube's inner surface of the transition zone possesses the highest stresses along the tube. At maximum expansion pressure, as a result of bending moment, the axial stress is at its maximum positive value on the inner surface, reaching yield at the expansion transition zone interface and dropping down abruptly to a minimum negative value reaching yield. The maximum hoop stress at the expansion pressure reaches yield at this junction, but drops down to yield in compression right after, but over the whole plastic region of transition zone.

FUTURE WORK

The proposed analytical model showed a relatively good agreement with the FE model, and its performance in determining the residual stresses at the transition zone of the expanded tube is acceptable. The model enables the calculation of the axial and hoop stresses during loading and unloading sequences in the transition zone, which was divided into the plastic and the elastic regions. The model predicts better stress distributions in the elastic region than the plastic region.

Nevertheless, some improvements are required in order to better predict the residual stresses in the transition zone. There are several influencing factors that should be considered in the analysis of the connection's risk of failure. Therefore, it is suggested to investigate the effect of the following parameters as future work:

1) Study the effect of clearance on the residual stresses in the transition zone: As demonstrated from previous work, clearance has a significant effect on the residual stresses in the expansion zone, especially for high strain hardened materials. In particular, the effect emerges notably at the junction where the expansion zone is tied to the transition zone.
2) Study the effect of stain hardening on the residual stresses in the transition zone: This factor needs particular attention due to its complexity and the lack of a theory to model the collapse of a tube subject to band pressure with a strain hardening behavior. The strain hardening effect must be accounted for in order to optimize tube-to-tubesheet joints.
3) Improve the model to include the local effect of the expansion-transition zone: As is clearly manifested by the final results, this junction shows a transition effect where stresses change signs drastically. The assumption that the transition zone is stretched into the expansion zone simplifies the analysis but ignores the stress change at this point. An improved analytical solution is necessary to improve the residual stress predictions.
4) Study the effect of thinning in both zones: Tube thinning and its variation in the transition zone may be important in assessing stress concentration and stress

corrosion cracking. The measurement of this parameter may be a good technique to detect tube expansion defects and the need for retubing or replacing the tubes.

APPENDIX I

MATLAB PROGRAM TO CALCULATE RESIDUAL STRESSES AT TRANSITION ZONE

The program below was written to calculate the residual stresses at the transition zone of the tube for loading and unloading steps, according to Von Mises and Tresca yield criteria. In fact, these stresses are determined and plotted separately and normalized by the tube yield stress.

```
!!!!!!!!!!!!!!!!!!!!!!!!!!!!!!!!!!!!!!!!!!!!!!!!!!!!!!!!!!!!!!!!!!!!!!!
!!! DETERMINATION OF RESIDUAL STRESSES AT THE TRANSITION !!!
!!!                ZONE OF EXPANDED TUBE                 !!!
!!!!!!!!!!!!!!!!!!!!!!!!!!!!!!!!!!!!!!!!!!!!!!!!!!!!!!!!!!!!!!!!!!!!!!!

% function [cas2]=cylinder(ro,t,Syt,Et,nut)
      clear
      clc
      J=0.3;
      ro=12.5;
      t=2.0;

%Tube material properties 10#
      Syt=238;
      Et=209000;
      nut=0.3;
      syms p;
      mm=[];
      nn=[];
      qq=[];
      xx=[];

%Loading

criteria=1; %1 VM 2 Tresca
      ni=21;% number of point along transition length
      xmax=p;
      xmin=p;

if criteria==1
m=-2/3^(1/2)*((tan(p))^2*log(tan(p/2))+1/cos(p));
    n=-tan(p)*log(tan(p/2));
    dm=diff(m,p);
    q=(2*int(n*dm,[xmin,pi]))^(1/2);
    qo=(2*int(n*dm,0,pi))^(1/2);

%xtrans_zone=int(dm/q,0,xmax);
xmin=0.001;
```

```
    xtrans_zone=quad(@distance,xmin,pi);
    xtrans_zone=real(double(vpa(xtrans_zone)));
end

if criteria==2
    n1=1+p;
    m1=4*p*(1+p);
    dm1=diff(m1,p);
    q1s=int(n1*dm1,[xmin,0]);

q1sc=int(n1*dm1,[-0.5,0]);
    n2=1-p;
m2=4*p*(1-p);
dm2=diff(m2,p);
q2=(2*int(n2*dm2,[xmin,0.5]))^(1/2);

q2sc=int(n2*dm2,[0,0.5]);
    qo=(2*(q1sc+q2sc))^(1/2);
    q1=(2*((int(n1*dm1,[xmin,0]))+q2sc))^(1/2);
    x1=int(dm1/q1,[-0.5,xmax]);

x1sc=int(dm1/q1,[-0.5,0]);
    x1sc=real(vpa(x1sc));
    x2s=int(dm2/q2,[0,xmax]);
x2=x1sc+x2s;
    x2sc=int(dm2/q2,[0,0.5]);
real(vpa(x2sc));

xtrans_zone= real(vpa(x1sc))+x2sc;
end

qo=real(double(vpa(qo)));%vpa(qo, 8);

for i=1:ni
if criteria==1
        pp=(i-1)*pi/(ni-1);
if (pp == pi/2) | (pp == 0)
            pp=pp+0.001;
else
            pp=pp;
end
xmin=pp;
xmax=pp;
        x=quad(@distance,0.001,xmax);
xp=real(x);
q=(2*int(n*dm,[xmin,pi-0.001]))^(1/2);
qp=real(double(vpa(q)));
end

if criteria==2
        pp=-0.5+(i-1)/(ni-1);
if (pp<=0) && (pp>=-0.5)
            n=n1;
            m=m1;
```

```
xmin=pp;
xmax=pp;
            dm=dm1;
            q=(2*((int(n1*dm1,[xmin,0]))+q2sc))^(1/2);
            x=int(dm1/q1,[-0.5,xmax]);
xp=real(double(vpa(x)));
qp=real(double(vpa(q)));
end
if (pp>0) && (pp<=0.5)
n=n2;
m=m2;
xmin=pp;
xmax=pp;
            dm=dm2;
            q=(2*int(n2*dm2,[xmin,0.5]))^(1/2);
x2s=int(dm2/q2,[0,xmax]);
            x=x1sc+x2s;
xp=real(double(vpa(x)));
qp=eval(q);
end
end
       p=pp;
mp=real(eval(m));
np=real(eval(n));
xx=[xx xp];
       qq=[qq qp];
mm=[mm mp];
nn=[nn np];
end;

figure(1)
 plot(xx,qq,'*-',xx,mm,'-^',xx,nn,':+')%,xx,p,'-..')

% plot(mm,nn,'*-')% limit diagram

% plot(xx,(mm.^2+nn.^2-mm.*nn).^2,'*-')% VM

% plot(xx,mm+nn,'*-')% Tresca

% set(findobj(gca,'type','line'),'MarkerSize',5)

grid on
      title('Graph of normalized shear, bending & hoop')
      legend ('shear','bending','hoop','Location','SouthWest')

% legend ('colapse','Location','SouthWest')
      r=ro-t/2;
      qlx=qq/2*Syt*t*(t/r)^0.5;
      Nt=nn*Syt*t;
      Mx=mm*Syt*t^2/4;
      xd=xx/2*(r*t)^0.5;
      Strtzti=Nt./t;
      Strtzto=Nt./t;
```

```
if criteria==2
Strtzli=-sign(Mx).*(Strtzti.*(1-sign(Mx))/2-Syt);
Strtzlo=sign(Mx).*(Strtzto.*(sign(Mx)+1)/2-Syt);
else
    Strtzli=(Strtzti+sign(Mx).*(Strtzti.^2-4*(Strtzti.^2-Syt^2)).^0.5)/2;
    Strtzlo=(Strtzto-sign(Mx).*(Strtzto.^2-4*(Strtzto.^2-Syt^2)).^0.5)/2;
end

% if criteria==2

% Strtzli=-sign(Mx).*(Strtzti.*(1-sign(Mx))/2-Syt);

% Strtzlo=sign(Mx).*(Strtzto.*(sign(Mx)+1)/2-Syt);

% else

% Strtzli=(Strtzti-(Strtzti.^2-4*(Strtzti.^2-Syt^2)).^0.5)/2;

% Strtzlo=(Strtzto+(Strtzto.^2-4*(Strtzto.^2-Syt^2)).^0.5)/2;

% end

Strtzs=qlx/t;

figure(2)

plot(xd,Strtzti,'*-',xd,Strtzto,'s-',xd,Strtzli,'-
^',xd,Strtzlo,':+',xd,Strtzs,'-..')

grid on

title('Graph of stresses during loading')
legend ('hoop i','hoop o','bending i','bending
o','shear','Location','SouthWest')

% Strtzs=0;
% Strtzti=0;
% Strtzto=0;
% Strtzli=0;
% Strtzlo=0;

%Unloading

%last=length(Uro);
      k=Et*t/r^2;
      beta=(3*(1-nut^2))^.25/(r*t)^0.5;

%Po=(-max(Uro)+Uro(last))*k/beta;
      Po=qo/2*Syt*t*(t/r)^0.5;

%Mxeu=Po/(2*beta)*exp(-beta*xd).*(sin(beta*xd)-cos(beta*xd));
```

```
      Mxeu=-Po/beta*exp(-beta*xd).*sin(beta*xd)-Mx(1)*exp(-
      beta*xd).*(cos(beta*xd)+sin(beta*xd));

%qxeu=Po*exp(-beta*xd).*cosbeta*xd);
      qxeu=Po*exp(-beta*xd).*(cos(beta*xd)-sin(beta*xd))+Mx(1)*exp(-
      beta*xd).*sin(beta*xd);

%uxzt=Po*beta/k*exp(-beta*xd).*(cos(beta*xd)+sin(beta*xd));
      uxzt=-2*Po*beta/k*exp(-beta*xd).*cos(beta*xd)-2*Mx(1)*beta^2/k*exp(-
      beta*xd).*(cos(beta*xd)-sin(beta*xd));
      Strtzti=Strtzti+Et*uxzt./r+6*nut*Mxeu./t^2;
      Strtzto=Strtzto+Et*uxzt./r-6*nut*Mxeu./t^2;
      Strtzli=Strtzli+6*Mxeu./t^2;
      Strtzlo=Strtzlo-6*Mxeu./t^2;
      Strtzs=Strtzs-qxeu./t;

if criteria==2
for i=1:ni
if Strtzli(i)<0
Strtzei(i)=Strtzti(i)-Strtzli(i);
else
Strtzei(i)=max(Strtzti(i),Strtzli(i));
end
if Strtzlo(i)<0
Strtzeo(i)=Strtzto(i)-Strtzlo(i);
else
Strtzeo(i)=max(Strtzto(i),Strtzlo(i));
end
end

else
       Strtzei=(Strtzti.^2+Strtzli.^2-Strtzti.*Strtzli).^0.5;
      Strtzeo=(Strtzto.^2+Strtzlo.^2-Strtzto.*Strtzlo).^0.5;
end

figure(3)

plot(xd,Strtzti,'*-',xd,Strtzto,'s-',xd,Strtzli,'-
^',xd,Strtzlo,':+',xd,Strtzs,'-..')

%plot(xd,Strtzei,'*-',xd,Strtzeo,'-^');

% plot(mm,nn,'*-')% limit diagram

%plot(xx,(mm.^2+nn.^2-mm.*nn).^2,'*-')% VM

%plot(xx,mm+nn,'*-')% Tresca

%set(findobj(gca,'type','line'),'MarkerSize',5)

grid on
title('Graph of stresses during unloading')
```

```
legend ('hoop i','hoop o','bending i','bending
o','shear','Location','SouthWest')

%legend ('inside','oustside','Location','SouthEast')

% end

%legend ('shear','bending','hoop','Location','SouthWest')

% legend ('colapse','Location','SouthWest')
```

APPENDIX II

ANSYS PROGRAM TO DETERMINE THE RESIDUAL STRESSES AT THE TRANSITION ZONE OF CASE 1

1.1 Units

TABLE-A II.1 Model units

Unit System	Metric (mm, t, N, s, mV, mA) Degrees rad/s Celsius
Angle	Degrees
Rotational Velocity	Rad /s
Temperature	Celsius

1.2 Model (A4)

1.2.1 Geometry

TABLE-A II.2
Model > Geometry

Object Name	*Geometry*
State	Fully Defined
Definition	
Type	DesignModeler
Length Unit	Meters
Element Control	Program Controlled
Display Style	Body Color
Bounding Box	
Length X	70. mm
Length Y	21.12 mm
Length Z	21.12 mm
Properties	
Volume	6693.7mm³
Mass	0. t

TABLE-A II.2 (Continued)

Scale Factor Value	1.
Statistics	
Bodies	3
Active Bodies	3
Nodes	121617
Elements	25953
Mesh Metric	None
Basic Geometry Options	
Parameters	Yes
Parameter Key	DS
Attributes	No
Named Selections	No
Material Properties	No
Advanced Geometry Options	
Use Associativity	Yes
Coordinate Systems	No
Reader Mode Saves Updated File	No
Use Instances	Yes
Smart CAD Update	No
Compare Parts On Update	No
Attach File Via Temp File	Yes
Analysis Type	3-D
Decompose Disjoint Geometry	Yes

TABLE-A II.3
Model > Geometry > Body Groups

Object Name	*Tube*
State	Meshed
Graphics Properties	
Visible	Yes

TABLE-A II.3 (Continued)

Definition	
Assignment	Tube
Coordinate System	Default Coordinate System
Bounding Box	
Length X	70. mm
Length Y	8.725 mm
Length Z	8.725 mm
Properties	
Volume	917.96 mm³
Mass	0. t
Centroid X	0. mm
Centroid Y	0. mm
Centroid Z	0. mm
Moment of Inertia Ip1	0. t·mm²
Moment of Inertia Ip2	0. t·mm²
Moment of Inertia Ip3	0. t·mm²
Statistics	
Nodes	50848
Elements	9825
Mesh Metric	None

TABLE-A II.4
Model > Geometry > Tube > Parts

Object Name	*Tube-1*	*Tube-2*
State	Meshed	
Graphics Properties		
Visible	Yes	
Transparency	1	
Definition		
Suppressed	No	

TABLE-A II.4 (Continued)

Stiffness Behavior	Flexible	
Coordinate System	Default Coordinate System	
Reference Temperature	By Environment	
Material		
Assignment	Tube	
Nonlinear Effects	Yes	
Thermal Strain Effects	No	Yes
Bounding Box		
Length X	50. mm	20. mm
Length Y	8.725 mm	
Length Z	8.725 mm	
Properties		
Volume	655.69 mm^3	262.27 mm^3
Mass	0. t	
Centroid X	45. mm	10. mm
Centroid Y	5.2245 mm	
Centroid Z	-5.2245 mm	
Moment of Inertia Ip1	0. t·mm^2	
Moment of Inertia Ip2	0. t·mm^2	
Moment of Inertia Ip3	0. t·mm^2	
Statistics		
Nodes	35794	15336
Elements	6900	2925
Mesh Metric	None	

TABLE-A II.5
Model > Geometry > Parts

Object Name	*Tubesheet*
State	Meshed
Graphics Properties	
Visible	Yes
Transparency	1
Definition	
Stiffness Behavior	Flexible
Coordinate System	Default Coordinate System
Reference Temperature	By Environment
Material	
Assignment	Tubesheet
Nonlinear Effects	Yes
Thermal Strain Effects	Yes
Bounding Box	
Length X	20. mm
Length Y	21.12 mm
Length Z	21.12 mm
Properties	
Volume	5775.8mm³
Mass	0. t
Centroid X	10. mm
Centroid Y	10.054 mm
Centroid Z	-10.054mm
Moment of Inertia Ip1	0. t·mm²
Moment of Inertia Ip2	0. t·mm²
Moment of Inertia Ip3	0. t·mm²
Statistics	
Nodes	70769
Elements	16128
Mesh Metric	None

TABLE-A II.6
Model > Construction Geometry

Object Name	*Construction Geometry*
State	Fully Defined
Display	
Show Mesh	No

TABLE-A II.7
Model > Construction Geometry > Paths

Object Name	Path-Tube outer length	Path-Tube inner length	Path-Tube middle length	
State	Fully Defined			
Definition				
Path Type	Two Points			
Path Coordinate System	Global Coordinate System			
Number of Sampling Points	139.		39.	139.
Suppressed	No			
Start				
Coordinate System	Global Coordinate System			
Start X Coordinate	0. mm		20. mm	0. mm
Start Y Coordinate	8.725 mm	7.709 mm	8.725 mm	8.217 mm
Start Z Coordinate	0. mm			
End				
Coordinate System	Global Coordinate System			
End X Coordinate	70. mm		40. mm	70. mm
End Y Coordinate	8.725 mm	7.709 mm	8.725 mm	8.217 mm
End Z Coordinate	0. mm			

1.2.2 Coordinate Systems

TABLE-A II.8
Model > Coordinate Systems > Coordinate System

Object Name	*Global Coordinate System*	*Cylindrical*
State	Fully Defined	
Definition		
Type	Cartesian	Cylindrical
Coordinate System ID	0.	12.
Coordinate System		Manual
Suppressed		No
Origin		
Origin X	0. mm	
Origin Y	0. mm	
Origin Z	0. mm	
Define By		Geometry Selection
Geometry		Defined
Directional Vectors		
X Axis Data	[1. 0. 0.]	[0. 1. 0.]
Y Axis Data	[0. 1. 0.]	[0. 0. 1.]
Z Axis Data	[0. 0. 1.]	[1. 0. 0.]
Principal Axis		
Axis		X
Define By		Global Y Axis
Orientation About Principal Axis		
Axis		Y
Define By		Global Z Axis
Transformations		
Base Configuration		Absolute
Transformed Configuration		[0. 0. 0.]

1.2.3 Symmetry

TABLE-A II.9
Model > Symmetry

Object Name	*Symmetry*
State	Fully Defined

TABLE-A II.10
Model > Symmetry > Front

Object Name	*Front*	*Bottom*
State	Fully Defined	
Scope		
Scoping Method	Geometry Selection	
Geometry	3 Faces	
Definition		
Scope Mode	Manual	
Type	Symmetric	
Coordinate System	Global Coordinate System	
Symmetry Normal	Z Axis	Y Axis
Suppressed	No	

1.2.4 Connections

TABLE-A II.11
Model > Connections

Object Name	*Connections*
State	Fully Defined
Auto Detection	
Generate Automatic Connection on Refresh	Yes
Transparency	
Enabled	Yes

TABLE-A II.12
Model > Connections > Contacts

Object Name	*Contacts*
State	Fully Defined
Definition	
Connection Type	Contact
Scope	
Scoping Method	Geometry Selection
Geometry	All Bodies
Auto Detection	
Tolerance Type	Slider
Tolerance Slider	0.
Tolerance Value	0.19026mm
Use Range	No
Face/Face	No
Face/Edge	No
Edge/Edge	No
Priority	Include All
Group By	Bodies
Search Across	Bodies
Statistics	
Connections	1
Active Connections	1

TABLE-A II.13
Model > Connections > Contacts > Contact Regions

Object Name	*Frictional - Multiple To Tubesheet*
State	Fully Defined
Scope	
Scoping Method	Geometry Selection
Contact	2 Faces

TABLE-A II.13 (Continued)

Target	1 Face
Contact Bodies	Multiple
Target Bodies	Tubesheet
Definition	
Type	Frictional
Friction Coefficient	0.15
Scope Mode	Manual
Behavior	Program Controlled
Trim Contact	Program Controlled
Advanced	
Formulation	Program Controlled
Detection Method	Program Controlled
Penetration Tolerance	Program Controlled
Elastic Slip Tolerance	Program Controlled
Normal Stiffness	Program Controlled
Update Stiffness	Program Controlled
Stabilization Damping Factor	0.
Pinball Region	Program Controlled
Time Step Controls	None
Geometric Modification	
Interface Treatment	Add Offset, No Ramping
Offset	0. mm
Contact Geometry Correction	None
Target Geometry Correction	None

1.2.5 Mesh

TABLE-A II.14
Model > Mesh

Object Name	*Mesh*
State	Solved
Display	
Display Style	Body Color
Defaults	
Physics Preference	Mechanical
Relevance	0
Sizing	
Use Advanced Size Function	Off
Relevance Center	Coarse
Element Size	Default
Initial Size Seed	Active Assembly
Smoothing	Medium
Transition	Fast
Span Angle Center	Coarse
Minimum Edge Length	1.0160 mm
Inflation	
Use Automatic Inflation	None
Inflation Option	Smooth Transition
Transition Ratio	0.272
Maximum Layers	5
Growth Rate	1.2
Inflation Algorithm	Pre
View Advanced Options	No
Patch Conforming Options	
Triangle Surface Mesher	Program Controlled
Patch Independent Options	
Topology Checking	No

TABLE-A II.14 (Continued)

Advanced	
Number of CPUs for Parallel Part Meshing	Program Controlled
Shape Checking	Standard Mechanical
Element Midside Nodes	Program Controlled
Straight Sided Elements	No
Number of Retries	Default (4)
Extra Retries For Assembly	Yes
Rigid Body Behavior	Dimensionally Reduced
Mesh Morphing	Disabled
Defeaturing	
Pinch Tolerance	Please Define
Generate Pinch on Refresh	No
Automatic Mesh Based Defeaturing	On
Defeaturing Tolerance	Default
Statistics	
Nodes	121617
Elements	25953
Mesh Metric	None

TABLE-A II.15
Model > Mesh > Mesh Controls

Object Name	*Contact Sizing*	*Edge Sizing-Tube front ID*	*Edge Sizing-Tube back ID*	*Edge Sizing-Tube front OD*	*Edge Sizing-Tube back OD*	*Edge Sizing-Tube front ID down*	*Edge Sizing-Tube back ID down*	*Edge Sizing*
State	Fully Defined							
Scope								

TABLE-A II.15 (Continued)

	Multiple To Tubesheet						
Scoping Method		Geometry Selection					
Geometry		1 Edge					4 Edges
Definition							
Suppressed	No						
Type	Element Size	Number of Divisions					Element Size
Element Size	0.5 mm						0.1 mm
Number of Divisions		40	60	40	60	40	60
Behavior		Hard					Soft
Bias Type		_ _ ___ _____	_____ ___ _ _	_ _ ___ _____	_____ ___ _ _		No Bias
Bias Option		Bias Factor					
Bias Factor		3.					
Reverse Bias		No Selection					

1.3 Static Structural (A5)

TABLE-A II.16
Static Structural > Analysis

Object Name	*Static Structural (A5)*
State	Solved
Definition	
Physics Type	Structural
Analysis Type	Static Structural
Solver Target	Mechanical APDL
Options	

TABLE-A II.16 (Continued)

Environment Temperature	22. °C
Generate Input Only	No

TABLE-A II.17
Static Structural > Analysis Settings

Object Name	*Analysis Settings*
State	Fully Defined
Step Controls	
Number Of Steps	1.
Current Step Number	1.
Step End Time	1. s
Auto Time Stepping	Program Controlled
Solver Controls	
Solver Type	Program Controlled
Weak Springs	Program Controlled
Solver Pivot Checking	Program Controlled
Large Deflection	Off
Inertia Relief	Off
Restart Controls	
Generate Restart Points	Program Controlled
Retain Files After Full Solve	No
Nonlinear Controls	
Newton-Raphson Option	Program Controlled
Force Convergence	Program Controlled
Moment Convergence	Program Controlled
Displacement Convergence	Program Controlled
Rotation Convergence	Program Controlled
Line Search	Program Controlled
Stabilization	Off
Output Controls	

TABLE-A II.17 (Continued)

Stress	Yes
Strain	Yes
Nodal Forces	No
Contact Miscellaneous	No
General Miscellaneous	No
Store Results At	All Time Points
Analysis Data Management	
Future Analysis	None
Scratch Solver Files Directory	
Save MAPDL db	No
Delete Unneeded Files	Yes
Nonlinear Solution	Yes
Solver Units	Active System
Solver Unit System	Nmm

TABLE-A II.18
Static Structural > Loads

Object Name	*Pressure*	*Displacement-Tube back edge*	*Displacement-Tubesheet front head*	*Displacement-Tube front head*	*Fixed Support-Tubesheet Vertex 1*
State	Fully Defined				
Scope					
Scoping Method	Geometry Selection				
Geometry	1 Face	1 Edge		1 Face	1 Vertex
Definition					
Type	Pressure	Displacement			Fixed Support

TABLE-A II.18 (Continued)

		Components		
Magnitude	Tabular Data			
Suppressed	No			
Coordinate		Cylindrical	Global Coordinate System	
System				
X Component			Free	0. mm (ramped)
Y Component			0. mm (ramped)	Free
Z Component			Free	
Tabular Data				
Independent Variable	Time			

TABLE-A II.19
Static Structural > Pressure

Time [s]	Pressure [MPa]
0.	0.
0.5	228.

APPENDIX III

ANSYS PROGRAM TO DETERMINE THE RESIDUAL STRESSES AT THE TRANSITION ZONE OF CASE 2

1.1 Units

TABLE-A III.1 Model units

Unit System	Metric (mm, t, N, s, mV, mA) Degrees rad/s Celsius
Angle	Degrees
Rotational Velocity	Rad/s
Temperature	Celsius

1.2 Model (A4)

1.2.1 Geometry

TABLE-A III.2
Model > Geometry

Object Name	*Geometry*
State	Fully Defined
Definition	
Type	DesignModeler
Length Unit	Meters
Element Control	Program Controlled
Display Style	Body Color
Bounding Box	
Length X	70. mm
Length Y	21.5 mm
Length Z	21.5 mm
Properties	

TABLE-A III.2 (Continued)

Volume	7216.4 mm³
Mass	0. t
Scale Factor Value	1.
Statistics	
Bodies	3
Active Bodies	3
Nodes	159607
Elements	35132
Mesh Metric	None
Basic Geometry Options	
Parameters	Yes
Parameter Key	DS
Attributes	No
Named Selections	No
Material Properties	No
Advanced Geometry Options	
Use Associativity	Yes
Coordinate Systems	No
Reader Mode Saves Updated File	No
Use Instances	Yes
Smart CAD Update	No
Compare Parts On Update	No
Attach File Via Temp File	Yes
Analysis Type	3-D
Decompose Disjoint Geometry	Yes

TABLE-A III.3
Model > Geometry > Body Groups

Object Name	*Tube*
State	Meshed
Graphics Properties	
Visible	Yes
Definition	
Suppressed	No
Assignment	Tube
Coordinate System	Default Coordinate System
Bounding Box	
Length X	70. mm
Length Y	12.5 mm
Length Z	12.5 mm
Properties	
Volume	2529. mm³
Mass	0. t
Centroid X	0. mm
Centroid Y	0. mm
Centroid Z	0. mm
Moment of Inertia Ip1	0. t·mm²
Moment of Inertia Ip2	0. t·mm²
Moment of Inertia Ip3	0. t·mm²
Statistics	
Nodes	139727
Elements	30800
Mesh Metric	None

TABLE-A III.4
Model > Geometry > Tube > Parts

Object Name	*Tube-1*	*Tube-2*
State	Meshed	
Graphics Properties		
Visible	Yes	
Transparency	1	
Definition		
Stiffness Behavior	Flexible	
Coordinate System	Default Coordinate System	
Reference Temperature	By Environment	
Material		
Assignment	Tube	
Nonlinear Effects	Yes	
Thermal Strain Effects	No	Yes
Bounding Box		
Length X	50. mm	20. mm
Length Y	12.5 mm	
Length Z	12.5 mm	
Properties		
Volume	1806.4 mm³	722.57 mm³
Mass	0. t	
Centroid X	45. mm	10. mm
Centroid Y	7.3209 mm	
Centroid Z	-7.3209 mm	
Moment of Inertia Ip1	0. t·mm²	
Moment of Inertia Ip2	0. t·mm²	
Moment of Inertia Ip3	0. t·mm²	
Statistics		
Nodes	84247	56507
Elements	18480	12320
Mesh Metric	None	

TABLE-A III.5
Model > Geometry > Parts

Object Name	*Tubesheet*
State	Meshed
Graphics Properties	
Visible	Yes
Transparency	1
Definition	
Stiffness Behavior	Flexible
Coordinate System	Default Coordinate System
Reference Temperature	By Environment
Material	
Assignment	Tubesheet
Nonlinear Effects	Yes
Thermal Strain Effects	Yes
Bounding Box	
Length X	20. mm
Length Y	21.5 mm
Length Z	21.5 mm
Properties	
Volume	4687.4 mm³
Mass	0. t
Centroid X	10. mm
Centroid Y	11.13 mm
Centroid Z	-11.13 mm
Moment of Inertia Ip1	0. t·mm²
Moment of Inertia Ip2	0. t·mm²
Moment of Inertia Ip3	0. t·mm²
Statistics	
Nodes	19880
Elements	4332
Mesh Metric	None

TABLE-A III.6
Model > Construction Geometry

Object Name	*Construction Geometry*
State	Fully Defined
Display	
Show Mesh	No

TABLE-A III.7
Model > Construction Geometry > Paths

Object Name	Path-Tube outer length	Path-Tube inner length	Path-Tube middle length	
State	Fully Defined			
Definition				
Path Type	Two Points			
Path Coordinate System	Global Coordinate System			
Number of Sampling Points	139.		39.	139.
Suppressed	No			
Start				
Coordinate System	Global Coordinate System			
Start X Coordinate	0. mm		20. mm	0. mm
Start Y Coordinate	12.5 mm	10.5 mm	12.5 mm	11.5 mm
Start Z Coordinate	0. mm			
Location	Defined			
End				
Coordinate System	Global Coordinate System			
End X Coordinate	70. mm		40. mm	70. mm
End Y Coordinate	12.5 mm	10.5 mm	12.5 mm	11.5 mm

TABLE-A III.7 (Continued)

End Z Coordinate	0. mm
Location	Defined

1.2.2 Coordinate Systems

TABLE-A III.8
Model > Coordinate Systems > Coordinate System

Object Name	*Global Coordinate System*	*Cylindrical*
State	Fully Defined	
Definition		
Type	Cartesian	Cylindrical
Coordinate System ID	0.	12.
Coordinate System		Manual
Suppressed		No
Origin		
Origin X	0. mm	
Origin Y	0. mm	
Origin Z	0. mm	
Define By		Geometry Selection
Geometry		Defined
Directional Vectors		
X Axis Data	[1. 0. 0.]	[0. 1. 0.]
Y Axis Data	[0. 1. 0.]	[0. 0. 1.]
Z Axis Data	[0. 0. 1.]	[1. 0. 0.]
Principal Axis		
Axis		X
Define By		Global Y Axis
Orientation About Principal Axis		
Axis		Y
Define By		Global Z Axis
Transformations		

TABLE-A III.8 (Continued)

Base Configuration		Absolute
Transformed Configuration		[0. 0. 0.]

1.2.3 Symmetry

TABLE-A III.9
Model > Symmetry

Object Name	*Symmetry*
State	Fully Defined

TABLE-A III.10
Model > Symmetry > Front

Object Name	*Front*	*Bottom*
State	Fully Defined	
Scope		
Scoping Method	Geometry Selection	
Geometry	3 Faces	
Definition		
Scope Mode	Manual	
Type	Symmetric	
Coordinate System	Global Coordinate System	
Symmetry Normal	Z Axis	Y Axis

1.2.4 Connections

TABLE-A III.11
Model > Connections

Object Name	*Connections*
State	Fully Defined
Auto Detection	

TABLE-A III.11 (Continued)

Generate Automatic Connection On Refresh	Yes
Transparency	
Enabled	Yes

TABLE-A III.12
Model > Connections > Contacts

Object Name	*Contacts*
State	Fully Defined
Definition	
Connection Type	Contact
Scope	
Scoping Method	Geometry Selection
Geometry	All Bodies
Auto Detection	
Tolerance Type	Slider
Tolerance Slider	0.
Tolerance Value	0.1908 mm
Use Range	No
Face/Face	No
Face/Edge	No
Edge/Edge	No
Priority	Include All
Group By	Bodies
Search Across	Bodies
Statistics	
Connections	1
Active Connections	1

TABLE-A III.13
Model > Connections > Contacts > Contact Regions

Object Name	*Frictional - Multiple To Tubesheet*
State	Fully Defined
Scope	
Scoping Method	Geometry Selection
Contact	2 Faces
Target	1 Face
Contact Bodies	Multiple
Target Bodies	Tubesheet
Definition	
Type	Frictional
Friction Coefficient	0.15
Scope Mode	Manual
Behavior	Program Controlled
Trim Contact	Program Controlled
Suppressed	No
Advanced	
Formulation	Program Controlled
Detection Method	Program Controlled
Penetration Tolerance	Program Controlled
Elastic Slip Tolerance	Program Controlled
Normal Stiffness	Program Controlled
Update Stiffness	Program Controlled
Stabilization Damping Factor	0.
Pinball Region	Program Controlled
Time Step Controls	None
Geometric Modification	
Interface Treatment	Add Offset, No Ramping
Offset	0. mm
Contact Geometry Correction	None
Target Geometry Correction	None

1.2.5 Mesh

TABLE-A III.14
Model > Mesh

Object Name	*Mesh*
State	Solved
Display	
Display Style	Body Color
Defaults	
Physics Preference	Mechanical
Relevance	0
Sizing	
Use Advanced Size Function	Off
Relevance Center	Coarse
Element Size	Default
Initial Size Seed	Active Assembly
Smoothing	Medium
Transition	Fast
Span Angle Center	Coarse
Minimum Edge Length	2.0 mm
Inflation	
Use Automatic Inflation	None
Inflation Option	Smooth Transition
Transition Ratio	0.272
Maximum Layers	5
Growth Rate	1.2
Inflation Algorithm	Pre
View Advanced Options	No
Patch Conforming Options	
Triangle Surface Mesher	Program Controlled
Patch Independent Options	
Topology Checking	No

TABLE-A III.14 (Continued)

Advanced	
Number of CPUs for Parallel Part Meshing	Program Controlled
Shape Checking	Standard Mechanical
Element Midside Nodes	Program Controlled
Straight Sided Elements	No
Number of Retries	Default (4)
Rigid Body Behavior	Dimensionally Reduced
Mesh Morphing	Disabled
Defeaturing	
Pinch Tolerance	Please Define
Generate Pinch on Refresh	No
Automatic Mesh Based Defeaturing	On
Defeaturing Tolerance	Default
Statistics	
Nodes	159607
Elements	35132
Mesh Metric	None

TABLE-A III.15
Model > Mesh > Mesh Controls

Object Name	*Contact Sizing*	*Edge Sizing-Tube front ID*	*Edge Sizing-Tube back ID*	*Edge Sizing-Tube front OD*	*Edge Sizing-Tube back OD*	*Edge Sizing-Tube front ID down*	*Edge Sizing-Tube back ID down*	*Edge Sizing*
State	Fully Defined							
Scope								
Contact Region	Frictional - Multiple To Tubesheet							

TABLE III.15 (Continued)

Scoping Method		Geometry Selection					
Geometry		1 Edge					4 Edges
Definition							
Type	Element Size	Number of Divisions					Element Size
Element Size	0.5 mm						0.1 mm
Number of Divisions		40	60	40	60	40	60
Behavior		Hard					Soft
Bias Type		_ _ ___ _____	_____ ___ _ _	_ _ ___ _____	_____ ___ _ _		No Bias
Bias Option		Bias Factor					
Bias Factor		3.					
Reverse Bias		No Selection					

1.3 Static Structural (A5)

TABLE-A III.16
Static Structural > Analysis

Object Name	*Static Structural (A5)*
State	Solved
Definition	
Physics Type	Structural
Analysis Type	Static Structural
Solver Target	Mechanical APDL
Options	
Environment Temperature	22. °C
Generate Input Only	No

TABLE-A III.17
Static Structural > Analysis Settings

Object Name	*Analysis Settings*
State	Fully Defined
Step Controls	
Number Of Steps	1.
Current Step Number	1.
Step End Time	1. s
Auto Time Stepping	Program Controlled
Solver Controls	
Solver Type	Program Controlled
Weak Springs	Program Controlled
Solver Pivot Checking	Program Controlled
Large Deflection	Off
Inertia Relief	Off
Restart Controls	
Generate Restart Points	Program Controlled
Retain Files After Full Solve	No
Nonlinear Controls	
Newton-Raphson Option	Program Controlled
Force Convergence	Program Controlled
Moment Convergence	Program Controlled
Displacement Convergence	Program Controlled
Rotation Convergence	Program Controlled
Line Search	Program Controlled
Stabilization	Off
Output Controls	
Stress	Yes
Strain	Yes
Nodal Forces	No
Contact Miscellaneous	No

TABLE-A III.17 (Continued)

General Miscellaneous	No
Store Results At	All Time Points
Analysis Data Management	
Future Analysis	None
Scratch Solver Files Directory	
Save MAPDL db	No
Delete Unneeded Files	Yes
Nonlinear Solution	Yes
Solver Units	Active System
Solver Unit System	nmm

TABLE-A III.18
Static Structural > Loads

Object Name	*Pressure*	*Displacement-Tube back edge*	*Displacement-Tubesheet front head*	*Displacement-Tube front head*	*Fixed Support-Tubesheet Vertex 1*
State	Fully Defined				
Scope					
Scoping Method	Geometry Selection				
Geometry	1 Face	1 Edge		1 Face	1 Vertex
Definition					
Type	Pressure	Displacement			Fixed Support
Define By	Normal To	Components			
Magnitude	Tabular Data				
Coordinate System		Cylindrical	Global Coordinate System		

TABLE-A III.18 (Continued)

X Component		Free	0. mm (ramped)	
Y Component		0. mm (ramped)	Free	
Z Component			Free	
Tabular Data				
Independent Variable	Time			

TABLE-A III.19
Static Structural > Pressure

Time [s]	Pressure [MPa]
0.	0.
0.5	240.
1.	0.

BIBLIOGRAPHY

Alexander, J. M. and Ford, H. 1956. «Experimental Investigation of the Process of Expanded Boiler Tubes ». Proceeding of institute of mechanical Engineering, Vol. 171, 351-367.

Allam, M., Bazergui, A. and Chaaban, A. 1998b. «The effect of tube strain hardening level on the residual contact pressure and residual stresses of hydraulically expanded tube-to-tubesheet joint ». Proceedings, of the ASME Pressure Vessel and Piping Conference, 375.; 1998. p. 447–55.

Allam, M., Chaaban, A. and Bazergui, A. 1998a. «Estimation of residual stresses in hydraulically expanded tube-to-tubesheet joints ». Journal of Pressure Vessel Technology, Transactions of the ASME, v 120, n 2, 1998, p 129-137.

Allam, M., Chaaban, A. and Bazergui, A. 1995. «Residual Contact Pressure of Hydraulically Expanded Tube-to-Tubesheet Joint: Finite Element and Analytical Analyses ». ASME Conference, PVP-Vol, 305.

Bazergui, A. and Allam, M. 2002. «Axial strength of tube-to-tubesheet joints: Finite element and experimental evaluations ». Journal of Pressure Vessel Technology, Transactions of the ASME, v 124, n 1, p 22-31.

Bouzid, H. and Kazeminia, M. 2015. «Effect of reverse yielding on the Residual contact stresses of tube-to-tubesheet joints subjected to hydraulic expansion». Proceedings of the ASME 2015 Pressure Vessels & Piping Conference PVP2015, Boston, Massachusetts, USA.

Cassidy P. R. 1935. «The trend of modern boiler design», presented at a meeting of the engineers' Society of western Pensylvania, Oct. 15, 1935).

Chaaban, A., Ma, H. and Bazergui, A. 1992. «Tube-tubesheet joint: a proposed equation for the equivalent sleeve diameter used in the single-tube model ». ASME Journal of Pressure Vessel Technollgy1992, 114:19–22.

Chaaban, A., Morin, E., Ma, H. and Bazergui, A. 1989. «Finite Element Analysis of Hydraulically Expanded Tube-To-Tubesheet Joints: A Parametric Study ». ASME PVP conference, 19-25.

Culver, L. E. and Ford, H. 1959. «Experimental Study of Some Variables of the Tube Expanding Process ». Proceeding of Institute of Mechanical Engineering Vol. 173, 399-413.

Denton, A. A. 1966. «Determination of residual stresses ». Met. Reviews (101), J. Inst. Met., Vol. II (1966), pp. 1-23.

Dudley F. E. 1953. «Electronic Control Methodfor the Precision, Expanding of Tubes ». ASME Winter Annual Meeting, Paper No. 53-A-133.

Fisher, F. F. and Brown, G. J. 1954. «Tube Expanding and related subjects ». Transaction of ASME, Vol. 75, 563-584.

Fisher, F. F. and Cope, E. T. 1943. « Automatic Uniform Rolling–In of Small Tubes ». Transaction of ASME, Vol. 65, 53-60.

Flesch, B. and al. 1993. «Operating Stresses and Stress Corrosion Cracking in Steam Generator Transition Zones (900-MWe PWR) ». Int. J. Pres. Ves. & Piping 56 (1993) 213-228, Commissariat ~ l'Energie Atomique, Cadarache, France.

Green, S. J. 1986. «Methods for Preventing Steam Generator Failure or Degradation». Int. J. Pres. Ves. & Piping 25, 1986, 359-391.

Haslinger, K. H. and Hewitt, E. W. 1983. «Leak Tight, High Strength Joints for Corrosion Resistant Condenser Tubing ». Joint Power Generation, ASME paper 83-JPGC-Pwr-39.

Hwang, J. Harrod, D. and Middlebrooks, W. 1993. «Analytical Evaluation of the Hydraulic Expansion of Stream Generator Tubing in to Tubesheet ». International Conferences on Expanded and Rolled Joint Technology, Toronto, CANADA, C98-C113.

José, L. O. and Pablo, G. F. 2004. «Failure analysis of tube–tubesheet welds in cracked gas heat exchangers ». Engineering Failure Analysis 11 (2004) 903–913.

Kasriae, B. and Porowski, J. S. 1983. «Elastic-Plastic Analysis of Tube Expansion in Tubesheet». Pressure Vessel and Piping Conference, Portland, Ore.

Kohlpaintner, W. R. 1995. «Calculation of Hydraulically Expanded Tube-to-Tubesheet Joints ». ASME J. Pressure Vessel Technol., 117, pp. 24–30.

Krips, H. and Podhorsky, M. 1976. «Hydraulic Expansion –A New Method for Anchoring of Tubes ». Journal of Pressure Vessel Technology, Vol. 117, 24-30.

Kyu, I. S. and al. 2001. «Simulation of stress corrosion crack growth in steam generator tubes». Nuclear Engineering and Design 214 (2002) 91–101.

Laghzale N. and Abdel-Hakim Bouzid, 2009, "Analytical Modeling of Hydraulically Expanded Tube-To-Tubesheet Joints", ASME Journal of Pressure and Vessel Technology, Volume 131 / 011208.

Laghzale Nor-eddine and Abdel Hakim Bouzid, "Theoretical Analytical of Hydraulically Expanded Tube-To-Tubesheet Joints with Linear Strain Hardening Material Behavior", ASME Journal of Pressure and Vessel Technology, Volume 131 / 061202.

Livieri, P., and Lazzarin, P., 2002, « Autofrettaged cylindrical vessels and Bauschinger effect: an analytical frame for evaluating residual stresses distribution. » ASME J. Pressure Vessel Technol., 114.Pp.19-22.

LI Xiaotian and HE Shuyan. 2004. «Fatigue analysis of steam generator in Htr-10 ». 2nd International Topical Meeting on HIGH TEMPERATURE REACTOR TECHNOLOGY, Beijing, China, September 22-24, 2004.

Maxwell, C. A. 1943. «Practical aspects of Marking Expended Joint ». Transaction of ASME, Vol. 65, 507-514.

Merah, N., Al-Zayerb, A., Shuaib, A. and Arif, A. 2003. «Finite element evaluation of clearance effect on tube-to-tubesheet joint strength». International Journal of Pressure Vessels and Piping 80, 2003, 879–885.

Middlebrooks, W. B., Harrod, D. and Gold, R.E. 1991. «Residual Stresses Associated with the Hydraulic Expansion of Steam Generator Tubing into Tubesheets». Transaction of the 11th International Conference on Structural Mechanics in Reactor Technology Atomic Energy Society of Japan, Vol. F.

Oppenheimer P.H. 1927. «Rolling Tubes in Boiler Plates ». Power, 300-303.

Osgood, W. R. 1954. «Residual Stresses in Metals and Metal Construction». Prepared for the Ship Struct. Comm., Committee on Residual Stresses, Nat. Academy of Sciences Nat. Res. Council, Reinhold Publ. Corp., N.Y., 1954.

Ramu, S. A., Krihnan, A. and Dxit, K. 1987. «Finite Element Analysis of Elastic-plastic Stresses in Channel Rolled Joints ». 9th.International Conference on Structural Mechanic in Reactor Technology, Vol. 8, T 359-368.

Roark's Formulas for stress and strain, 7edition, Warren C. Young and Richard G. Budynas.

Sachs, G. 1947. «Note on the Tightness of expanded tube joints ». Journal of Applied Mechanics.A285-A286.

Sang, Z., Zhu, Y. a Widera, G. 1996. «Reliability factors and tightness of tube-to-tubesheet joints ». ASME J Press Vessel Technol, 1996;118: 137–41.

Sawczuk A. and P. G. Hodge JR., 1960. « Comparison of yield conditions for circular shells». Franklin Institute -- Journal, v 269, p 362-374, May, 1960.

Scott, D. A., Wolgemuth, G.A. and Aikin, J.A., 1984. «Hydraulically Expanded Tube-to-Tubesheet Joints». Journal of Pressure vessel technology, pp. 104-109.

Scott, D., Dammak, M. and Paiement, G. 1991. «Hydraulic Expanded Tube-to-Tubesheet joints ». Transactions of ASME, Journal of Pressure Vessels Technology, Vol. 1O6, 104-109.

Seong, S. H. and Hong, P. K. 2005. «Leak behavior of SCC degraded steam generator tubings of nuclear power plant ». Nuclear Engineering and Design 235 (2005) 2477–2484.

Toba, A. 1966. «Residual Stress and Stress Corrosion Cracking in the Vicinity of Expanded Joint of Aluminum Brass Tube Condensers». Journal of Japan Petroleum Institute Vol. 9, No. 5, 30-34.

Updike D. P., Kalnins A. and S. M. Caldwell 1988. « A method for calculating residual stresses in transition zone of heat exchanger tubes» PVP, v 139, p 113-118, 1988.

Updike D. P., Kalnins A. and S. M. Caldwell 1989. « Residual stresses in transition zones of heat exchanger tubes» PVP, v 175, p 39-44, 1989.

Uragami, K. 1982. «Experimental Residual Stress Analysis of Tube to Tube Sheet Joints During Expansion ». Pressure Vessel and Piping. ASME, 82-PVP-61.

Wang, H. F. and Sang, Z. F. 2005. «Effect of Geometry of Grooves on Connection Strength of Hydraulically Expanded Tube-to-Tubesheet Joints». Journal of Pressure Vessel Technology, Transactions of the ASME, Vol. 127, NOVEMBER 2005.

Wang, Y. et Soler, A. I. 1988. «Effect of Boundary Conditions on The Tube-Tubesheet Joint Annulus Model- Finite Element Analysis ». ASME PVP Conference, Vol. 139.

Wilson, R. M. 1978. «The Elastic-Plastic Behavior of a Tube During Expansion ». ASME, paper 78-PVP-112.

Yokell, S. 1992. «Expanded and Welded-and-Expanded Tube-to-Tubesheet Joints ». ASME J. Pressure Vessel Technology, 114, pp. 157–165.

Yokell, S. 1982. «Heat-exchanger tube-to-tubesheet connections ». Journal of Chemical Engineering, pp.78-94, Feb. 8.